Chemical composition of volcanic plumes:

Application of ground-based in-situ and remote sensing measurements for the determination of C, S and halogens species and analytical progress to determine molecular halogens in volcanic plumes

Dissertation

vorgelegt von

Xochilt Carolina Gutiérrez Gutiérrez

geboren in San Salvador, El Salvador

1. Berichterstatter: █████████████████████████████

2. Berichterstatter: ████████████████████████

Tag der mündlichen Prüfung:

I hereby declare that I wrote the dissertation submitted without any unauthorized external assistance and used only sources acknowledged in the work. All textual passages which are appropriated verbatim or paraphrased from published and unpublished texts as well as all information obtained from oral sources are duly indicated and listed in accordance with bibliographical rules. In carrying out this research, I complied with the rules of standard scientific practice as formulated in the statutes of Johannes Gutenberg-University Mainz to insure standard scientific practice.

Mainz, February 17, 2022

"Caminante no hay camino, se hace camino al andar"

<div align="right">

Written by: Antonio Machado

Singed by: Joan Manuel Serrat y Joaquín Sabina

Said by: **Rubén Eduardo Gutiérrez Flores**

</div>

Zusammenfassung

Aktive Vulkane können große Mengen an Gasen und Partikeln in die Atmosphäre emittieren, entweder durch passive Entgasung oder während eruptiver Ereignisse. SO_2-Emissionen werden als grundlegendes Überwachungsinstrument betrachtet und Fernerkundungstechniken werden hauptsächlich zu ihrer Messung eingesetzt. Häufig werden diese Messungen mit In-situ-Gasmessungen von SO_2 und anderen flüchtigen Stoffen (CO_2, H_2S, Cl, F) kombiniert, um Veränderungen der vulkanischen Aktivität zu bewerten und sogar Eruptionen vorherzusagen (e.g. Noguchi, 1963, Menyailov, 1975, Duffel et al., 2003; Aiuppa, 2009; Lee et al., 2018). Nur wenige Studien haben sich bislang mit Brom und Jod befasst, was zum Teil daran liegt, dass diese viel selteneren Halogene nur mit erhöhtem Aufwand zu analysieren sind. Dennoch wurden seit der Entdeckung von BrO in Vulkanfahnen durch Bobrowski et al. (2003) BrO und BrO/SO_2-Verhältnisse an verschiedenen Vulkanfahnen mit Fernerkundungstechniken beobachtet (e.g. Bobrowski et al., 2003; Kern et al., 2009; Bobrowski und Giuffrida, 2012; Lübcke et al., 2014; Dinger et al., 2018; Warnach et al., 2019). Diese Beobachtungen deuten auf komplexe chemische Reaktionen insbesondere von Brom in der Vulkanfahne hin, die u. a. Auswirkungen auf den atmosphärischen Ozonhaushalt haben.

Die vorliegende Dissertation zielt darauf ab, das Verständnis der Chemie von Vulkanfahnen und ihrer Auswirkungen auf die Atmosphäre besser zu verstehen, und zwar indem verschiedene Halogenspezies analytisch erfasst werden mit der langfristigen Perspektive auch Zusammenhänge mit der vulkanischen Aktivität (präeruptiver Indikator) zu verstehen. Insbesondere zwei Vulkane in El Salvador (Santa Ana und San Miguel) stehen im Mittelpunkt dieser Studien.

Zu den ersten Studien, die durchgeführt wurden, gehört die Verwendung von mit cis- und trans-Silbenen (CST, TST) beschichteten Diffusion-denuder für die In-situ-Derivatisierung zur Bestimmung reaktiver Halogenspezies (RHS). Die Beschichtungen sammeln selektiv molekulare Halogene (Cl_2 und Br_2) und möglicherweise Interhalogene (BrCl). CST hat sich als geeigneteres Reagenz erwiesen, da eine höhere Wiederfindungsrate als bei TST beobachtet wurde. Die Derivatisierungsprodukte konnten mittels GC-MS nachgewiesen werden, wobei für jede

dihalogenierte Verbindung ein Signal erhalten wurde und zwischen verschiedenen RHS unterschieden werden konnte. Die Verwendung dieser Beschichtungen in Kombination mit Diffusion-denuder wird jedoch aufgrund der geringen Ausbeute bei kurzen Probenahmezeiten (15 – 60 min) als nicht wirklich geeignet bewertet.

Daher wurde in einer zweiten Studie die Effizienz von Stilben-Stereoisomeren sowie von Octenol (OC) unter Verwendung von Spritzenfiltern als RHS-Probenahmetechnik anstelle von Diffusionsabscheidern unter Verwendung einer Chlorgasquelle untersucht. Der Grund für die Verwendung von Spritzenfiltern ist ihre geringe Größe und ihr geringes Gewicht, wodurch sie sich nicht nur für die Probenahme am Kraterrand, sondern auch für unbemannte Luftfahrzeuge eignen. Diese Effizienzstudien wurden mit handelsüblichen elektrochemischen Sensoren als Echtzeitsysteme zur Überwachung der Leistung der verschiedenen Beschichtungen durchgeführt. Auch hier zeigte CST eine höhere Sammeleffizienz als TST und Octenol. Dennoch wurden geringe Wiederfindungsraten erzielt, was möglicherweise auf die Verdampfung der Beschichtung während der Probenahme zurückzuführen ist. Trotz dieser Ergebnisse zeigten beschichtete Filter eine bessere Effizienz für Reaktionen mit Chlorgas bei niedrigen Beschichtungsraten im Vergleich zu Diffusionsabscheidern, mit einer Verbesserung von 5% Ausbeute bei Diffusionsabscheidern auf 23% Ausbeute bei Spritzenfiltern.

Zusätzlich zu dieser grundlegenden analytischen Entwicklungsarbeit umfasst die vorliegende Arbeit auch die Anwendung etablierter vulkanologischer In-situ-Messverfahren. Alkalifallen, MultiGAS und 1,3,5-Trimethoxybenzol (TMB)-beschichtete Diffusions-denuder für die In-situ-Derivatisierung von RHS wurden verwendet. Feldanwendungen wurden am Vulkan Masaya (Nicaragua), am Krater La Fossa, am Vulkan Vulcano (Italien) sowie an den Vulkanen Santa Ana und San Miguel (El Salvador) durchgeführt. Der Gesamtschwefelgehalt und die Halogene wurden mit Hilfe von Alkalifallen-Probenahmen und anschließenden IC- und ICP-MS-Messungen bestimmt, während der Gesamt-RHS-Wert von Chlor und Brom mit Hilfe von TMB-beschichteten Diffusionsabscheidern und anschließender GC-MS-Analyse gemessen wurde. Diese In-situ-Techniken wurden in unterschiedlichen Abständen vom Emissionsschlot durchgeführt. Die Daten zeigen die Halogenspeziation in Abhängigkeit vom Alter der Abgasfahne, wobei das Verhältnis von RHS zu Schwefel im Bereich von $10^{-6} – 10^{-5}$ in der Nähe des

Schlots und zwischen $10^{-5} - 10^{-4}$ in größerer Entfernung liegt. Darüber hinaus wurde auf Vulcano eine zusätzliche Messung in der Nacht durchgeführt, die zeigt, dass die Halogenchemie auch während der Nacht stattfindet.

Schließlich wurde eine erweiterte Auswertung von Langzeit-DOAS-Beobachtungen der NOVAC-Stationen Santa Ana und San Miguel durchgeführt, die SO_2-, BrO- und BrO/SO_2-Messungen umfasst und den ersten Datensatz seiner Art für Langzeit-DOAS-Beobachtungen an diesen Vulkanen darstellt.

Abstract

Active volcanoes can emit large amounts of gases and particles into the atmosphere, either through passive degassing or during eruptive events. SO_2 emissions are considered a fundamental monitoring tool, and remote sensing techniques are mainly used to measure them. Often, these measurements are combined with in situ gas measurements of SO_2 and other volatiles (CO_2, H_2S, Cl, F) to assess changes in volcanic activity and even predict eruptions (e.g., Noguri, 1963; Menzailov, 1975; Duffel et al., 2003; Aiuppa, 2009; Lee et al., 2018). Only few studies have addressed bromine and iodine, in part because these much rarer halogens have been difficult to analyze. Nevertheless, since the discovery of BrO in volcanic plumes by Bobrowski et al. (2003), BrO and BrO/SO_2 ratios have been observed at various volcanic plumes using remote sensing techniques (Bobrowski et al., 2003; Kern et al., 2009; Bobrowski and Giuffrida, 2012; Lübcke et al., 2014; Dinger et al., 2018; Warnach et al., 2019). These observations indicated complex chemical reactions especially of bromine in the volcanic plume with, e.g., implications for the ozone budget.

The present PhD thesis aims to improve the understanding of volcanic plume chemistry and its atmospheric impact by investigating halogen-related chemical processes and their potential correlation with volcanic activity (pre-eruptive indicator). In particular, two volcanoes in El Salvador (Santa Ana and San Miguel) are in the focus of these studies.

Among the first studies performed is the use of diffusion denuders coated with cis- and trans-stilbenes (CST, TST) for in situ derivatization to determine reactive halogen species (RHS). The coatings selectively collect molecular halogens (Cl_2 and Br_2) and possibly interhalogens (BrCl). CST was shown to be a more suitable reagent, as a higher recovery rate than for TST was observed. The derivatization products could be detected by GC-MS, obtaining a signal for each di-halogenated compound and distinguishing between different RHS. However, the use of these coatings in combination with diffusion denuders is not really evaluated as suitable due to the low yield obtained with short sampling times (15 – 60 min).

Therefore, in a second study, the efficiency of stilbene stereoisomers as well as octenol (OC) was investigated using syringe filters as an RHS sampling technique instead of glass denuders using a chlorine gas source. The motivation for using syringe filters is their small size and light weight, which makes them suitable not only for crater rim sampling but also for unmanned aerial vehicles. These efficiency studies were conducted using commercially available electronic sensors as on-line systems to monitor the performance of the various coatings. Again, CST showed higher collection efficiency than TST and octenol. Nevertheless, low recoveries were obtained, possibly due to evaporation of the coating during sampling. Despite these results, coated filters showed better collection efficiency for chlorine gas at low coating rates compared to denuders, with an improvement from 5 % yield for denuders to 23 % yield for syringe filters.

In addition to this basic analytical development work, the present work also includes the application of established volcanological in situ measurement techniques (alkali traps and MultiGAS), and 1,3,5-trimethoxybenzene (TMB)-coated denuders were also used for in situ derivatization of RHS. Field applications were conducted at Masaya volcano (Nicaragua), La Fossa crater, Vulcano volcano (Italy), and Santa Ana and San Miguel volcanoes (El Salvador). Total sulfur and halogens were determined by alkaline trap sampling followed by IC and ICP-MS measurements, while total RHS of chlorine and bromine were measured by diffusion denuder sampling followed by GC-MS analysis. These in situ techniques were performed at different distances from the emission vent. The data show the halogen speciation in relation to the age of the plume, with the ratio of RHS to sulfur in the range of $10^{-6} - 10^{-5}$ near the vent and between $10^{-5} - 10^{-4}$ at greater distances. Moreover, an additional measurement was performed at night on Vulcano, showing that halogen chemistry continues during the night through heterogeneous reactions.

Finally, an extended evaluation of long-term DOAS observations from NOVAC's Santa Ana and San Miguel stations was performed, which included SO_2, and BrO measurements and represents the first data set of its kind for long-term DOAS observations at these volcanoes.

Table of contents

1.   Introduction

1.1.   Volcanic degassing and the atmosphere

1.1.1.   Chemical composition of volcanic gas emissions

Volcanic gases are a mixture of volatiles released from volcanoes e.g., as large emissions by open vent volcanoes, or as invisible degassing through soil. They are generated when volatiles exsolve from magmas as a function of processes such as: (1) vapor-melt separation during the generation and rise of the magmas; (2) re-equilibration in response to cooling and dilution by meteoric water and/or hydrothermal systems; and (3) increase of volatiles concentrations in the melt due to crystallization (Giggenbach, 1996; Shinohara et al., 2008).

Volatiles play a central role in governing the ascent and eruption of magma, since the degassing process affects its physical properties (i.e., viscosity, temperature, density). In general, increasing the quantity of volatiles within a magma, increases the explosive activity of a volcano, when they don't find a way to separately scape, as a consequence of the large pressure upturns as the volatiles exsolved from the magma during it ascends towards shallow levels and/or the surface (Delmelle et al., 2002). Once volcanic gases ascend to the surface, they can give insights to the volcanic system below the surface. For instance, they can give information about the type of magma from which they were exsolved and its level in the volcanic edifice as well as about the source of the gas (e.g., magmatic, hydrothermal).

1.1.1.1. Constituents of volcanic emissions

Volcanic gases mainly consist of H_2O, acidic gases (CO_2, SO_2, H_2S HCl, HF), non-condensable gases (H_2, He, N_2, Ar, CH_4, and CO), metallic trace elements, and organic matter (Lee et al., 2018; Textor, 2003). Their composition varies widely between volcanoes and is dependent on the individual volcano's state of activity, magma type, and tectonic settings. This chapter is focused on the main components of the volcanic gases (H_2O, CO_2, S species) and halogens.

1.1.1.1.1. Water

Water is usually the component with the highest contribution to the total volatile contribution with 50 – 90% by volume. Its solubility in silicate melts is a function of pressure, composition and temperature. Thus, basaltic magmas (silica-poor melts) show a wide range of H_2O contents, ranging from 0.5 to 8 wt%; while rhyolitic magma (silica-rich melts) show often contents higher than 6 wt% (Wallace et al., 1999; Wallace, 2005).

1.1.1.1.2. Carbon dioxide

Carbon dioxide (CO_2) is the predominant C-containing species with a contribution to the volcanic mixture ranging from 1 to 40% by volume (Textor, 2003). Its solubility in silica melts is strongly dependent on pressure. However, CO_2 solubility is 50–100 times less, by weight, than the solubility of H_2O at comparable pressure and temperature.

Among the major volatile species, CO_2 is the least soluble in magmatic melts and the least affected by hydrothermal scrubbing (Symonds et al., 2001). CO_2 exsolves at higher pressures (deeper) than H_2O, being virtually completely exsolved from its parent magmas by the time it reaches the surface. Therefore, relative proportions of CO_2 and H_2O can provide constraints on depths of magma degassing (Gonnermann et al., 2013). Also, CO_2 is considered an invaluable indicator of eruptions since it is a conservative component because there are no major sources and sinks for CO_2.

1.1.1.1.3. Sulfur species

The next most important constituents of volcanic emissions are the sulfur species (SO_2, H_2S, COS, CS_2 and elemental sulfur), contributing typically with 2 to 35% by volume, with concentrations of several thousand of ppm in arc and back-arc magmas (Wallace, 2005). Sulfur concentrations in melt inclusions show large variation as silica content increases. For example, basaltic magmas often contain > 1000 ppm of sulfur species while rhyolitic magmas can contain < 100 ppm (Shinohara, 2008).

The predominant sulfur component is sulfur dioxide (SO_2), which is more soluble in magma than CO_2, and will thus be released at lower pressure. This property makes it an indicator of eruptions since its emission rates likely increases as magmatic degassing gets stronger or

when magma ascends at lower depths. Unlike carbon dioxide, SO_2 can be affected by leaching of overlying meteoric aquifers, making it more difficult for eruption prediction in such cases (Rouwet et al., 2019; Symonds et al., 2001). The second important S-species is hydrogen sulfide (H_2S). This gas is usually observed by direct sampling at fumaroles and can likewise serve as a geochemical signal that indicate volcanic unrest because it is less affected by scrubbing than SO_2, although such consideration requires to account the origin of H_2S since it is likely to be formed from fluid-rock interaction. The H_2S fraction increases with increasing depth and with decreasing temperature and oxygen concentration of the magma, according to the reaction (Giggenbach, 1987):

$$SO_2 + 3H_2 \rightarrow H_2S + 2H_2O$$
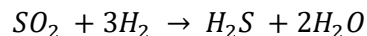
Consequently, if a magma ascends sufficiently close to the surface (~5 bar), volcanic H_2S flux is expected to be low, making SO_2 the dominant sulfur species (Giggenbach, 1975).

1.1.1.1.4.   *Halogens*

Halogens constituents are the fourth most abundant group of gases emitted by volcanoes, present in the low-pressure discharges mainly in the form of hydrogen halides (Giggenbach, 1996). Primary halogen volatiles are Cl and F, occurring at major to trace element concentrations (1-10% and < 1 % vol, respectively), while Br and I occur as trace components (ppt to ppm ranges).

Halogen release may occur during low-pressure and crystallization-driven degassing. Cl and F are also used to constrain depths of volatile exsolution since they are more soluble in silicate melt than S.

As SO_2, halogens are affected by interaction with hydrothermal systems. Their high solubility in water makes them sometimes to be completely washed out from the magmatic gas phase in the subsurface (Symonds et al., 2001). Nonetheless, when renewed magmatic recharges, the hydrothermal systems can act as a source of halogens due to re-evaporation of acidic brines or previously-deposited hydrothermal minerals. Either process can affect the halogen contents in volcanic gases.

1.1.2. Impact of volcanic degassing on the atmosphere
1.1.2.1. Volcanic inputs to the atmosphere

Active volcanoes can inject large quantities of gases and particles into the stratosphere, especially when an eruption column penetrates the tropopause, which happens at least once every two years (Textor, 2003), altering its chemical composition. However, smaller eruptions and continuously passive degassing volcanoes can also contribute to the alteration of the atmosphere, these are emitted to the troposphere. The short-term climatic impact of volcanic eruptions is mostly due to the interaction of sulfur and halogen species in volcanic gases with atmospheric gases (H_2O, N_2, O_2).

In the stratosphere, SO_2 will become rapidly oxidized by OH radicals to SO_3, which finally forms H_2SO_4 ("sulfate") aerosols due to reactions with water vapor. These volcanic aerosols have the potential to alter the chemistry of the stratosphere, including ozone with significant impacts on both longwave and shortwave radiative fluxes because they provide surfaces for heterogeneous reactions at all latitudes and all times of the year (Staunton-Sykes et al., 2021).
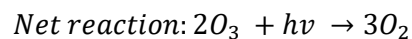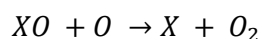
1.1.2.2. Radiative forcing

Sulfate aerosols particles in the stratosphere have also the ability to change the radiative budgets of the atmosphere since they are about the same size as the wavelength of visible light, this property allows them to strongly interact with solar radiation. In the lower stratosphere, the atmosphere is heated by absorption of both near-IR solar radiation (at the top of the layer), and terrestrial radiation (at the bottom of the layer). Some of the light is backscattered, reflecting sunlight back to space, increasing the net planetary albedo and reducing the amount of solar energy that reaches the Earth's surface (Timmreck, 2012). This backscattering is the dominant radiative effect at the surface, and results in a net cooling since the amount of solar energy that reaches the Earth's surface is reduced (McCormick et al., 1995; Robock, 2000; Robock and Oppenheimer, 2003) (Figure 1.1). Volcanic aerosols can be important causes of temperature changes for several years following large eruptions, and even on a 100-year time scale they can be important when their cumulative effects are taken into account (Table 1.1).

Table 1.1. Effect of large explosive eruptions on weather and climate (modified from Robock, 2003)

Effect	Mechanism	Start time	Duration (years)
Stratospheric warming	Stratospheric absorption of short-wave and long-wave radiation	1 – 3	1 – 2
Global cooling	Blockage of short-wave radiation	Immediately	1 – 3
Global cooling from multiple eruptions	Blockage of short-wave radiation	Immediately	Up to decades
Winter warming of North Hemisphere continents	Differential stratospheric heating, dynamical interaction with troposphere	0.5 – 1.5 years	1 – 2 winters
Ozone depletion, enhanced UV	Dilution, heterogeneous chemistry on aerosols	1 day	1 – 2

It is well known that stratospheric ozone has significant effects on ultraviolet and long-wave radiative fluxes. Decreasing ozone concentration causes less UV absorption in the stratosphere, which modifies the aerosol heating effect. Ozone depletion allows more UV to reach the Earth's surface than is backscattered by the aerosols (Robock, 2000). Sulfate aerosols in the stratosphere can catalyze heterogeneous reactions that affect global ozone abundance. These heterogeneous processes occurring on the surface of sulfate particles can convert stable halogen reservoirs (e.g., HX, HOX, $XONO_2$) into photochemically active species (e.g., X_2, X) that are active in ozone destruction (Bluth et al., 1997; Textor et al., 2003; Oppenheimer et al., 2011):

$$X + O_3 \rightarrow XO + O_2$$

$$O_3 + hv \rightarrow X + O_2$$

$$XO + O \rightarrow X + O_2$$

$$Net\ reaction{:}\ 2O_3 + hv \rightarrow 3O_2$$
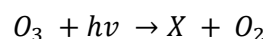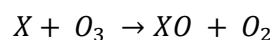
Other reaction sequences that involve Cl, ClO, HO_2, NO_2 HOCl and $ClNO_3$ catalytically consume O_3, but the reactions shown above make up the most important cycle (Cicerone, 1987). The reduced O_3 absorption of shortwave and long-wave radiation reduces the

stratospheric heating effect and can affect the winter warming phenomenon described above (Robock and Oppenheimer, 2003).
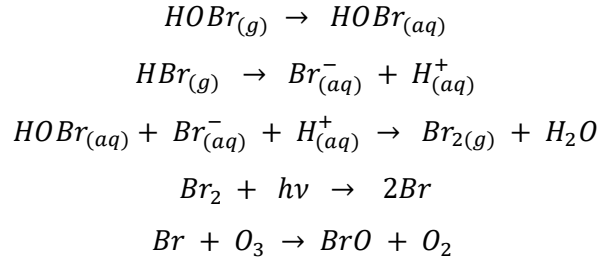
1.1.2.3. Halogens compounds and ozone

As mentioned in section 1.1.1.4, volcanogenic halogens are emitted and injected into the atmosphere mainly as halogen halides (HCl, HBr, HF, which were initially assumed to be washed out in the troposphere (Tabazadeh and Turco, 1993). However, a series of studies have shown the stratospheric halogen injection during explosive eruptions (Textor et al.; 2003; Schönhardt et al., 2017, Stauton and Sykes, 2021). The detection of BrO in the volcanic plume of Soufriéré Hills (Bobrowski et al., 2003) in the troposphere showed that volcanic HBr emissions can be transformed into reactive bromine in a short time scale of minutes. The mechanism for reactive bromine specie such as BrO, has been proposed to occur via a volcanic version of the autocatalytic "bromine explosion".

1.1.2.3.1. Formation of halogen reactive species (RHS)

The formation of RHS is influenced by factors such as temperature, humidity, dilution (entrainment of background air) and aerosols loading. Numerical models using atmospheric chemistry schemes have been developed and applied to two different scenarios to propose the formation of RHS by : (1) the halogen speciation at near-vent due to high-temperature reactions (Bobrowski et al., 2007; Martin et al., 2006; Mather, 2015; Roberts et al., 2009); and (2) the atmospheric chemistry in plume due to low-temperature reactions that causes a sustained halogen cycling that impacts tropospheric ozone (von Glasow, 2010; Roberts et al., 2009; Surl et al., 2021). When present, halogens in the stratosphere are notably involved in the destruction of ozone, being bromine significantly more efficient than chlorine. As stated before, the formation mechanism for bromine monoxide in volcanic plumes might be very similar to the so-called "bromine explosion". Figure 1.2 summarize the principal acid catalyzed and photolysis reactions involved in this process. A key step in this mechanism is the uptake of bromine from the gas phase by airborne aerosol particles in form of HOBr and HBr. An acid catalyzed reaction in the aqueous phase leads to the

subsequent release of Br_2 back to the gas phase. As described before, the resulting Br radicals react with O_3 producing BrO as follows:

$$HOBr_{(g)} \rightarrow HOBr_{(aq)}$$
$$HBr_{(g)} \rightarrow Br^-_{(aq)} + H^+_{(aq)}$$
$$HOBr_{(aq)} + Br^-_{(aq)} + H^+_{(aq)} \rightarrow Br_{2(g)} + H_2O$$
$$Br_2 + h\nu \rightarrow 2Br$$
$$Br + O_3 \rightarrow BrO + O_2$$

BrO is rapidly photolyzed and the resulting O atom quickly recombines with O_2 to form O_3, which in turn reacts with Br atoms to re-form BrO. The key ozone destruction steps in the reaction scheme are the next reactions:

$$BrO + BrO \rightarrow 2\,Br + O_2$$
$$BrO + BrO \rightarrow Br_2 + O_2$$
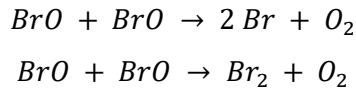
Finally, BrO reacts with HO_2 to form $HOBr_{(gas)}$, which closes the cycle starting with:

$$BrO + HO_2 \rightarrow HOBr + O_2$$
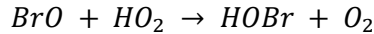
1.2. Volcanic gas monitoring

Volcanic gas monitoring aims to track changes in chemical composition and gas fluxes released from a volcano in order to recognize precursory signals of volcanic unrest. However, the behavior of a volcano has to be followed for a large period of time so the background and the deviations from the background can be established.

Systematic volcano monitoring began in the 1840's with the completion of the Ossevatorio Vesuviano, followed by other observatories and networks around the world. Nowadays, the World Organization of Volcano Observatories includes more than 80 partner observatories that charged with the global coordination and dissemination of volcanic activity information (Costa et al., 2019; Pyle et al., 2013; Sparks et al., 2012)
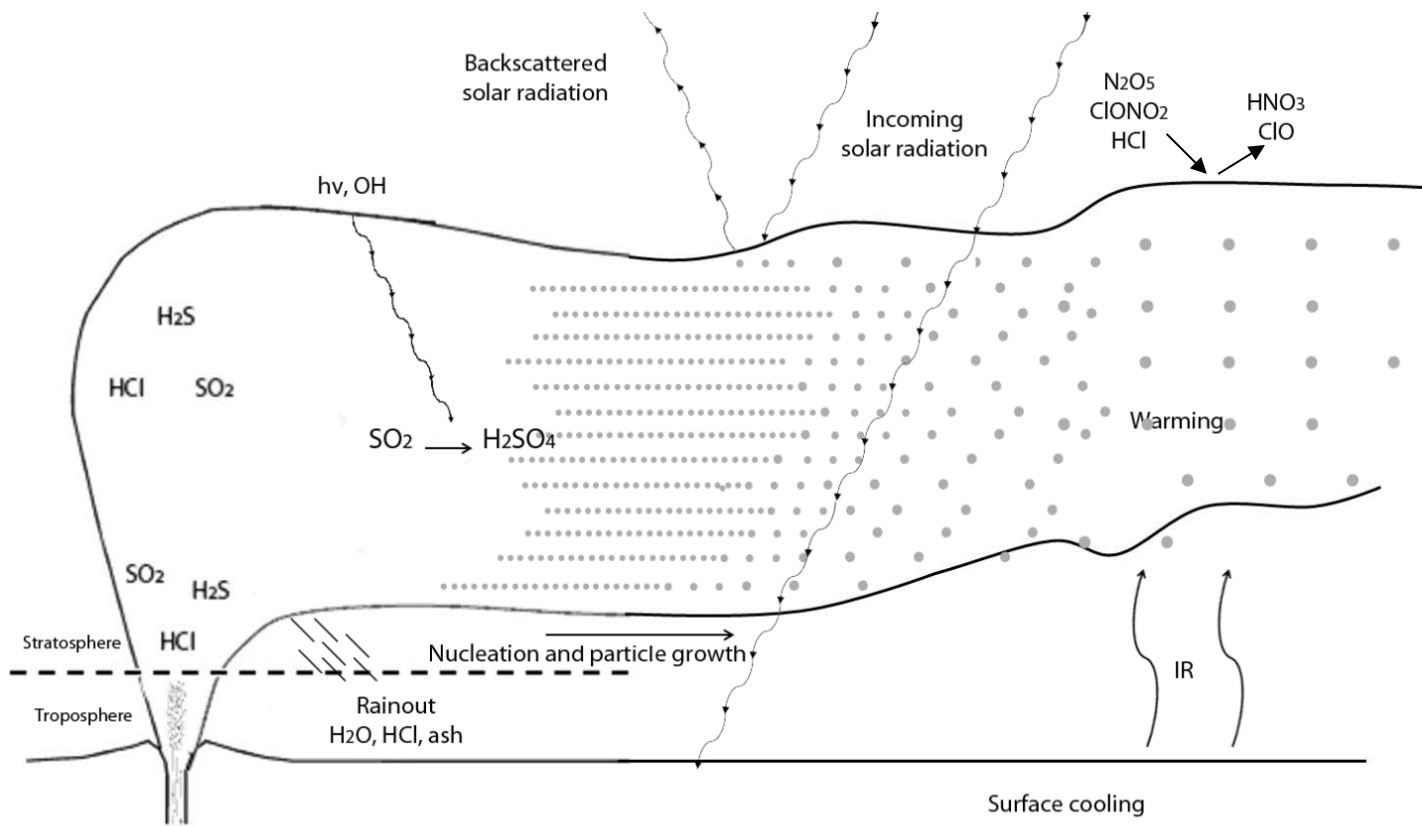
Figure 1.1. Diagram of sulfur compounds volcanic inputs to the atmosphere and their effects (after McCormick et al., 1995)

+ ClO

+ BrO

+ hv

BrO

+ hv

Br

hv +

BrCl

+ O₃

+ NO₂

HO₂ +

+ hv

+ hv

BrNO₃

Br₂

+ OH

HOBr

+HCHO + HO₂
× + CH₃OOH

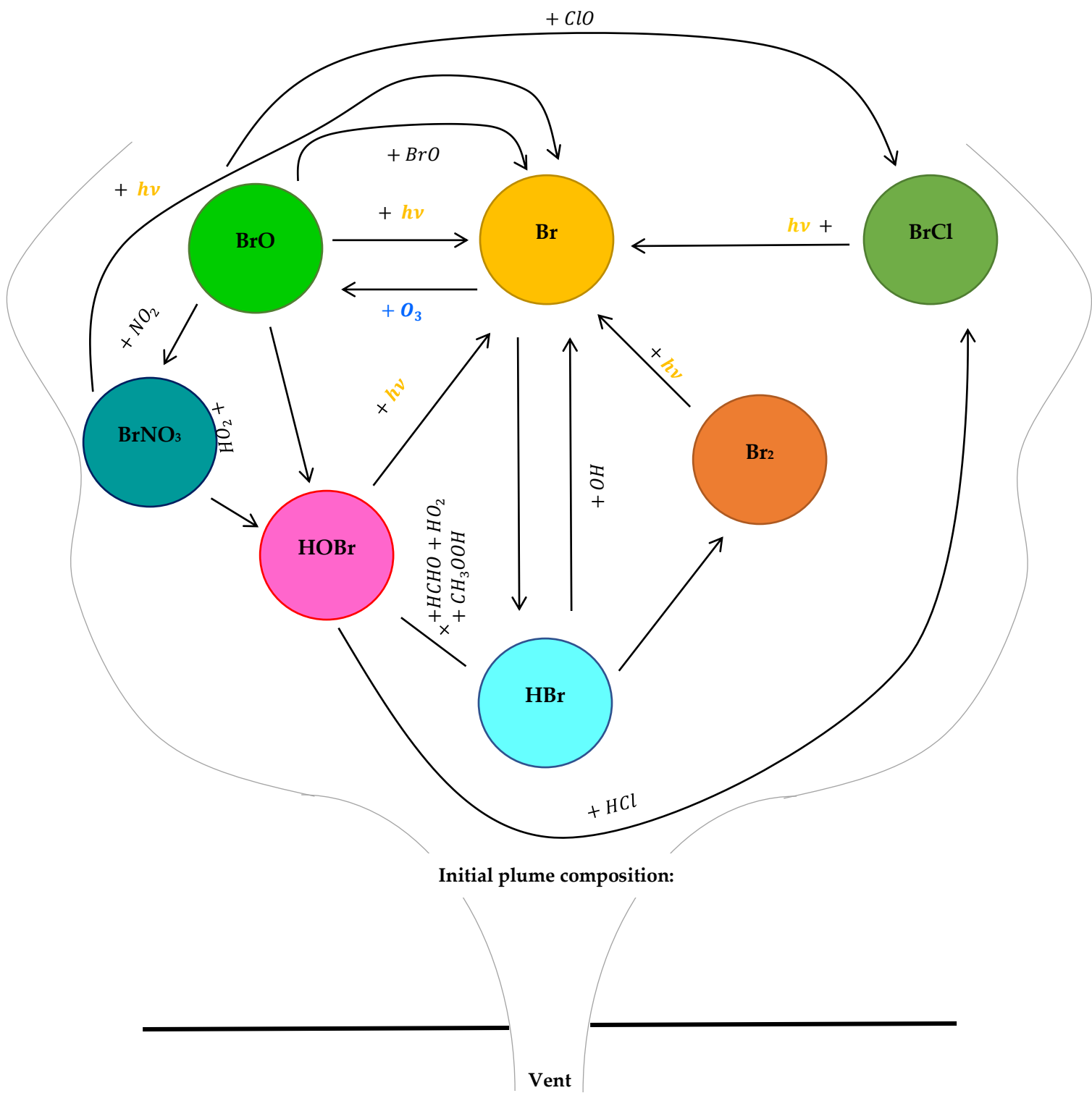**HBr**

+ HCl

Initial plume composition:

Vent

Figure 1.2. Major reaction of bromine cycle within a volcanic plume (modified from Surl et al., 2021)

As mentioned above, active volcanoes release volatiles during passive and eruptive periods. Characterizing the chemical and isotopic compositions of these volatiles allows the identification of changes in any parameter. The range of geochemical techniques used for the detection of the degassed volatiles from magmas is wide and its use depends on the volcano's state of activity, the accessibility to the craters and logistical difficulties. The different sampling techniques used in this study will be explained in the next chapters.

1.3. Motivation and objectives

Volcanic emissions are a source of halogens emitted into the atmosphere with environmental and climate impacts. Approaches to estimate the degassed halogens include petrological studies (Freundt et al., 2014; Kutterolf et al., 2015; Wallace, 2005) and direct measurements (Aiuppa et al., 2005; Roberts et al., 2012; Rüdiger et al., 2017; Wittmer et al., 2014). Yet, the emitted budgets are still poorly constrained for the heavy halogens bromine and iodine. The development of analytical methods for the accurate speciation of certain bromine compounds (HBr, Br_2, Br, $BrCl$, $HOBr$, etc.) are necessary to understand the chemistry of halogens in volcanic plumes and will also help to improve the estimates of global emissions.

This research aims to improve the understanding of the chemistry of volcanic plumes and their impact on the environment by the investigation of halogen related chemical processes, in particular focusing on bromine chemistry in volcanic plumes, to understand its behavior and further also its potential correlation to volcanic activity (pre-eruptive indicator) as well as environmental impacts. Also, this research aims to extend the characterization and thus prediction availability of two volcanoes in El Salvador (Santa Ana and San Miguel) in order to pursue an establishment of a baseline of halogen species, as there is no former known plume composition regarding the content of these gases.

2. Experimental methods

2.1. Development of sampling techniques for the determination of reactive halogen species (RHS) in volcanic plumes

2.1.1. Diffusion denuder samplers

Denuders are systems for gas-particle separation used for the sampling of gaseous compounds in the atmosphere since the 1930's (Ali et al., 1989). In its most elementary form, a denuder is a cylindrical tube coated with a reagent, which selectively samples a specific gaseous or volatile component from aerosols (Figure 2.1). The flow conditions can be easily adjusted so that particulate matter passes through the tube and gaseous components diffuse to the tube wall, where they can be trapped on the coating (solvent or a sorbent).
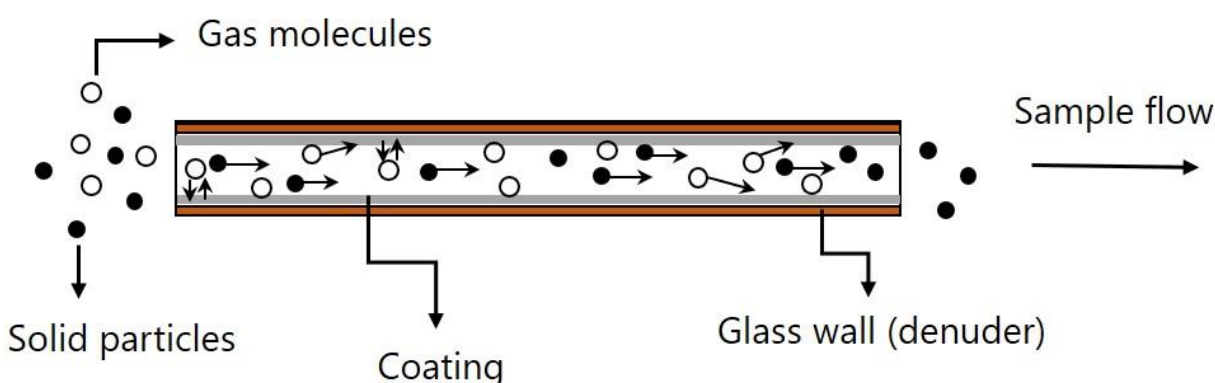
Figure 2.1. Schematics of the separation of gases and particulate matter (after Klokowski et al., 2012)

Recently, Huang and Hoffmann (2008) developed a coupled diffusion denuder system for the measurements of inorganic gaseous halogens species in marine atmosphere. The method is based on in-situ selective derivatization with 1,3,5-trimethoxybenzene (TMB), followed by gas chromatography mass spectrometry (GC-MS). The derivatization is based on the reaction of a series of halogen species (X_2, XY, HOX, and $XONO_2$ – X and Y: Cl, Br, I), with the activated aromatic compound (TMB), which results in the formation of the respective 1-halogen-2,4,6-trimethoxybenzene (1-X-2,4,6-TMB). Later, Rüdiger et al. (2017, 2018) adapted this method for measurements of halogens in the volcanogenic gas plumes at Mt. Etna and Stromboli, Italy, as

well as Masaya, Nicaragua. This method demonstrated the importance of in-situ measurements not just for monitoring volcanic emissions but to understand their role in the atmosphere.

However, the method only allows for a differentiation between the amount of total halogen and the sum of the reactive gaseous halogens, when applied simultaneously with alkaline traps. A coating that allows to further distinguish between RHS species is still needed.

Here we selected trans- and cis-stilbenes as derivatization agents since they are active organic compounds (activated toward electrophilic addition, Figure 2.2) able to react with halogens. Previous work in this research group already reported the reaction between cis- and trans-stilbenes and molecular bromine (Gutmann, 2015; Sehring, 2016). Moreover, these stilbenes are separable from their products, which makes them easily achievable by gas chromatography. Trans-stilbene is a relatively unreactive colorless solid compound, while cis-stilbene an oily yellow liquid. For the trans-stilbene the reaction will be as gas-solid reaction whereas for its cis-isomer it will be gas-liquid.

Bromination occurs in both cases, when the double bond undergoes an electrophilic addition reaction by the bromine reagent, in this case bromine gas, which proceeds via a cyclic bromonium ion. The addition of bromine begins at one side of the double bond (either side is equally likely, but only one option is drawn) and is followed by attack of bromide ion on the bromonium ion (again, attack could occur at either carbon since the ion is symmetric, but only one option is drawn). The product is the trans- dibromide, as shown in Figure 2.2. The products are the brominated meso- and dl-stilbenes that differ only by their stereochemistry. Because of its smaller size and lesser polarizability, chlorine is not as effective as bromine in bridging for any particular alkene. Bromination therefore generally gives a higher degree of anti- addition than chlorination, all other factors being the same (Carey and Sunderberg, 2007).

2.1.1.1. Experimental procedures

2.1.1.1.1.   Chemicals and materials

Molecular bromine (99.5 %) and hydrochloric acid (ACS reagent, 37.0 %), potassium permanganate (ACS reagent, $\geq$ 99.0 %), 1,2,4,5-Tetrabromobenzene (97.0 %), 1,2-dichloro-1,2-diphenylethane, cis- stilbene and sodium thiosulphate ($\geq$ 98.0 %) were purchased from
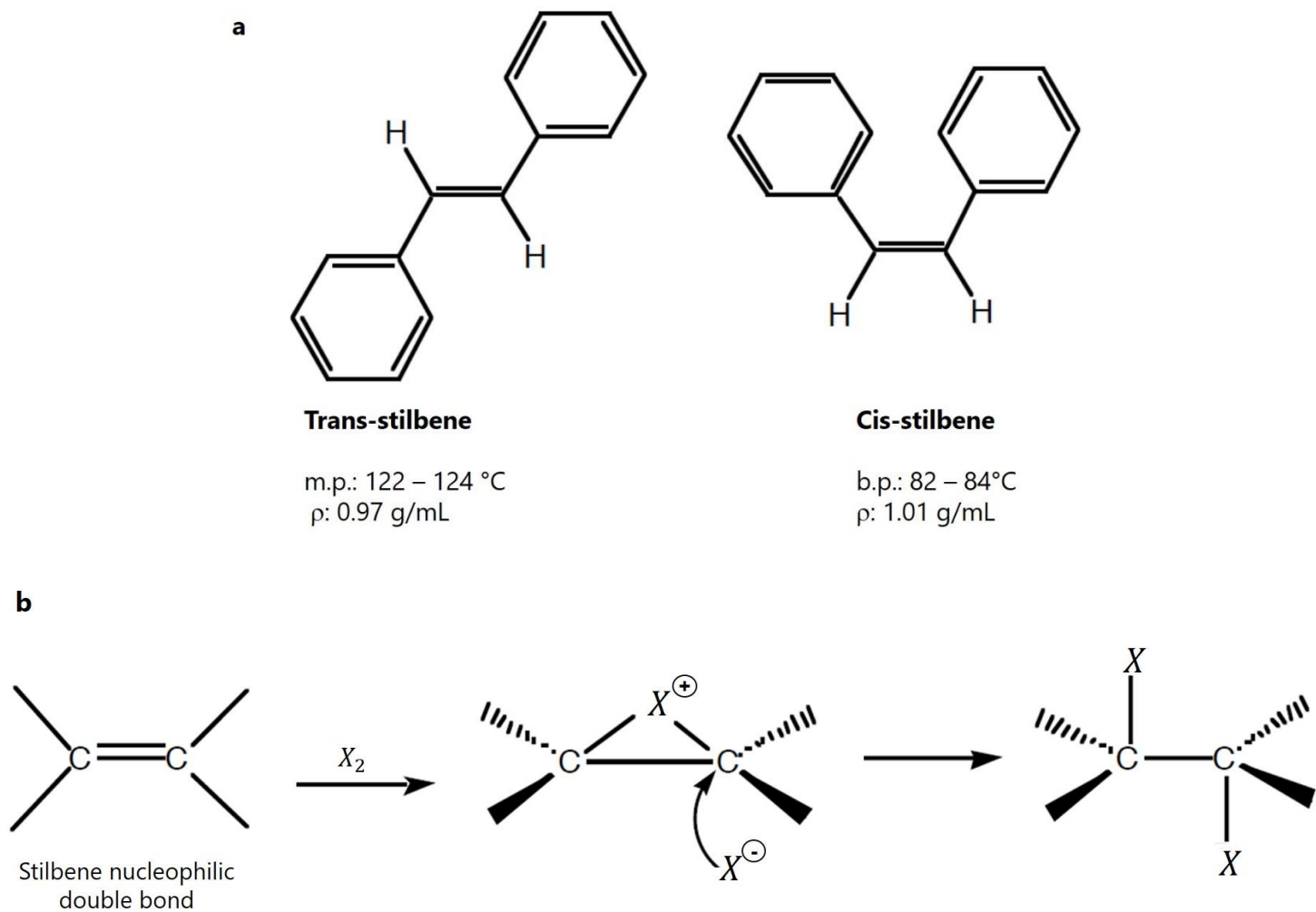
Figure 2.2. (a) Structure of trans- and cis-stilbene isomers. (b) Halogenation of the nucleophilic double bond by electrophilic addition reaction (X: Cl, Br, I)

Sigma-Aldrich (Steinheim, Germany). Trans-stilbene (> 98.0 %) was obtained from TCI Tokio Chemical Industry Co., LTD (Zwijndrecht, Belgium). Meso-1,2-dibromo-1,2-diphenylethane (97.0 %) and acetone (Analytical reagent grade, ≥ 99.8 %) were available from Alfa Aesar (Kandel, Germany) and Fischer Scientific (Lougborough, UK), respectively. 2,3-dibromo-3-phenylpropiophenone (98.0 %) was purchased from Acros Organics (Geel, Belgium). Hydrochloric acid (37.0 %), toluene and Acetone for gas chromatography MS SupraSolv® (≥ 99.8 %) were obtained from Merck KGaA (Darmstadt, Germany). Acetic acid glacial AnalaR NORMAPUR was purchased from VWR International S.A.S (Fontenay-sous-Bois, France). perfluoroalkoxy alkanes (PFA) Tube Fitting Union (1/4 in.) and PFA Plug (1/4 in.) were available by Swagelok (Ohio, USA). Brown borosilicate glass tubes (7 mm i.d., 9 mm o.d. length 15 – 16.5 cm and 50 cm) were purchased from HWS Labortechnik (Mainz, Germany).

2.1.1.1.2. *Gas sources*

With the aim to verify the reliability of the sampling system (denuder), gaseous standards are essential for atmospheric simulation in this study. In this research, permeation tubes for Br_2 and HCl were constructed according to Rüdiger et al. (2017) using 70-mm-long glass vials (6 mm outer diameter, 1 mm wall thickness) and PFA sealing caps (Swagelok). The chlorine source was made adding concentrated hydrochloric acid into potassium permaganate to form molecular chlorine and condensing it inside the test tube at -78 °C with an acetone/dry ice mixture, according to (Geil, 2021). The permeation tubes were placed in a doubled walled glass chamber and kept under a constant temperature of 30 °C. Nitrogen was flushed continuously through the thermostatic glass vessel. The output rate of the individual test gas sources was measured by the mass loss of the tubes, which were determined by periodically weighing the tubes using a microbalance.

2.1.1.1.3. *Preparation of denuders*

The diffusion denuders are prepared using brown borosilicate glass tubes. Trans-stilbene (TST, 0.15, 0.5, 1.5, 3.0 and 15 mM) and cis-stilbene (CST, 0.14 and 0.48 mM), in acetone. To obtain a uniform TST-coating along the whole tube, six 0.5 mL portions of the individual solution were alternately pipetted into both openings of the 50 cm slightly sloped glass tube. For CST, two 140 μL portions of solution were alternately pipetted into both openings of a 20 cm glass tube. During

the coating procedure, the tubes were rotated by a geared motor and flushed with a gentle stream of nitrogen for drying. Afterwards, the coated denuders were sealed with polypropylene (PP) end caps and stored in the refrigerator until sampling. However, CST doesn't crystallize but rather remains liquid for which it was used immediately after preparation for the next experiments.

2.1.1.1.4.   *Experimental setup*

To test the sampling denuders, Br_2 and Cl_2 were passed individually through the stilbene-coated denuders using a two-denuder serial setup (**Figure 2.3**) for each compound with varying sampling times of 20 and 60 minutes at room temperature and at a flow rate of 250 mL min^{-1} according to Sehring (2016). Additionally, both sources were combined in the thermostated vessel and exposed to UV light using a 7 W UV lamp (Roxin) to produce bromine monochloride (BrCl). Afterwards, the sampled denuders were eluted 5 times with 2 mL of acetone (GC-MS grade). For the compensation of evaporation losses and dilution effects, an internal standard of 100 µL stock solution was added. This mixture was then evaporated at 30°C under a gentle N_2 gas stream to a volume of approximately of 100 µL, followed by the GC-MS analysis of each sample.
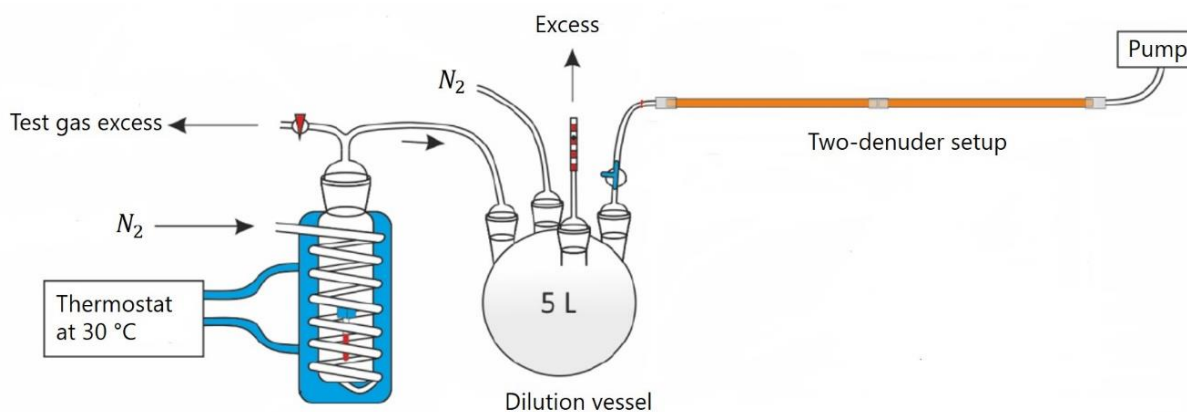

Figure 2.3. Experimental setup to test performance of cis- and trans-stilbenes coated denuders (modified from Rüdiger et al., 2017)

2.1.1.1.5.   *Internal standard and recovery rate*

Two internal standards (1,2,4,5-Tetrabromobenzene – TBB, and 2,3-dibromo-3-phenylpropiophenone - DBPP) were evaluated for its suitability to compensate the evaporation

during the pre-concentration process. To do so, 10 mL of acetone was spiked with 100 μL of stock solution of DCTST (0.1 and 1.0 mg/L) and 100 μL of internal standard (6 mg/L). The mixture was then evaporated to a final volume of ~100 μL. The recovery rates from this experiment were obtained by comparison of the analyte concentration in the evaporated sample with its stock solution by means of the ratio of the analyte signal to the internal standard signal. The same procedure was applied for the dibromo-derivative (DBTST). The recovery rate of sampled denuders was determined by the comparison between the retrieved amounts of analytes (with external calibration) and the known amount obtained by the gravimetric weight loss of the test gas sources (Cl_2: 146.4 ng, Br_2: 177.5 ng).

2.1.1.2. Analytical methods

2.1.1.2.1.   Gas chromatography – Mass spectrometry

GC-MS is an instrumental technique by which mixtures of volatiles can be separated, identified and, if needed, quantified. In order to analyze compounds by GC-MS, they have to be sufficiently volatile and thermally stable. MS detection enables the determination of molecular masses of the analytes and the elucidation of their molecular structure, due to the specific fragmentation patterns that organic compounds show upon bombardment with fast electrons in an MS ion source (electron ionization - EI), under which sample molecules lose an electron resulting in a molecular ion (M^+). Due to the high amount of energy (70 eV) impacted to the molecular ion it usually fragments producing further smaller ("daughter") fragments. On the MS, the detector separates the ions in vacuum based on their mass-to-charge ratios (m/z), and eventually measures the intensities of each ion. These intensities are recorded to produce a series of mass spectra. Since the halogens collected with the denuders undergo the derivatization process by reacting with the coating, the di-halogenated stilbene derivatives can be analyzed by the GC – MS technique.

The qualitative analysis of the derivatized products is realized by the GC retention time and the mass spectra of the respective analyte. With the hyphenated mass spectrometer (quadrupole mass analyzer) identification of the respective derivatized products is achieved. Using the single ion monitoring (SIM) mode, the quadrupole acts as a mass filter that enables the transmission of ions with selected mass-to-charge (m/z) ratios. Here, for the chromatographic analysis, an Agilent GC-MS system (Agilent 6850 Network GC and Agilent 5973 Network Mass Selective Detector, Agilent

Technologies, Inc. Santa Clara, CA, USA) was used with a fused silica capillary column (28.5 m × 0.25 mm I.D., df 0.25 µm, Rtx-5MS, Restek Co., Bellefonte, PA, USA). High-purity helium (99.999 %) was employed as a carrier gas. One microliter of sample solution was injected in the splitless mode. The temperature of the injector was set to 250 °C and the transfer line was set to 300 °C. The GC oven was programmed as follows: initial temperature 50 °C (hold 1 min), 35 °C min^{-1} to 250 °C (hold 4 min), 20 °C min^{-1} to 270 °C (hold 2 min). A solvent delay of 5.5 min was chosen, since the TST retention time is 6.0 min. The MS spectra acquisition covered a mass range of m/z 50 – 450 (70 eV (EI) mode). For quantification, characteristic m/z ratios were selected for the SIM mode: m/z 127/ 125 (M$^+$/2) for DCTST and m/z 261/ 259 (M$^+$ - Br), 180/179 (M$^+$ - 2Br) for DBTST.

2.1.1.2.2.   Calibration curve and detection limits

Once the output of the gas sources stabilized, standard solutions were prepared in order to achieve the trans-stilbene derivatives analysis by means of a calibration curve. The standard solutions were prepared freshly out of the solid pure standards, meso-1,2-dibromo-phenylethane (DBTST) and 1,2-dichloro-1,2-diphenylethane (DCTST), by sequential dilution with acetone with concentrations range 0.002 – 3.0 mg/L. Using blank samples (n = 6) and the calibration curve, the limit of detection (LOD) and the limit of quantification (LOQ) were determined.

2.1.2. Syringe filters

Up to now, the diffusion denuder samplers have been used to collect reactive chlorine, bromine and even iodine (Rüdiger et al., 2017; Rüdiger et al., 2021) on volcanic plumes. However, these samplers have the disadvantage of the fragility of the glass tubes in the field work and for transportation. Furthermore, they collect some particles when wind speed is high or when they are setup in an up-side down position, which implies some "dirt" within the samples during analysis. Huygen (1963), proposed the sampling of HF in air by means of an alkali-impregnated filters. More recently, this method has been applied at Stromboli and Etna by mounting the alkali-impregnated filters in series in the so called "filter packs" for the collection of acid gases such as SO$_2$, HF, HCl, HBr, HI (Wittmer et al., 2014). Here we propose the use of syringe filters coated with an organic compound to sample reactive halogen species (RHS) by means of derivatization (electrophilic addition). Furthermore, we suggest the use of syringe filters due to their small size which will make them useful not only for in-situ sampling but also on unmanned aerial vehicles

(UAVs). We use the same derivatizing agents as described in section 2.1 and 1-Octen-3-ol since they have a reactive double bond able to react in an electrophilic addition reaction. Cis- and trans-stilbene were used again to test if by using a different medium with open surface (a syringe filter instead of a glass denuder), their efficiency will improve, while the second is to test a new coating.

2.1.2.1. Experimental procedures

2.1.2.1.1.   Chemicals and materials

Hydrochloric acid (37.0 %), toluene and acetone for gas chromatography MS SupraSolv® (≥ 99.8 %) were obtained from Merck KGaA (Darmstadt, Germany). Cis-stilbene (96 %), 1-octen-3-ol (98%), 1,2-dichloro-1,2-diphenylethane and potassium permanganate (ASC reagent, ≥ 99 %) were purchased from Sigma- Aldrich (Steinheim, Germany). Trans-stilbene (> 98.0 %) was obtained from TCI Tokio Chemical Industry Co., LTD (Zwijndrecht, Belgium). Syringe filters (CHROMAFIL GF, 25 mm, 1 µm) were available from MACHEREY-NAGEL GmbH & Co. KG (Dueren, Germany). Chlorine sensor CL2-B1was obtained from Alphasense Sensor Technology House (Essex, UK).

2.1.2.1.2.   Chlorine gas source

The chlorine source was prepared as described in section 2.1.1.1.2, consisting of a permeation tube capped with a PTFE hex-nut and placed in a doubled walled glass chamber to keep it under a constant temperature of 30° C. The output rate of the chlorine gas source was measured by the mass loss of the tube, which were determined by periodically weighing of the tubes using a microbalance.

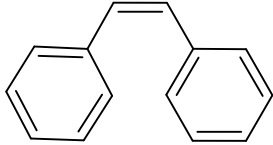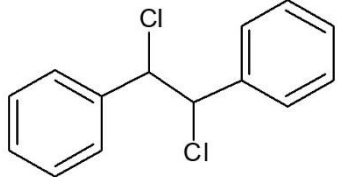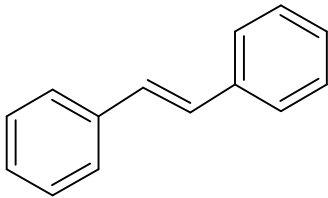*2.1.2.1.3.   Preparation of syringe filters*
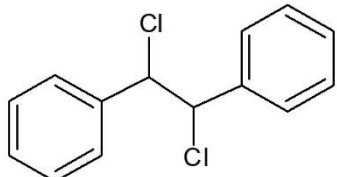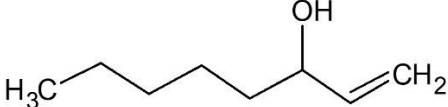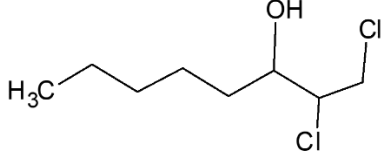
Impregnated-filters were prepared by multiple addition of a defined volume of a specific solution to achieve 1.5 µmol of coating (Table 2.1) onto the glass-fiber filters (25 mm, 1 µm). The filters were then dried by repeatedly passing air through the filter with the syringe until no more acetone could be perceived.

2.1.2.1.4.   Experimental setup and filter sampling

To test the coatings, a Cl_2 air mixture was passed through a coated-filter connected to a chlorine sensor in combination with a datalogger and a pump (Figure 2.4). The flowrate tested was of 750

mL min^{-1} with sampling time of ~ 60 minutes. To start an experiment, the pump was started at the desired flowrate and then the datalogger was started, giving ~ 2 – 5 minutes for the system to stabilize. Then the prepared filter was inserted into the apparatus. After each experiment, data acquisition was stopped and the filters were disconnected from the apparatus and sealed and stored if they were not to be analyzed immediately. The samples were prepared for analysis by extracting the filters with 20 × 0.5 mL portions of acetone. Then an aliquot of 100 µl was filled into a vial and finally analyzed by GC-MS.

Table 2.1. Summary of coatings used to impregnate the syringe filters with its structures and the expected product from reaction with chlorine gas

Compound	Structure	Chlorinated derivative
Cis-stilbene (CST)		
Trans-stilbene (TST)		
Octenol (EC)		

2.1.2.2. Analytical methods

2.1.2.2.1.   Electrochemical sensor, calibration and limit of detection

The electronic chlorine sensor outputs a current between 4 - 20 mA depending on the chlorine concentration. The sensor is designed for a working range of 0 - 20 ppm chorine. Here it is combined with a set of devices to read its signal on a computer (**Figure** 2.4). For more information on the electronic design of the sensor, see Karbach (2021). The sensor was then calibrated by changing the flow rate of the sample pump and thus the dilution of the chlorine source. The tested

concentration range was 0.0 - 0.75 ppm. Between measurements, the sensor had 3 minutes to adjust to the new flow rate. Subsequently, the detection limit was calculated from the standard deviation of the measured noise (n = 40) when the source was turned off (0.0 ppm Cl_2).
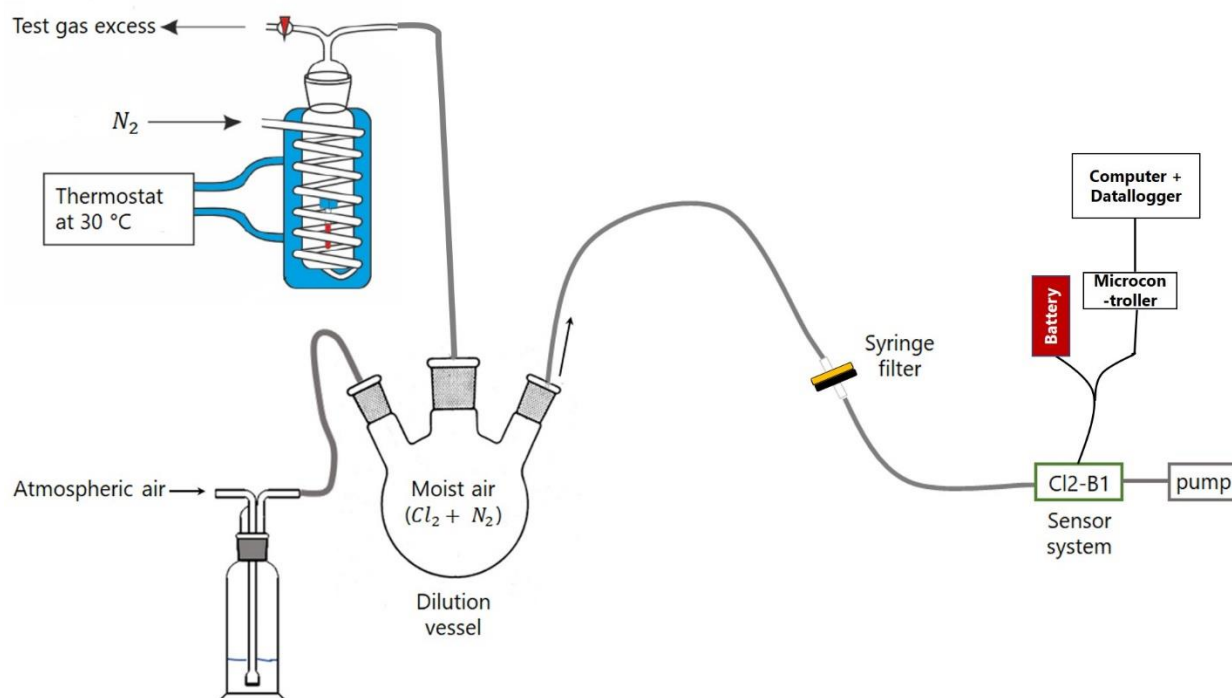

Figure 2.4. Laboratory setup to investigate the analytical performance of the impregnated filters (modified from Karbach, 2021)

2.1.2.2.2. Chromatography and detection

The derivatized products were identified by GC retention time and mass spectra of the respective analyte using an Agilent GC-MS system (Agilent 6850 Network GC and Agilent 5973 Network Mass Selective Detector, Agilent Technologies, Inc. Santa Clara, CA, USA). A fused-silica capillary column (27.6 m× 0.25 mm I.D., df 0.25 μm, Rtx-5MS, Restek Co., Bellefonte, PA, USA) was used as the separation column. The measurement conditions were the same as described in section 2.1.1.2.1, since the coatings were also stilbene derivatives. The GC oven was programmed as follows: Initial temperature 50 °C (hold for 1 min), 35 °C min-1 to 250 °C (hold for 4 min), 20 °C min-1 to 270 °C (hold for 2 min). MS spectra were recorded in a mass range of m/z 45 - 450 (70 eV (EI) mode). The yield was calculated based on the ratio between the recovered chlorine derivative and the total amount of chlorine that passed through the coating, where applicable.
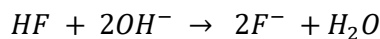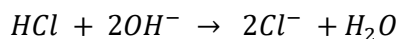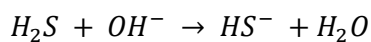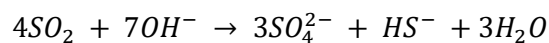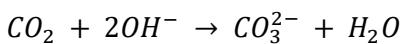
3. Field measurement methods and data analysis

3.1. In-situ sampling techniques

Direct sampling refers to techniques in which the volcanic gases are directly collected from fumaroles or plume gases, using open samplers filled or impregnated with an alkaline, neutral or acidic solution, that allows to trap them for later analysis by different techniques (i.e., ion chromatography, selective ion electrode, gas chromatography-mass spectrometry). Direct sampling permits to characterize undiluted and uncooled gas samples, and therefore detect a large number of chemicals down to the ppb level (Symonds et al., 1994). Furthermore, development of instrument-based techniques has been done in recent years (Aiuppa, 2005; Shinohara, 2005), allowing continuous and almost real-time field observations with portable instruments (e.g., MultiGAS) that are able to determined only few species (SO_2, CO_2) rather than bulk gas emissions. Each in-situ technique has its advantages and disadvantages, but its simultaneous use allows a more integrated approach to geochemically characterize a volcano (Aiuppa, 2015; Symonds et al., 1994).

3.1.1. Alkaline traps

Alkaline traps are the most common method applied for in-situ sampling. Solution-filled bottles are the most frequently gas sampling technique applied by (Giggenbach, 1975) using a 300 mL flask containing 50mL of 4N NaOH attached in a setup that allowed the acidic gases to be absorbed or "trapped" by the NaOH solution according to the following aqueous reactions:

$$CO_2 \ + \ 2OH^- \ \rightarrow \ CO_3^{2-} \ + \ H_2O$$

$$4SO_2 \ + \ 7OH^- \ \rightarrow \ 3SO_4^{2-} \ + \ HS^- + 3H_2O$$

$$H_2S \ + \ OH^- \ \rightarrow \ HS^- \ + H_2O$$

$$HCl \ + \ 2OH^- \ \rightarrow \ 2Cl^- \ + H_2O$$

$$HF \ + \ 2OH^- \ \rightarrow \ 2F^- \ + H_2O$$

Non-condensable gases (H_2, CO, CH_4, COS, N_2, Ar) are collected in the headspace of the bottle. Although, several modifications have been developed since then, the same principle is applied: the system use a pump that allows the volcanic gases to pass through a medium (e.g., filter,

impregnated filter, alkaline, neutral or acidic solution) that enables to trap these gases for its later analysis.
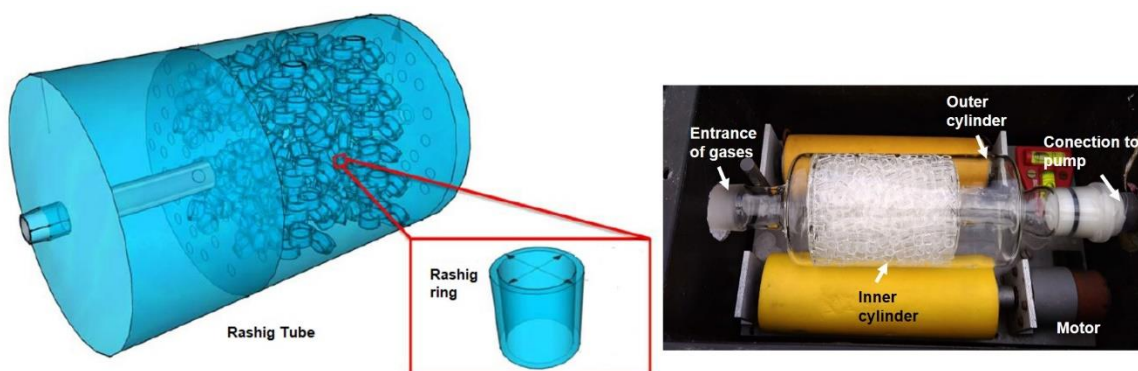

Figure 3.1. Close-up view of a Raschig tube instrument consisting of a two cylinders tube: (a) an inner cylinder, containing little glass rings, and (b) an outer cylinder connected to a geared motor (after Wittmer et al., 2014)

Alkaline traps, as used in this work, refers to the use of a Raschig-tube device (RT), that consists of a glass cylinder that contains little glass rings (Raschig rings), wetted with 50 mL of NaOH 1 M aqueous solution (EMSURE® ≥ 99.0 %, Sigma Aldrich) as a trapping medium (Figure 3.1). Homogeneous wetting is achieved by rotation of the RT during the sampling time by means of a geared motor. Previous each measurement, the tube is be cleaned using ultra-pure water. During sampling, the RT gathers the gases directly into its interior through an inlet at a flow rate of 4 L min^{-1} using a GilAir Plus™ pump (Sensidyne, St. Petersburg, FL, USA). The collected samples were stored, prepared and analysed according to (Wittmer et al., 2014) using an Ion Chromatograph (Dionex ICS-1100, Thermo Fischer Scientific, Massachusett, USA) equipped with an AS14A column (1 mL/min flow rate), an AERS 500e suppressor and using a 100 μL sample loop. Table 3.1 summarizes the field campaigns and laboratories where the samples were analyzed. Additionally, Masaya samples were also analysed by ICP-MS for HBr and HI. Carbon dioxide on this type of samples was determined by volumetric titration adding 0.1 M HCl solution to 0.5 mL of sample dissolved in 35 mL of CO_2-free water. HCl is added until pH of the solution reaches 6.36 and 10.25 (Geil, 2021). The volume of HCl used at each point is recorded.

Table 3.1. General information of RT samples collected in this study

Year	Volcano	Technique	Analyzed species	Laboratory
2019	Masaya, Nicaragua	IC/ICP-MS	S, HCl, HF/ HBr, HI	National Institute of Geophysics and Volcanology (INGV), Palermo Department
2019	Santa Ana, El Salvador	IC/ICP-MS	S, HCl, HF/ HBr, HI	INGV, Palermo Department
2019	San Miguel, El Salvador	IC/ICP-MS	S, HCl, HF/ HBr, HI	INGV, Palermo Department
2019	Vulcano, Italy	IC	S, HCl, HF, HBr	Institute of Inorganic and Analytical Chemistry, JGU Mainz in Germany
2020	Vulcano, Italy	IC	S, HCl, HF, HBr	Institute of Inorganic and Analytical Chemistry, JGU Mainz in Germany
2020	Santa Ana, El Salvador	IC	S, HCl, HF, HBr	Institute of Inorganic and Analytical Chemistry, JGU Mainz in Germany
2020	San Miguel, El Salvador	IC	S, HCl, HF, HBr	Institute of Inorganic and Analytical Chemistry, JGU Mainz in Germany

3.1.2. Multicomponent gas analyzer

Portable multi-sensor systems (MultiGAS) were developed in the mid-2000's to measure volcanic plumes (Aiuppa, 2005; Shinohara, 2005). A typical system consists of infrared and electrochemical gas sensors (e.g., CO_2 and SO_2), a pump and flow control units, a data logger and batteries. These are fully automated systems that can be used to make continuous, near real time field measurements. Most recently, these instruments have also been used as stationary systems to acquire permanent observations of the gas plume composition and further improvement has been done by addition of more sensors to record more gases (e.g., Roberts et al., 2017).

3.1.2.1. Optical sensors

This type of sensors is based on the principle of Non-Dispersive Infra-Red (NDIR), which measures how much infrared light of a specific wavelength is absorbed by the surrounding air, and using this measurement to calculate the concentration of the target gas. Usually, a sensor consists of: an infrared source, an optical cavity, a detector and internal thermistor. Gases from

the air diffuse into the optical cavity. Light from the infrared source passes through the optical cavity where it interacts with the gases before impinging on the detector. The active channel of the detector is fitted with a filter such that the only light with a wavelength that corresponds to an absorption band of the target gas is allowed to pass through. If the target gas is present in the optical cavity the intensity of light passing through the filter and hitting the active channel decreases. The reference channel of the detector is fitted with a filter that only allows wavelengths of light where there are no absorption bands to pass through. The intensity of light hitting the reference channel is not affected by the presence of gas. The detectors used are highly sensitive to the ambient temperature and so it is necessary to constantly monitor the temperature and compensate the output. The internal thermistor is used for this purpose (Alphasense Application Note AAN 201-06). In this research, our instruments have a CO_2 optical sensor K30-FR, purchased from SenseAir, Delsbo, Sweden.

3.1.2.2. Electrochemical sensors

Generally, this are electrochemical cells that generate a current proportional to the fractional volume of the target gas. The sensors are composed of three electrodes: (a) a working electrode, to optimize the oxidation or reduction of the target gas by being exposed to the outside air; (b) the counter electrode, to balance the reaction of the working electrode, and (c) a reference electrode, which anchors the working electrode potential to ensure that works in the correct region of the current-voltage curve (Alphasense Application Note AAN 104). Here a SO_2 electrochemical sensor CiTiceL 3MST/F is used, which was obtained from City Technology, Portsmouth, United Kingdom.

Both sensors were calibrated using test gas standards (200 ppm SO_2 in N_2, 5000 ppm CO_2 in N_2, All-in-Gas e.K., München, Germany) prepared in different gas mixtures in Tedlar® bags. The sensors were exposed to these gas mixtures by pumping the gas through the MultiGAS system. A calibration curve was obtained for each gas by plotting the response signal against the concentration of the gas mixtures (Figure 3.2).
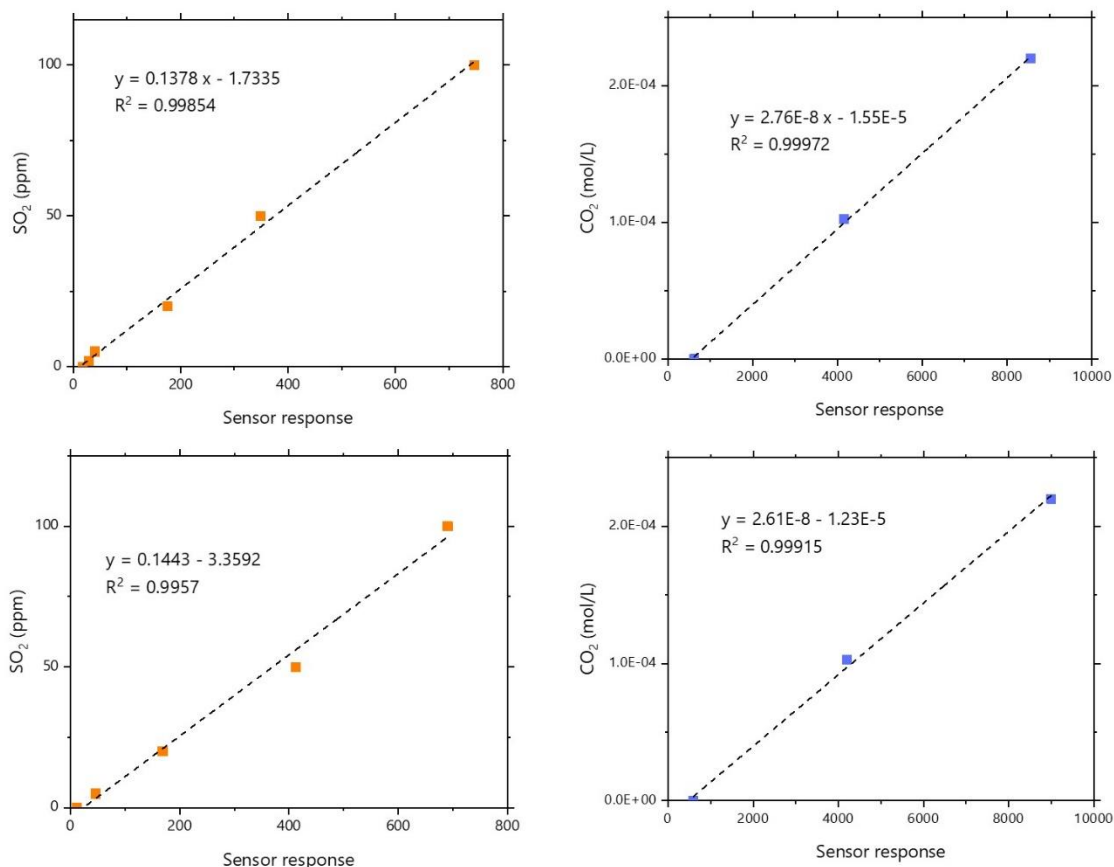
Figure 3.2. Example of calibration curves of SO_2 and CO_2 sensors contained within the MultiGAS instrument. Upper plots correspond to calibration for the 2019 survey, while lower plots correspond to the 2020 survey.

In the field, the MultiGAS instrument was set to perform ground-based measurements and when possible, on an Unmanned Aerial Vehicle (UAV). Table 3.2 describes the instruments used in this work. Generally, each device pumps the volcanic gases through a 45 μm pore size PTFE filter (Polytetrafluorethylene) using a small pump with a flow rate of 500 mL min^{-1} over the sampling time. The sensors are read out by a microcontroller with a micro SD card logger to store the measurements (Rüdiger et al., 2018). The recorded data was then post-processed using RatioCalc program (Tamburello, 2015) to obtain time series of CO_2/SO_2 mixing ratios. Specific acquisition time windows or subintervals were selected (Figure 3.3) and molar ratios were obtained by taking the best-fit regression line in scattered plots of volatile couples. No ratio calculated during the subintervals was considered when excessive dilution of volcanic gases (e.g., $SO_2 < 1.0$ ppmv) or when low correlation coefficient was obtained ($R^2 < 0.5$).

Instrument	Gas sensors	Volcano
Sunkist (SK)	CO_2, SO_2	Masaya, Santa Ana, San Miguel, Vulcano (ground-based), Santa Ana (aerial)
Pitsa (PT)	CO_2, SO_2	Santa Ana (ground-based)
Snet (SN)	CO_2, SO_2, H_2S and H_2	Santa Ana, San Miguel (ground-based)
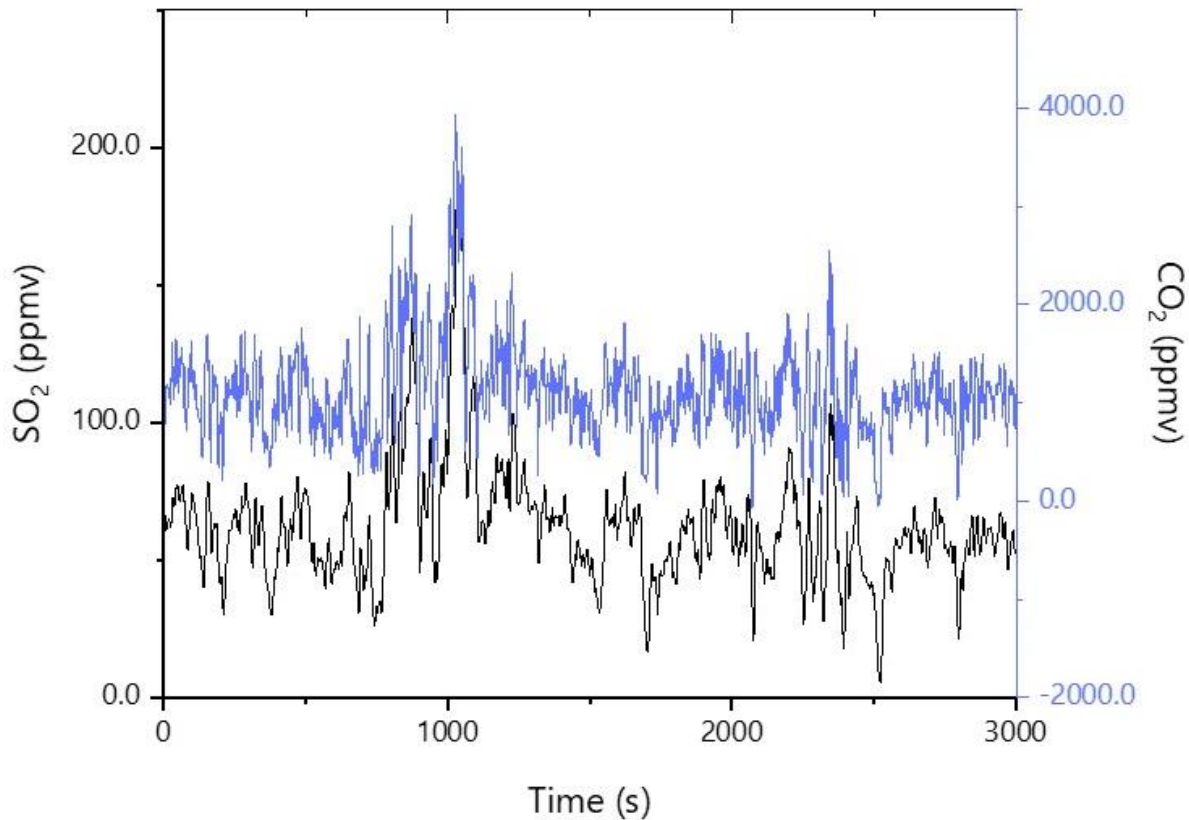
Figure 3.3. Variation of co-acquired CO_2 and SO_2 concentrations in the atmosphere during the fumarole plume measurement at La Fossa crater, Vulcano.

3.1.3. Diffusion denuder

Another in-situ sampling method for gases is the diffusion denuder systems, designed for gas-particle separation, as described in section 2.1.1.

Here we applied this method in all our field campaigns using TMB-coated denuders. These were prepared using brown borosilicate glass tubes (6 mm i.d., length 50 cm) coated with six 0.5 mL

portions of a 15 mM solution of TMB (≥ 99.0 %, Merck Germany) in methanol (HPLC-Grade, Merck Germany). During measurements, the discharged gases pass through a two-denuder serial setup with a GilAir Plus™ pump at 250 mL min^{-1} flow rate. The collected samples were stored, prepared and analysed according to Rüdiger et al. (2017), using an GC-MS system (Agilent 6850A Gas Chromatograph and Agilent 5973 Mass Selective Detector, Agilent technologies Inc., California, USA) with an oven temperature program of initial temperature 90 °C (hold 3 min), 30 °C min^{-1} to 210 °C, 7 °Cmin^{-1} to 235 °C, and 20 °C min^{-1} to 250 °C (hold 1 min). For quantification, characteristic m/z ratios were selected for the single ion monitoring mode (SIM), i.e., m/z 246 for 1-bromo-2,4,6-TMB and m/z 202 for 1-chloro-2,4,6-TMB.

3.2. Remote sensing

Remote sensing techniques enclose methods with which the measurements are made at a distance from the volcano, and the instrument and the observer are not actually in the gas plume. Apart from being much safer than monitoring by direct or in-situ sampling methods, gas emission monitoring by means of remote sensing techniques has the major advantage that these methods generally allow for automated acquisition of gas measurements and real-time data analysis, however they typically allow the quantification of selected species such as SO_2, so the number of gas species determined remotely is less than gas samples collected directly at the fumaroles. These techniques have been implemented on several platforms: from ground, on aircrafts, balloons and satellites.

Despite the abundance of H_2O and CO_2 in magmatic gas emissions, their quantification by means of remote sensing methods is exceedingly difficult, since they are also present in the ambient atmosphere in significant amounts. Remote measurements of magmatic volatiles have then strongly focused on SO_2, since it is readily detectable by ultraviolet and infrared spectroscopic methods, due to its strong absorption in distinctive narrow band wavelength ranges of the electromagnetic spectrum, and since its high abundance in the volcanic gas plume.

Due to their unique molecular structures, some gases in the plume (e.g., SO_2, BrO, OClO) absorb light at characteristic wavelengths in the UV or IR regions of the electromagnetic spectrum, resulting in distinct broad and narrow band optical absorption structures, which are

superimposed on each other in the measured light spectra, and thus reflect the composition of the light absorbing gas mixture (Figure 3.4). Here, we will focus on the UV-spectrometers, specifically the DOAS method.

3.2.1. Differential Optical Absorption Spectrometers (DOAS)

UV-spectrometers have been used for decades for the remote determination of volcanic SO_2 emissions, starting in the 1970's with the Correlation spectrometer (COSPEC), using the skylight as an ultraviolet source. This technique became a primary tool for remote measurements of SO_2 emissions and was used for the first assessments of global volcanogenic volatile fluxes to the atmosphere (Halmer et al., 2002; Andres and Kasgnoc, 1998). However, COSPEC has thus in many places gradually been displaced by an easily operated instrument based on robust lightweight miniature grating spectrometer and applying the DOAS. This allow fully automated acquisition of data at a frequency of several minutes per measurement during daytime and are thus used on an increasing number of volcanoes to permanently monitor SO_2 emission rates, enabling to study long-term degassing variations including periods of quiescence (Arellano et al., 2021; Galle et al., 2010). As the COSPEC, the DOAS method is based on the Lambert-Beer Law, which describes absorption of electromagnetic radiation by matter (Figure 3.5), in this case, the absorption of light by atmospheric constituents using either artificial light sources, scattered sunlight or direct sun- or moonlight, according to

$$I(\lambda, L) = I_0(\lambda) \times \exp\left(-\sigma(\lambda) \times \rho \times L\right)$$

with I_0 being the intensity of the light at wavelength λ before entering the absorber and $I(\lambda, L)$ the intensity after passing a layer of length L, with σ being the absorption cross section and ρ the concentration of the trace gas. However, on the atmosphere, several mechanisms affect the intensity of the light (absorption and scattering). The DOAS method separates the spectral structures in narrowband (e.g., by gas molecules) and broadband components (e.g., by aerosols, cloud droplets, gas molecules) in differential spectra, so that changes in narrowband absorptions can be detected. DOAS instruments operating within the framework of the global "Network for Observation of Volcanic and Atmospheric Change" (NOVAC) (Galle et al., 2010) utilize linear CCD sensors combined with a diffraction grating, and thus provide one-dimensional

hyperspectral measurements, which can in principle be used to simultaneously also quantify other light absorbing trace gases than SO_2, such as bromine monoxide (BrO; Bobrowski et al., 2003; Lübcke et al., 2014).

In this research, sulfur dioxide emission rates were acquired by two DOAS stations one installed at the southwest flank of Santa Ana and another one at San Miguel volcano, El Salvador, at distances of ~ 6 and ~ 8 Km downwind, respectively. These stations are part of the mentioned NOVAC network operated in El Salvador by the Ministerio de Medio Ambiente y Recursos Naturales (MARN) - Observatorio Ambiental, the national institution responsible for the study and research of natural phenomena in the country. El Águila (Santa Ana volcano) and Piedra Azul (San Miguel volcano) stations (instrument number D2J2167 and D2J2170, respectively) have operated since 2008. However, the instrument at Piedra Azul was removed due to technical problems and a new station was installed at San Jorge using another instrument. Summarizing information about the stations are presented on Table 3.3 and Figure 3.6 and Figure 3.7. Each station acquires spectra during daylight hours. Each instrument is mainly composed by an UV-spectrometer (Ocean Optics®, S2000) and a telescope connected via a quartz fiber, where a motor-driven mirror or prism collects the backscattered sunlight; each measurement sequence scans across the sky in a vertical plane of 180°, from horizon to horizon, with angular steps of 3.6°. The spectrometer operates in the wavelength range of about 280 – 425 nm, and the telescope has a field of view of 8 mrad. The instrument is controlled by microcomputer, also used to store and transmit the measurements to the observatory, where the measurements are downloaded and evaluated using the NovacProgram (Galle et al., 2010). The data collected by the stations was used here in order to retrieve SO_2 and BrO gas emissions from Santa Ana and San Miguel volcanoes for the period 2006 – 2020 and 2008 – 2019, respectively. The datasets were provided by the observatory, with some gaps due to failure of the instruments.
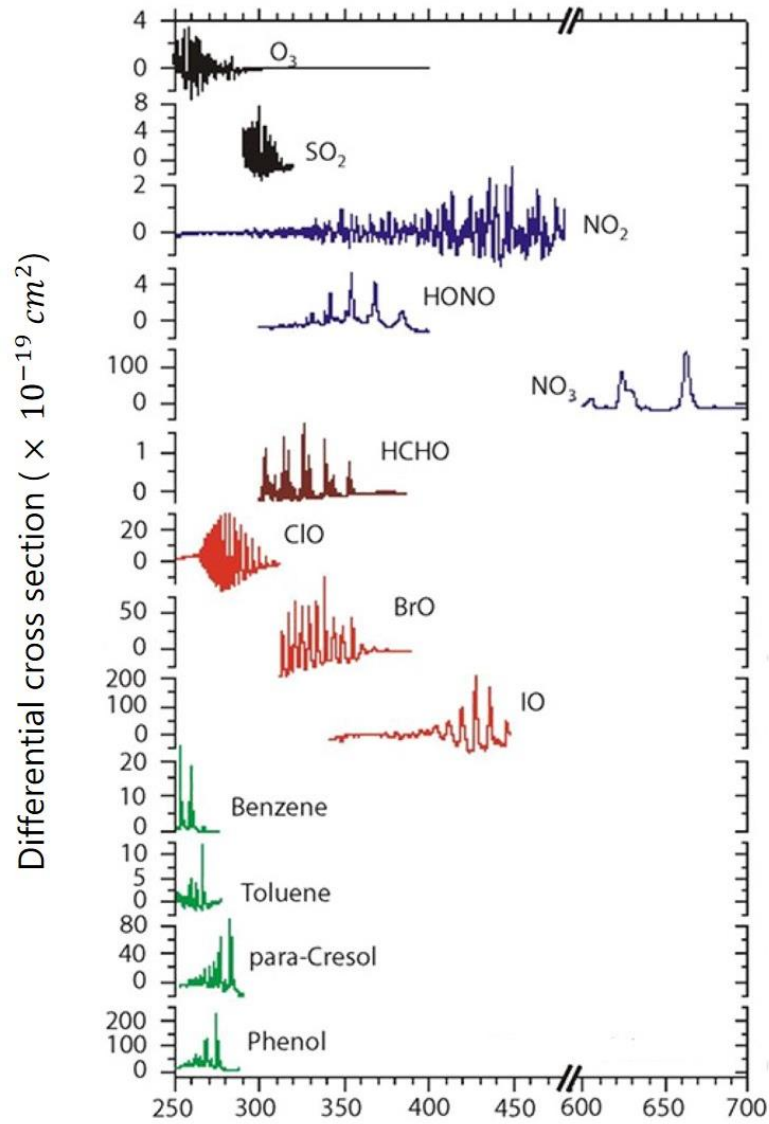
Figure 3.4. Differential cross section (σ') features of different gas species (Modified from Platt and Stutz, 2008)
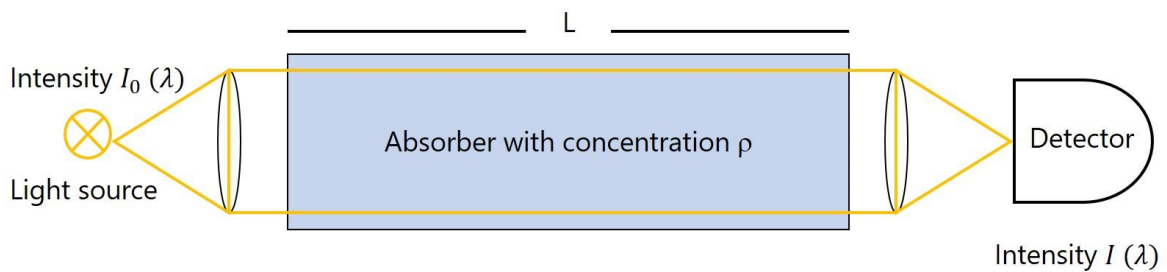

Figure 3.5. Image representing the Lambert Beer's law of absorption (After Platt and Stutz, 2008)

The evaluation is based on (Dinger et al., 2021), which performs: (1) a quality check of individual spectra of a scan, (2) a retrieval of the spatial SO$_2$ distribution, (3) spectral adding of scan spectra to perform the SO$_2$ and BrO DOAS fit, (4) spectral adding of consecutively recorded scans to further improve the signal-to-noise of the BrO fit. The output of this evaluation are the time series of SO$_2$ and BrO SCDs, and daily SO$_2$/BrO molar ratios. Furthermore, this approach allows the calculation of the SO$_2$ emission fluxes when meteorological data is available via

$$F_{SO_2} = M_{SO_2} \times v \times \cos(\omega - \beta) \times H \times \int_{-\infty}^{\infty} V_{SO_2}(\varepsilon) \, d(\tan(\varepsilon))$$

where M_{SO_2} is the SO$_2$ molar mass, v is the absolute wind speed, ω is the absolute wind direction, β is the orientation of the scan plane, H is the plume height and $\int_{-\infty}^{\infty} V_{SO_2}(\varepsilon) \, d(\tan(\varepsilon))$ is the SO$_2$ VCDs (vertical column densities) angular integral. In this work, meteorological data was obtained from the ERA-interim re-analysis database produced by the European Center for Medium-Range Weather Forecasts (ECMWF) since no meteorological data is available at the volcanic plume conditions. The ERA-Interim covers the period from 01.01.1979 to 31.08.2019. This model and reanalysis system was produced with a spatial resolution of 60 vertical levels up to 0.1 hPa (Berrisford et al., 2011). For each volcano, horizontal wind vectors were retrieved every 6 h, vertically interpolated to an altitude of 2,670 m.a.s.l. for Santa Ana and 2,310 m.a.s.l for San Miguel, with a grid of 0.125° × 0.125°, close to the location of the volcanic vent. Furthermore, wind information corresponding to September 2019 until December 2020 was additionally downloaded by the Observatory from the Global Data Assimilation System (GDAS) database produced by the National Oceanic and Atmospheric Administration (NOAA). The wind speed and wind direction were calculated based on the horizontal and vertical wind components, with a temporal resolution of 3 h, vertically interpolated to an altitude of 2,570 m.a.s.l. The model is currently produced at 64 layers in the vertical extending from the surface to the upper stratosphere (13-km horizontal resolution).

Table 3.3. NOVAC station settings for Santa Ana and San Miguel volcanoes

| Volcano	Station	Instrument number	Coordinates	Altitude (m.a.s.l)	Distance (Km)	Scan plane	Operation time
Santa Ana	El Águila	D2J2167	13.8509, -89.6295	1014	5.8	66°	2008 – present
San Miguel	Piedra Azul	D2J2170	13.3962, -88.3045	373	5.0	43°	2008 – 2010
San Miguel	Finca	D2J2205	13.4349, -88.2997	884	2.8	99°	2014 – 2016
San Miguel	San Jorge	I2J9304	13.4148, -88.3444	339	7.9	70°	2012 – 2014
San Miguel	San Jorge	I2J9304	13.4148, -88.3444	339	7.9	70°	2017 - present
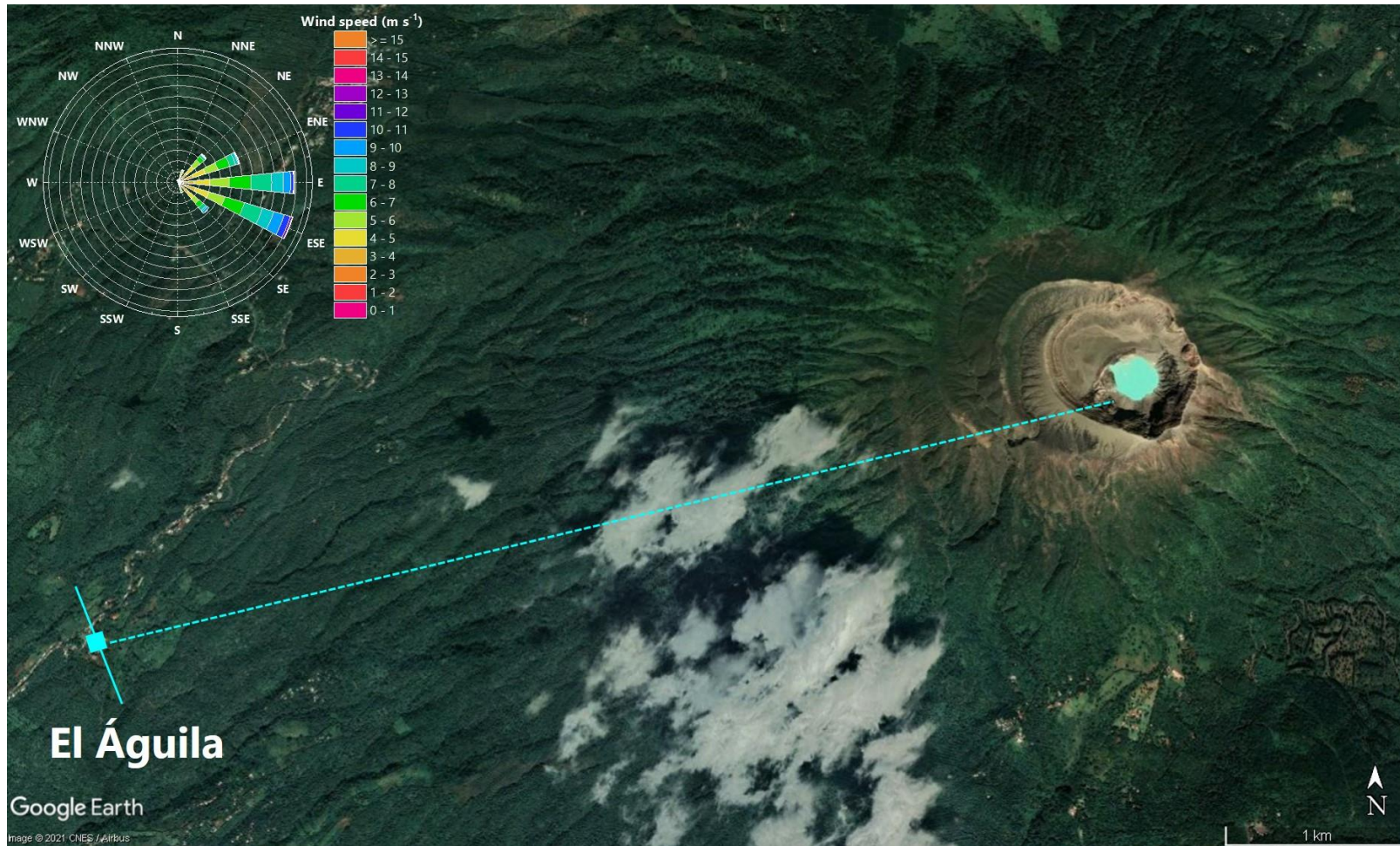
Figure 3.6. Scan geometry and wind rose at El Águila station, 5.8 Km from Santa Ana volcano
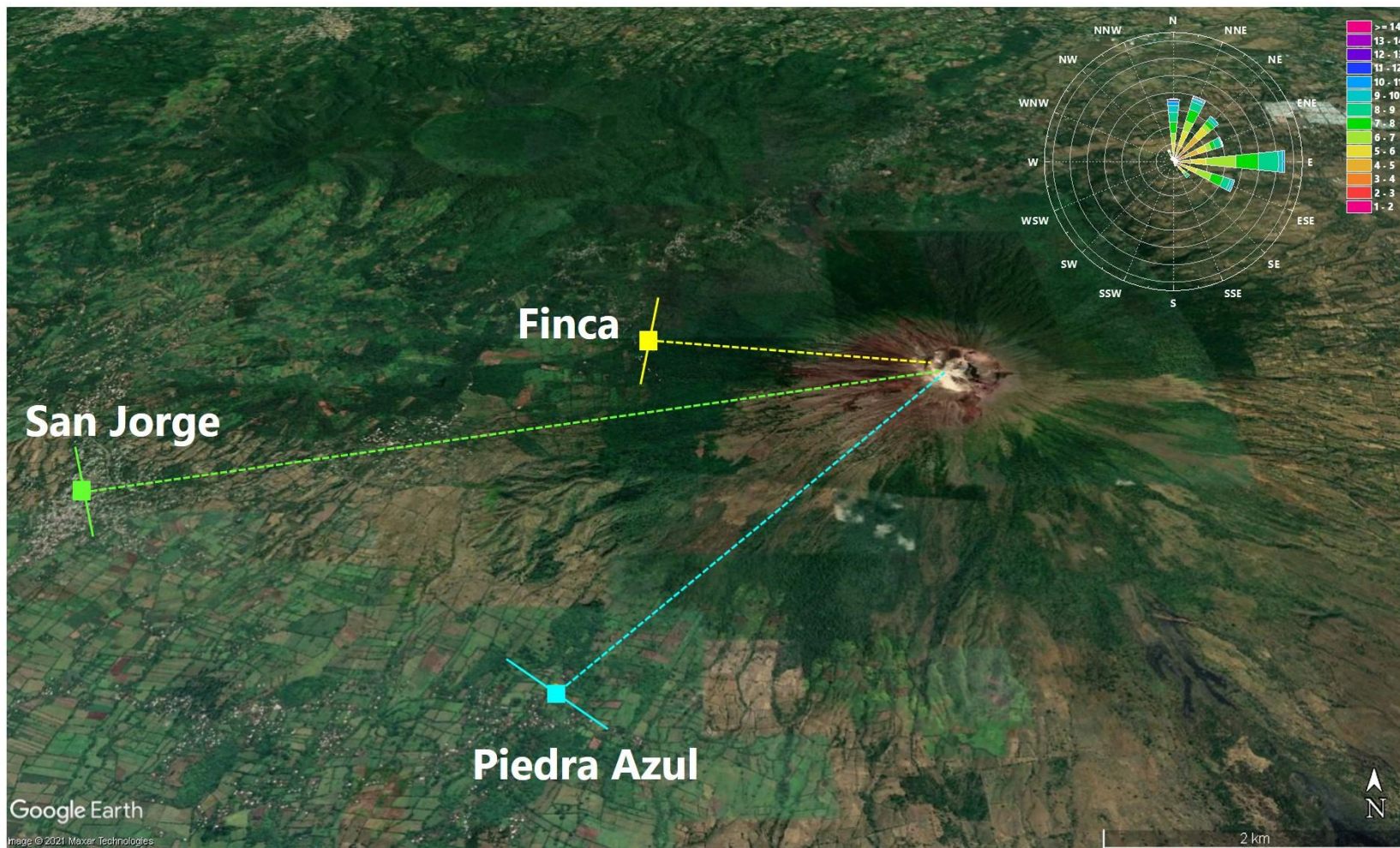
Figure 3.7. Scan geometries of Piedra Azul, Finca and San Jorge stations. Upper right, wind rose corresponding to the period of 2008 – 2019.

4. Results and discussion

4.1. Evaluation of stilbene-coated denuders as sampling technique for the determination of RHS in volcanic plumes

4.1.1. Laboratory results

4.1.1.1. Gas sources

The permeation tubes weight loss was monitored over time at a constant temperature of 30 °C. After a period of 1 – 2 weeks, the source reached equilibrium and a stable output rate was achieved. For each halogen, the slope of the least-square regression is given (**Figure** 4.1). The HCl permeation tube didn't achieve a stable output rate, for which it was not considered for the next experiments.

4.1.1.2. Linearity and limits of detection

The detector response was linear over the concentration range 0.002 – 3.3 mg/L (**Figure** 4.2). The linearity was further manifested by repetitive chromatograms under the same working conditions for the dichloro- and dibromo- derivatives, respectively (**Figure** 4.3). The LOD and the LOQ were determined to be in the lower nanogram scale for Cl_2 as shown in Table 4.1.

Table 4.1. Limit of detection (LOD) and quantification (LOQ) determined following the standard protocol DIN 32645 their corresponding mixing ratios, using typical sampling conditions: flow 250 mL/min, sampling time 20 min, 1 atm

Limit	Cl_2	Br_2
LOD (ng)	0.18	0.23
LOD (ppt)	4.04	2.34
LOQ (ng)	0.49	0.64
LOQ (ppt)	11.29	6.52

4.1.1.3. Cross-sensitivity between stilbenes and halogen species

The cross-sensitivity of the denuders towards halogens was tested by passing the Br_2, Cl_2 and BrCl gases through the CST- and TST-coated denuders. DCTST was obtained using both coatings. However, DBTST signal was only elucidated when CST was used as coating material. These di-halogenated stilbene derivatives were identified by GC-MS (**Figure** 4.4 and **Figure** 4.5) as a mixture of their meso- and dl-isomers. Since one of the isomers was available as standard, the identification of each one was possible. Furthermore, the retention time corresponds to the one observed with the standard solutions (**Figure** 4.3). Here we identify

signals for the BrCl derivative with a retention time between the DCTST and the DBTST (Figure 4.6).
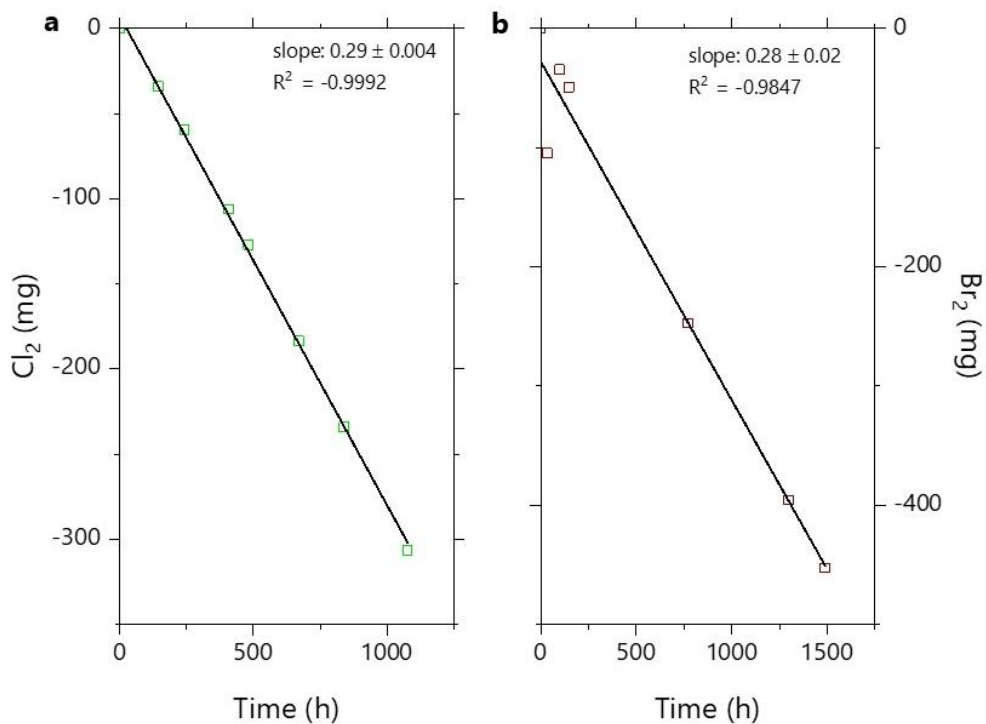

Figure 4.1. Thermogravimetric monitoring of (a) chlorine and (b) bromine permeation tubes. The plots show the weight loss vs. time, corresponding to a non-interrupted acquisition period of 1000 h and 1500 h, respectively.
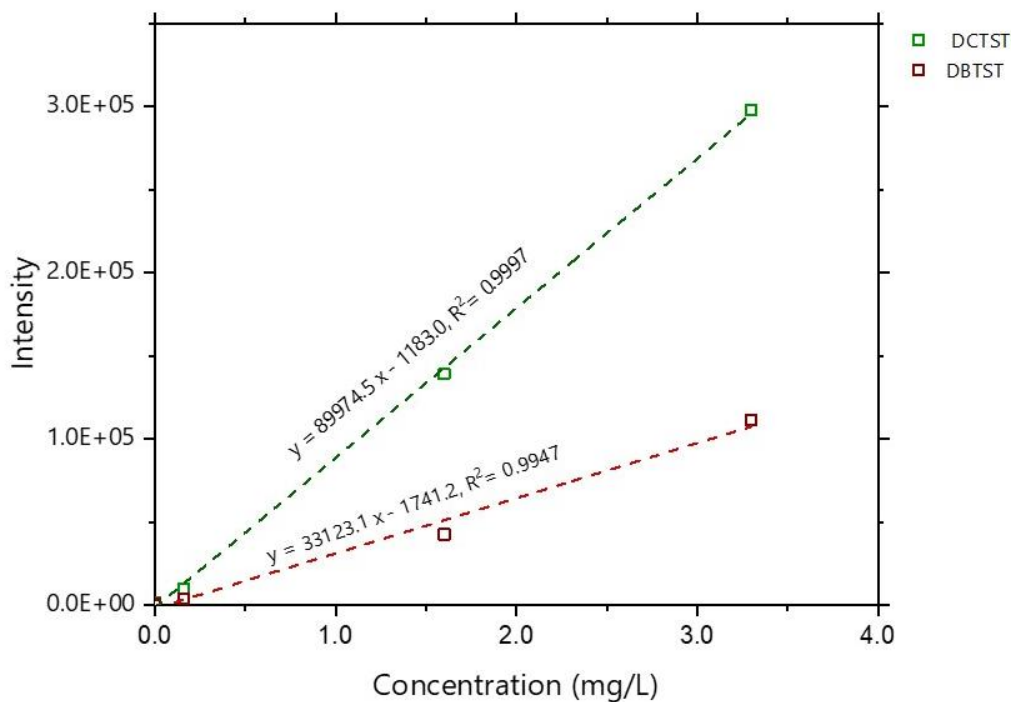

Figure 4.2. Calibration curves for DCTST (green cubes) and DBTST (red cubes) using standard solutions with its respective linear regression values.
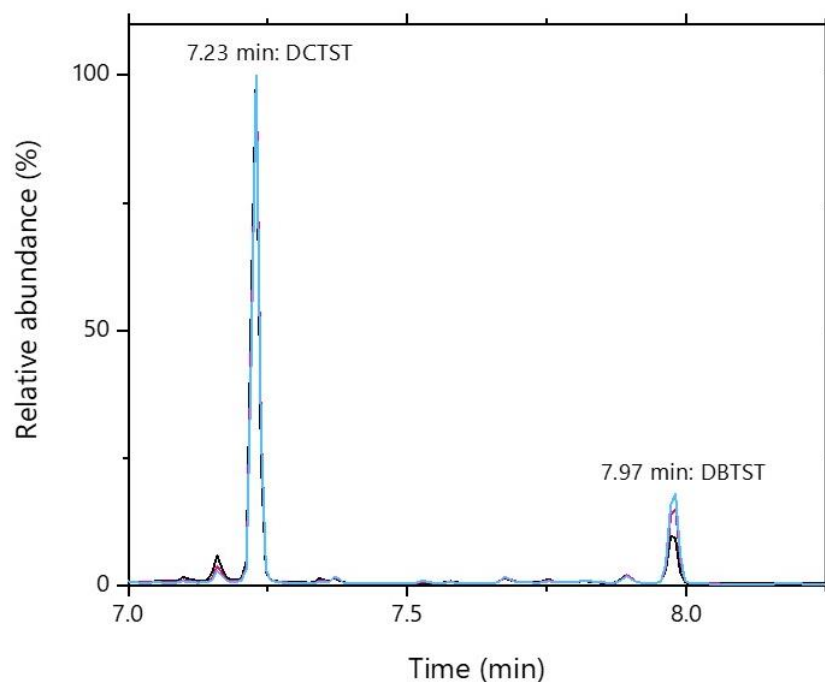
Figure 4.3. Typical chromatogram representing the reproducibility of the standards (n = 3).

For this compound three signals were found, recognizing the next fragments: 217/215 (M^+ – Br), 180/179/178 (M – Br – Cl), 171/169 ($M^+/2$ with Br), 165 (M – Me – Br – Cl), 127/125 ($M^+/2$ with Cl). Since no standard was available nor a theoretical MS spectrum, we can only assume from the m/z fragments and the retention time, that the presented chromatogram corresponds to the BrCl derivative.

4.1.1.4. Internal standard

Appreciable recovery rates were achieved using DBPP as internal standard, with recoveries of 72.5 % (0.1 mg/L) and 88.5 % (1.0 mg/L) for the DCTST, and 80 % (0.1 mg/L) and 120 % (1.0 mg/L) for the DBTST; whereas the recovery rates using TBB as internal standard ranged between 70 – 150 %, showing a different evaporation behavior as the halogenated-stilbene derivatives and not being considered for analysis. Even though the DBPP showed better results than TBB and there was repeatability in between measurements at the same condition of the same sample (n = 3), reproducibility was not achieved when repeating the internal standard performance experiment few months later, which means it is not reliable to use as an internal standard.

4.1.2. Analytical performance of stilbene-coated denuders
4.1.2.1. Recovery rate

Table 4.2 shows low recovery rates (5 – 9 %) for TST and CST, respectively. During the evaporation step, the eluted solution from denuders prepared with trans-stilbene 15 mM (0.045 mmol) doesn't contain the whole product since some of it recrystallizes on the wall of the evaporating vessel. This is a different behavior from the standard solution, tested with the same preparation procedure during the evaluation of the internal standard. Furthermore, these samples were too concentrated overloading the instrument and not being able to elucidate specific signals for the derivatives. On the other hand, samples prepared with lower concentration than the 15 mM, didn't present this recrystallization process during the evaporation step. Nonetheless, the chromatograms showed that most of the injected analyte was the coating itself, having in most cases no-signal or a small one below the LOQ (Figure 4.7). After this, the next samples were prepared by eluting the denuders with 5 times 0.5 mL of acetone and taking a 100 µL aliquot to be analyzed by GC-MS, avoiding the pre-concentration step (evaporation). The last procedure didn't improve the recovery rates, being still minor (< 10 %) to consider the denuder method for the quantitation of halogens. From 16 denuders prepared with TST only one sample gave results above the LOD and LOQ. In the case of CST, the same number of denuders was prepared obtaining results for 3 samples above the LOD and LOQ (Table 4.1).

Table 4.2. Recovery rates obtained from sampling coated denuders

Denuder number	Coating	Gas source	Sample preparation	Recovery (ng)
3B	TST 1.5 mM	Cl_2	Elution	13.9
18A	CST 0.48 mM	Cl_2	Evaporation	8.2
20A	CST 0.48 mM	Br_2	Evaporation	16.3
20B	CST 0.48 mM	Br_2	Evaporation	10.1

Figure 4.4. DCTST isomers chromatographic signals (left) with its respective MS spectrum (right). Numbers and arrows within the MS spectrum indicate the representative m/z fragments.
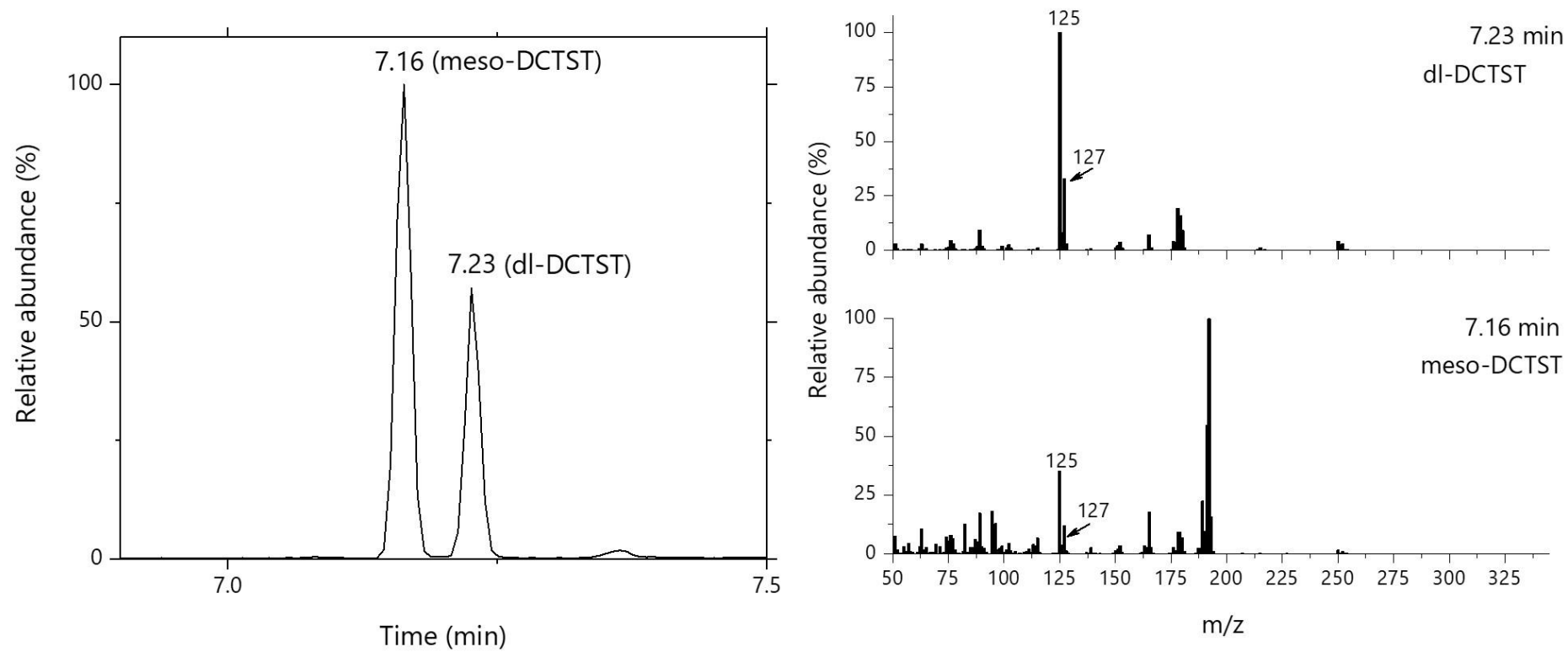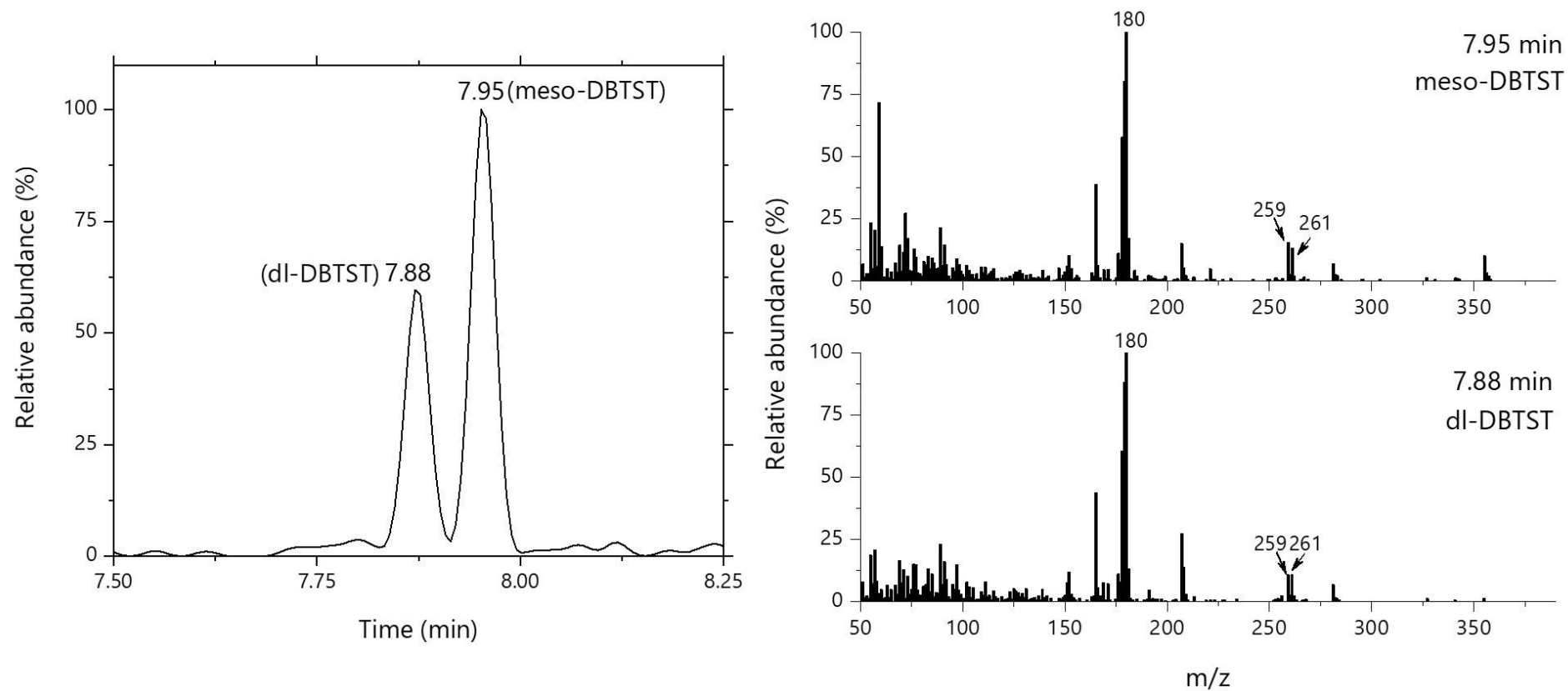
Figure 4.5. DBTST isomers chromatographic signals (left) with its respective MS spectrum (right). Numbers and arrows within the MS spectrum indicate the representative m/z fragments.
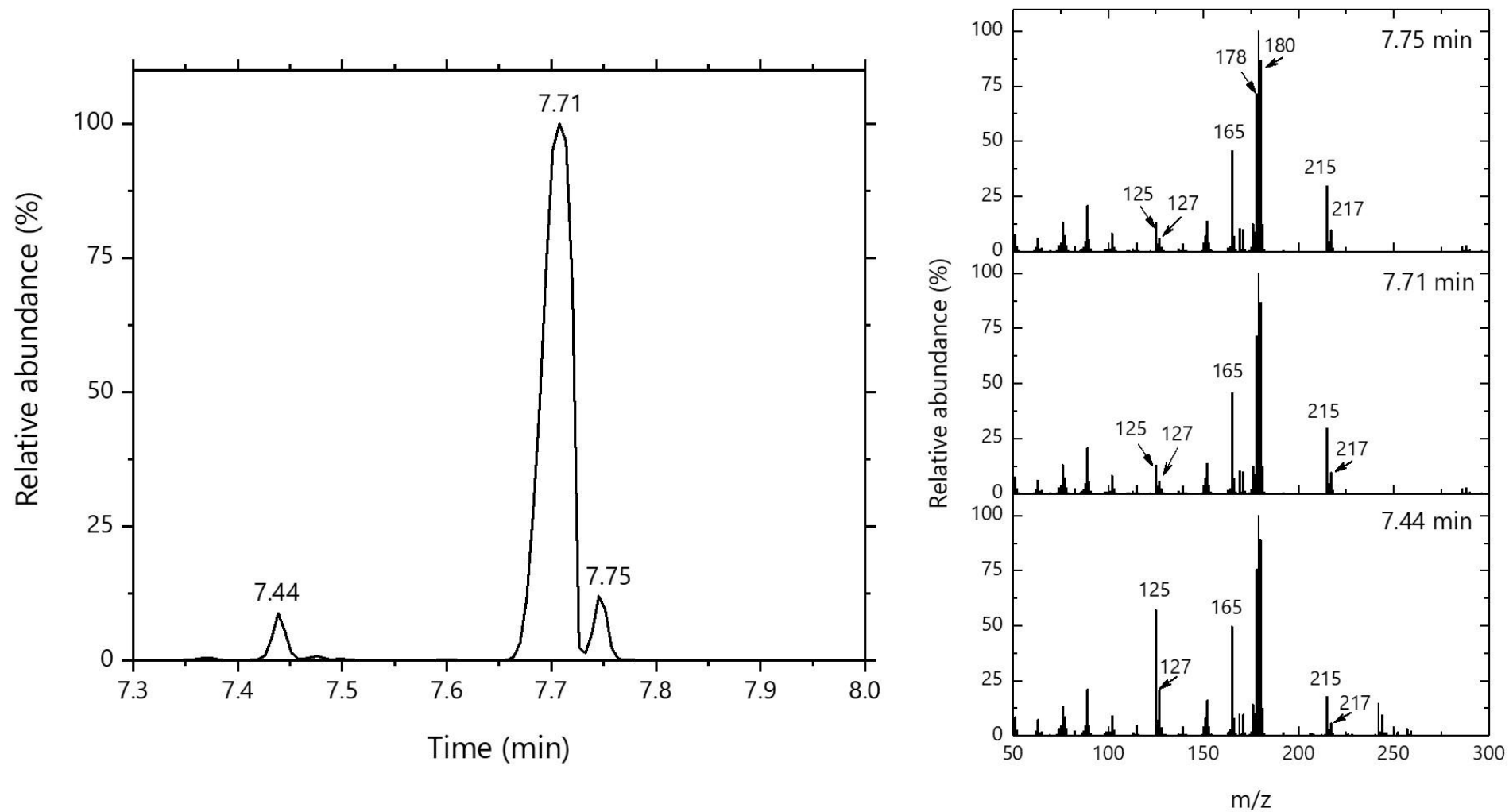
Figure 4.6. 1-bromo-2-chloro-1,2-diphenylethane chromatographic signals (left) with its respective MS spectrum (right). Numbers and arrows within the MS spectrum indicate the representative m/z fragments.
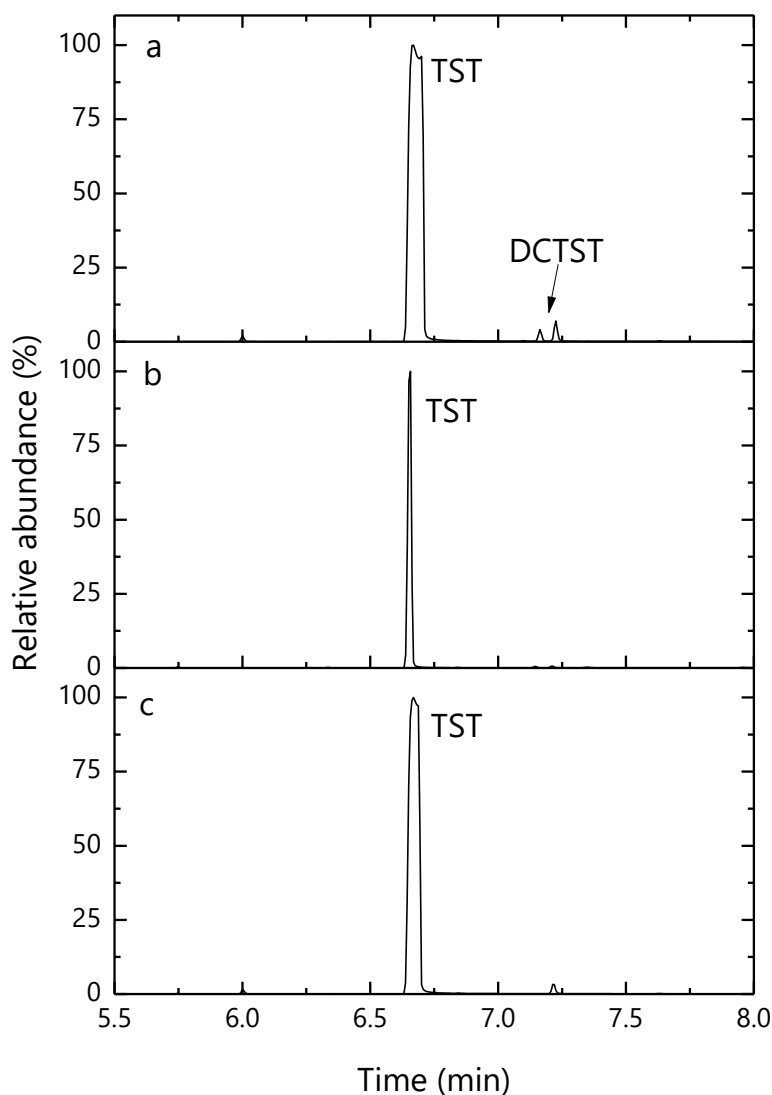
Figure 4.7. Examples of chromatograms obtained using (a) TST 1.5 mM and chlorine source, (b) TST 0.5 mM and the chlorine source, and (c) TST 1.5 mM and the bromine source. In each case, the coating is the main compound detected. As for the derivatives, only on (a) where the coating was more concentrated, very small signals of the derivative can be observed. However, this were below the LOQ.

Although stilbene isomers have shown effective halogen addition to its structure, the amount of recovered halogenated derivatives is very low. Kaupp and Matthies (1987) reported the halogenation of trans-stilbene in gas-solid state, achieving only 20 % yield of the halogenated products after 64 h at 22° C (Table 4.3). The incompleteness of the reaction (not fully quantitative) was attributed by Kaupp and Kuse (1998), to the third step of gas-solid reactions (crystal disintegration). Nevertheless, the authors overcame this problem by milling the trans-stilbene crystals to a grain size < 1μm and starting the reaction at 0 °C and 0.05 bar. Then, after 3 h the additions continued at room temperature for three more hours for Cl_2 (under 0.5 bar), and for 24 h at 0.1 bar for Br_2, with a 100 % yield in each case. In this work, the experiments were performed in much less time than the above described, at room pressure and room temperature, since the method was intended to be implemented in volcanogenic environments. The low yield obtained was, in most cases, close or below the limits of detection

and quantification (Table 4.1). Furthermore, during the re-crystallization of TST inside the denuders by the coating procedure, the crystal size was not controlled and therefore the surface area is not uniform. Consequently, the crystal disintegration step mentioned before was not carried out and the formation of fresh surface for further reaction was not achieved. Additionally, no improvement in the recovery rate was accomplished by changing the concentration of the coating (Figure 4.8). This can be explained by the reaction kinetics. (Kaupp, 2017) stated that gas-solid reactions taking place at constant gas pressure, have a reaction kinetics close to zero, which means the rate of the reaction is independent of the concentration of the reactants. Moreover, the author describes deviations in the kinetics due to the changing crystal sizes that can be overcome by milling, as described earlier. Unfortunately, in this work, milling of the crystals inside the denuders was not possible, so the reaction was limited at certain spots (probably packed crystals). Additionally, the reproducibility of the results was not feasible, possibly due to (1) the pre-concentration step in which not the whole analyte was contained in the solution, and (2) inhomogeneity of the coating to have effective reaction sites. Improvement of the halogenation has been reported also in "wet conditions" at room temperature (Tanaka et al, 1999). However, to reach the efficiency reported (88 % yield), the authors used milled TST and performed the reaction for a period of 15 h.

Cis-stilbene on the other hand, doesn't re-crystallize since its melting point is between 1 to 2 °C, resulting in a gas-liquid reaction. Bromination of CST has proven to be successful at room temperature over a long period of time in liquid-liquid conditions (Table 4.3), using bromine water and pyridinium bromide perbromide as brominating agents. Furthermore, (Al-hassan, 1989) described a rapid reaction of CST with Br_2 in CCl_4 at -12 °C (90 % yield). In this research, halogenation of CST was performed at room temperature for 20 min, using the gas sources of the pure halogens described above. These conditions permitted to achieve higher yields than its trans-isomer (Figure 4.9). Nevertheless, its collection efficiency needs to be tested perhaps using another sampling medium (e.g., filters, impingers) in order to rely on it as a successful material for sampling halogen compounds in volcanic environments, since repeatability was not accomplished in our experiments probably due to losses of the coating (evaporation and/or liquid dripping out of the denuder), that led to changes in the CST concentration.

Table 4.3. Published halogenation reaction of cis- and trans-stilbenes at different conditions

Material	Halogen source	Conditions	Reaction time (h)	Yield (%)	Reference
TST	Br_2	Gas-solid	64	20	Kaupp and Mathies, 1987
TST	Cl_2	Gas-solid	6	40	Kaupp and Mathies, 1987
TST	Cl_2 in CH_2Cl_2	Wet	2	91	Kaupp and Mathies, 1987
TST	Br_2 in CCl_4	Wet	0.5	93	Al-hassan, 1989
CST	Br_2 in CCl_4	Liquid-liquid	0.5	90	Al-hassan, 1989
TST	PBPB	Wet in water suspension	15	88	Tanaka et al., 1999
CST	PBPB in HOAc	Liquid-liquid		89	(Amburgey-Peters, Haynes, 2005)
CST	Br_2 in HOAc	Liquid-liquid		85	Amburgey-Peters and Haynes, 2005
CST	PBPB in CH_2Cl_2	Liquid-liquid		92	Amburgey-Peters and Haynes, 2005
CST	Br_2 in CH_2Cl_2	Liquid-liquid		93	Amburgey-Peters and Haynes, 2005

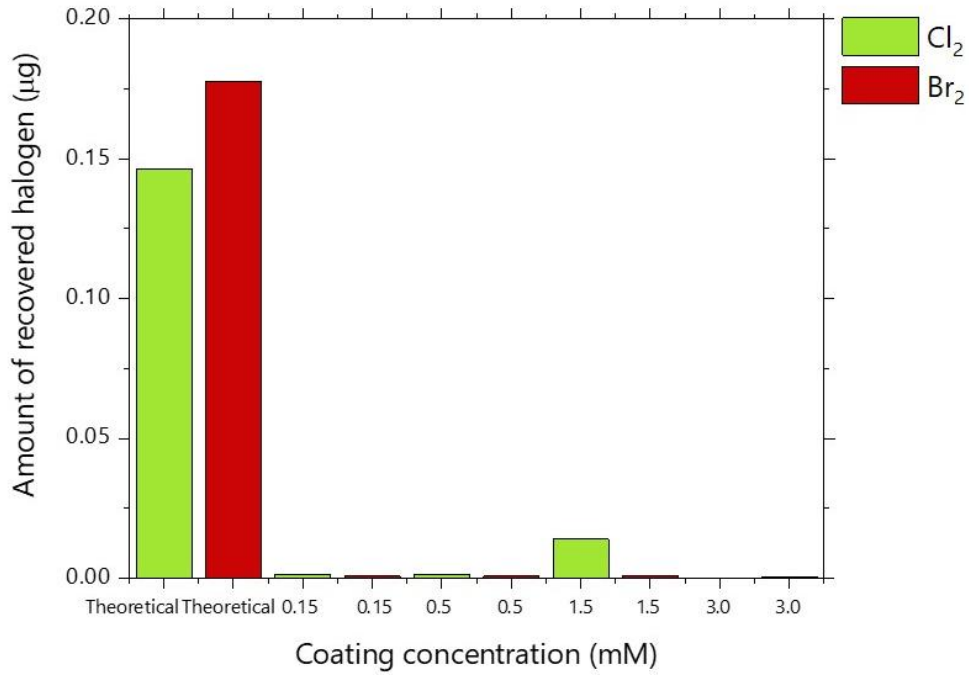* PBPB: Pyridinium bromide perbromide, OHAc: acetic acid glacial

Figure 4.8. Comparison of the sampled and determined amount of halogens with the theoretical output of the test gas sources, using different concentration of TST coating.
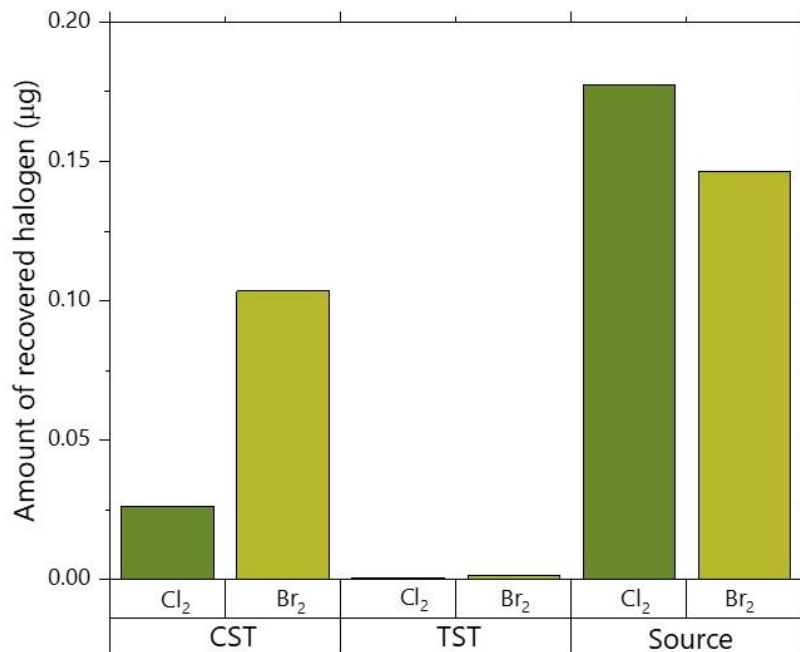

Figure 4.9. Comparison of the sampled and determined amount of halogens with the theoretical output of the test gas sources, using two different coatings with concentration 0.5 mM.

4.1.3. Summary

Cis- and trans-stilbene have proven to successfully react with molecular halogens (Cl_2 and Br_2), and possibly interhalogens (BrCl). Furthermore, the separation of the isomers is accomplished, having the possibility to obtain the proportion of each. More importantly, the qualitative speciation of the halogens by GC-MS is possible since there is a signal for each di-halogenated compound, which makes feasible to distinguish between halogen species. However, these are not considered suitable as coatings for the denuder method due to:

(1) Reaction conditions cannot be adjusted to the suggested in literature to achieve higher yields since this method was intended for in-situ sampling in volcanic environments where temperatures near vent are above 50° C and sampling times depend on the state of activity of the volcano and are rather smaller than the found on previous reports

(2) Incompleteness of the reaction between the gas and the solid coatings, which is necessary since halogens species at sampling sites are in the gas phase

(3) Difficult transport of CST denuders on the field since some loss of the liquid is forthcoming

(4) Reproducibility of results was not accomplished, which leads to no validation of the method

Furthermore, in this work only one of the meso- or dl-isomers can be quantitated since only one of them was commercially available. No synthesis of the other isomers was done since the diffusion denuder method was proving to be unsuccessful as sampling method in volcanogenic locations.

4.2. Development of a sampling technique with coated syringe filters for the determination of reactive halogen species (RHS)

4.2.1. Laboratory results

4.2.1.1. Gas source

As mentioned above, the chlorine source was the same as in section 4.1.1.1. The permeation rate by the time of the experiments was of 0.0011 ± 0.0001 mg min^{-1}, equivalent to 0.015 µmol min^{-1}, showing that this type of permeation tube is suitable for Cl$_2$ gas.
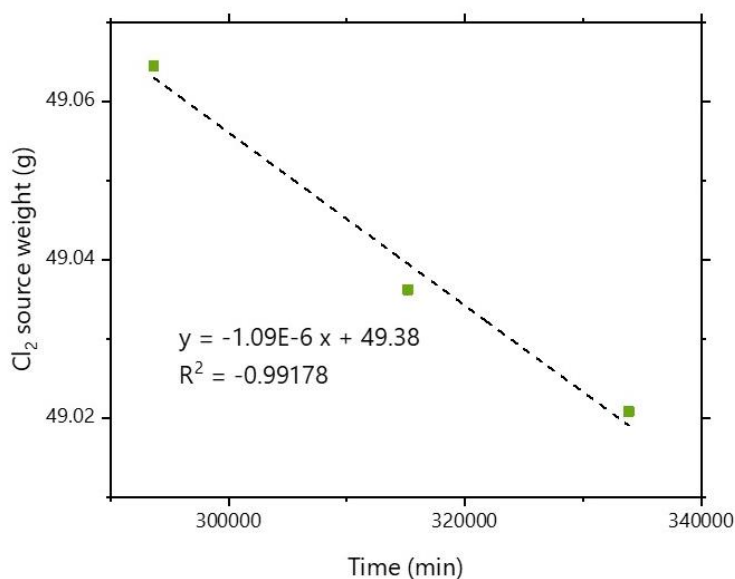
Figure 4.10. Gravimetric monitoring of the chlorine source as weight loss vs. time, corresponding to a non-interrupted 91 days acquisition period. Green squares indicate the weight during the period of the experiments performed in this study.

4.2.1.2. Calibration of sensor

The response of the sensor was linear over the concentration range studied (Figure 4.11), with a correlation coefficient of 0.98166. The limit of detection (LOD) and limit of quantitation (LOQ) were 0.03 ppm and 0.09 ppm, respectively, which are in the low ppm range. In addition, the repeatability of the sensor was evaluated in different measurement runs at a flow rate of 750 mL min^{-1}. The repeatability was ± 0.04 ppm (1 σ) with a relative repeatability of ± 8 %.

Figure 4.11. Calibration curve for DCTST using standard solutions. Dash line indicates the obtained linear fit.

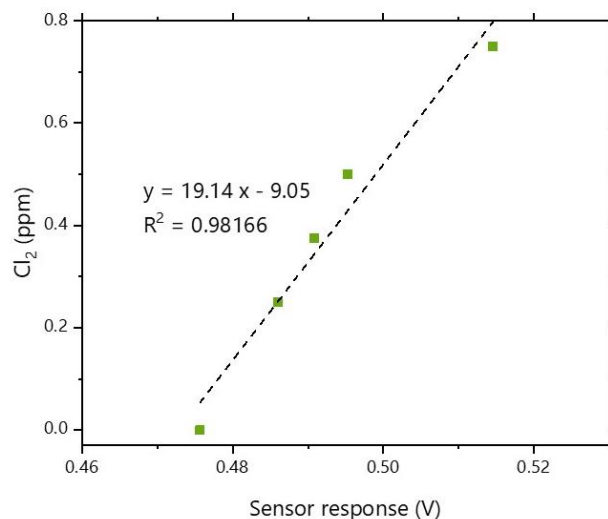### 4.2.2. Analytical performance of syringe-filters coated with alkenes
4.2.2.1. Collection efficiency

The collection efficiency of the impregnated-filters was evaluated using the experimental setup shown in Figure 4.12, by means of a sensor to monitor Cl_2 passing through the coated-filters. The collection efficiency (CE) of each coating was determined by comparing the output amount of the Cl_2 source (C_i) and the amount obtained after its reaction with the coating (C_f): $CE = 1 - \frac{C_f}{C_{i,}}$. In our experiments, TST showed a collection efficiency of 45.8 ± 23.4 %, whereas OC achieved a collection efficiency of 34.9 ± 25.5 %, with a poorly stable signal. Nonetheless, CST showed the highest efficiency of 100.7 ± 22.7 % for the first $6-7$ minutes of the experiment. Then, the efficiency starts to decrease, which it is thought to occur due to evaporation process of CST (Figure 4.12c). In theory, this can be overcome by applying an excess of CST to the filter. This excess is equivalent to the amount of coating lost due to evaporation and can be calculated with the vapor pressure of the coating (1 Pa, 26 °C) and the total volume of gas sampled by means of the ideal gas law ($n_{lost} = \frac{p_v \times V_t}{R \times T}$).

4.2.2.2. Factors influencing the efficiency

Following the previous experiments with different coatings, further experiments were conducted to test the performance of CST due to its high initial efficiency. First, the amount of coating was increased from 1.5 to 2.5 µmol using the same flowrate as before (750 mL min⁻¹). The results show a small increase in the collection efficiency with increasing amount of coating,
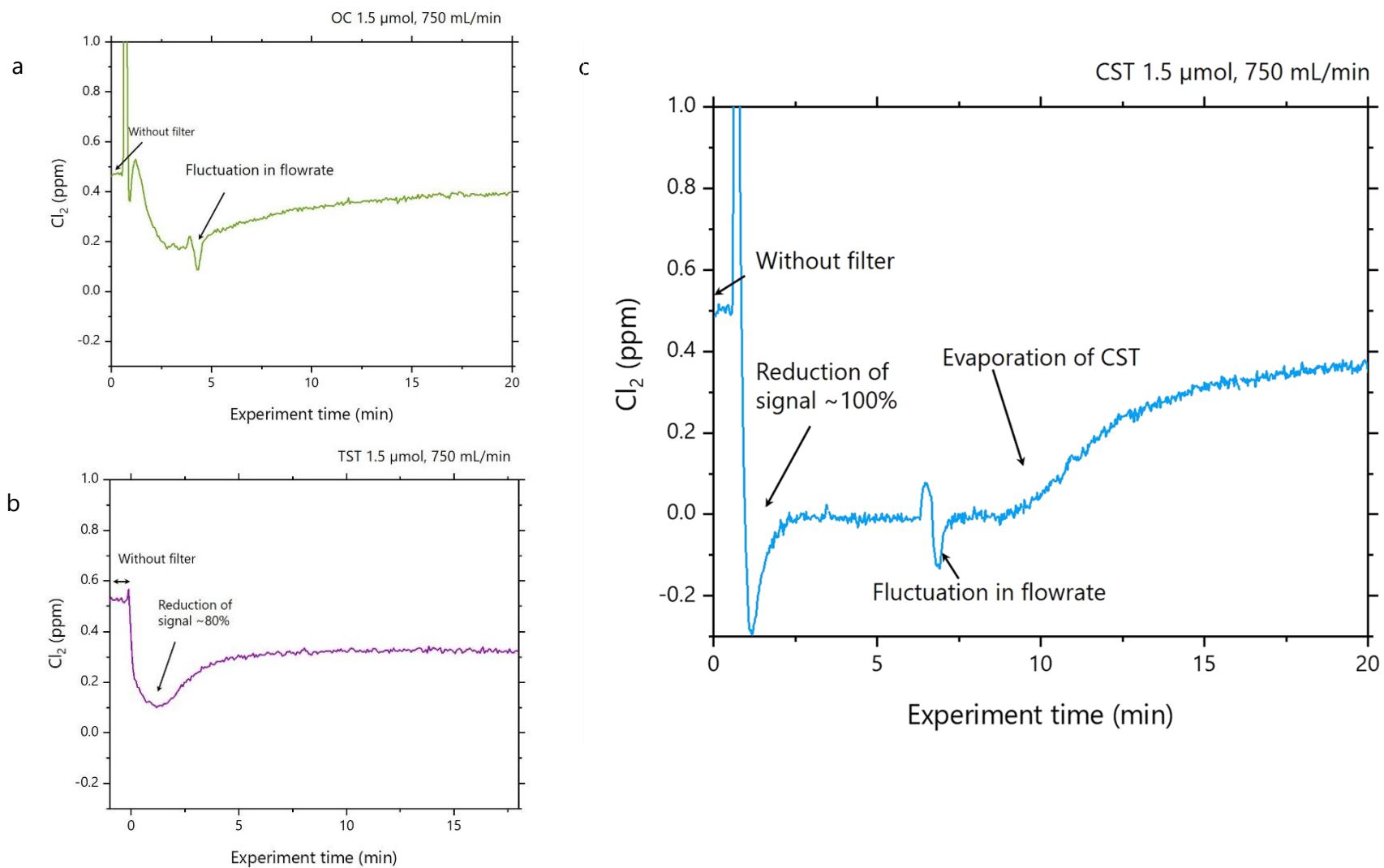
Figure 4.12. Comparison of collection efficiency of different coatings using a chlorine sensor: (a) trans-stilbene, (b) octenol, and (c) cis-stilbene. The plots show the drop of the measured Cl2 concentration when the coated-filters are connected to the system.

although the evaporation of the coating is slower (Figure 4.13). Also, another set of experiments was done by changing the flowrate with a sampling time of 15 minutes. Table 4.4 summarizes the results obtained. Like the amount of coating, the flow rate also affects the efficiency of the CST, as it was observed that the efficiency decreases with increasing flow rate. This is likely due to faster evaporation of the coating, so this effect must be considered when sampling at higher flow rates.

Table 4.4. Comparison of the averaged collection efficiency of CST at different flowrates during the first 15 minutes experiments

Coating (µmol)	Flowrate (mL min^{-1})	Collection efficiency (%)
1.5	750	85.7 ± 29.1
1.5	1000	62.0 ± 11.0
1.5	1500	46.8 ± 21.1

4.2.2.3. Storage behavior

Table 4.5 summarizes the results obtained from the different storage conditions. Very little variations are observed between the filters stored at room temperature (covered and not covered with aluminum foil to exclude light), suggesting that there is loss of coating over time (evaporation) and little or no photoisomerization happens since very little trans-stilbene is observed in the chromatograms (Annex). A coated-filter stored at 4 °C did not show a decrease in efficiency (63 ± 11 %) in comparison to a freshly prepared filter, evidencing that the storage temperature is the main factor that has a significant influence on the later performance of the filters.

Table 4.5. Storage conditions of coated cis-Stilbene syringe filters before usage. The experiments were conducted with a flowrate of 1000 mL/min and a sampling duration of 15 minutes.

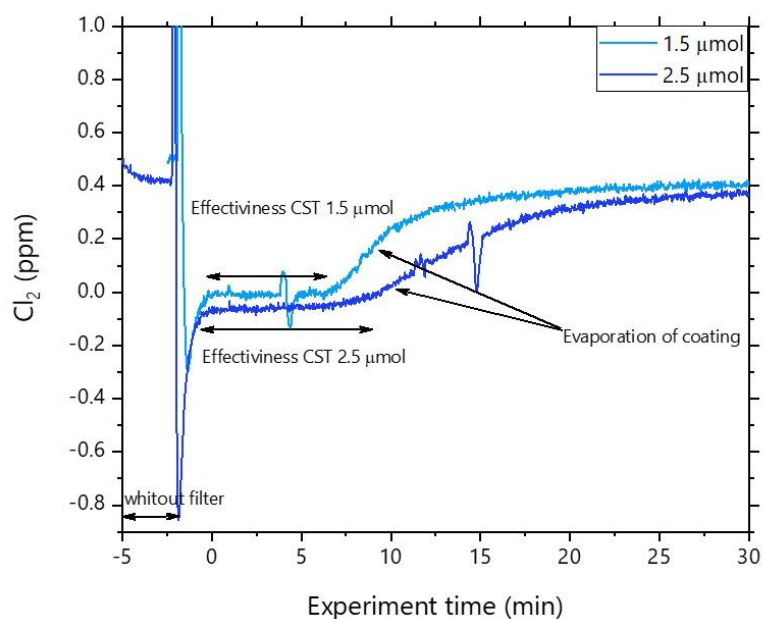| Sample number	Temperature (°C)	Storage time (d)	Conditions	Efficiency (%)
1	25	4	In fumehood	45 ± 11
2	25	1.8	In desiccator	49 ± 11
3	25	1.8	In desiccator and covered	49 ± 11
4	25	1.8	In fumehood and covered	48 ± 11
5	4	1.8	In frezzer and covered	63 ± 11

Figure 4.13. Comparison of the efficiency of the CST-coated filter method using different amounts of coating for the first 30 minutes of the experiment.

4.2.2.4. Recovery rates

To further test the performance of the CST, two experiments were conducted impregnating the filters with 1.5 μmol CST at a flowrate of 1000 mL min^{-1} with sampling times of 15 and 60 minutes. After each experiment the filters were washed with 10 mL of acetone, as described in section 2.1.2, and a 100 μL aliquot was used for its analysis by GC-MS. Prior to the analysis of the samples, a calibration was performed using the standard chlorinated derivative solutions as described in section 2.1.1.2.2, with a concentration range between 0.05 – 10 ppm. From the analysis, it was confirmed that the reaction of the CST with chlorine is occurring, since the signal of the di-chlorinated product was elucidated at 7.06 and 7.12 min (Figure 4.14). However, the signal of the coating (5.94 min) is higher than the signal of the derivative, as if most of the coating didn't react, even when the sensor response suggests that all of the coating has evaporated since the efficiency dropped to nearly 0%. If one assumes that after 6 minutes at least the first layer of the coating has evaporated completely and the next layers remain evaporating, probably this reduces the reaction rate since the surface area with effective reactive sites is getting reduced. The obtained yields were of 23.9 % for the 15 minutes experiment and 2.2 % for the 60 minutes experiment. Furthermore, the isomerization of cis- to trans-stilbene during sampling was considered. However, only a small signal of TST was observed, corresponding to less than 10% with respect to the CST signal, evidencing that there

was no large isomerization of the coating (Figure 4.14) during sampling. Additionally, the possibility of the elimination reaction is also discarded since this elimination mechanism has been described as time-consuming (with reaction times from hours to weeks) and requiring a substrate to take place at temperatures ranges of 34 – 101 °C (Buckles et al., 1962; Cristol and Bly, 1960; Tsai Lee et al., 1970), obtaining as product a mixture of trans-, cis-stilbene and other compounds depending on the reagent used. The samples here were prepared right after the experiment with the Cl_2 source for its analysis by washing the filters with acetone at room temperature, so no elimination reaction could have taken place during its preparation nor contamination with other reagents since only acetone was used. Moreover, the products described by the literature were not found on the chromatogram neither the mono-chlorinated derivative. Therefore, it is concluded that the evaporation of the coating has a major influence on the recovery rate experiments.

Buckles et al. (1962) described the bromination of cis-stilbene with the dl-isomer as the major product. Assuming that chlorine behaves like bromine, our results are consistent with this, since we obtained mainly dl-stilbene dichloride (retention time: 7.12 min)
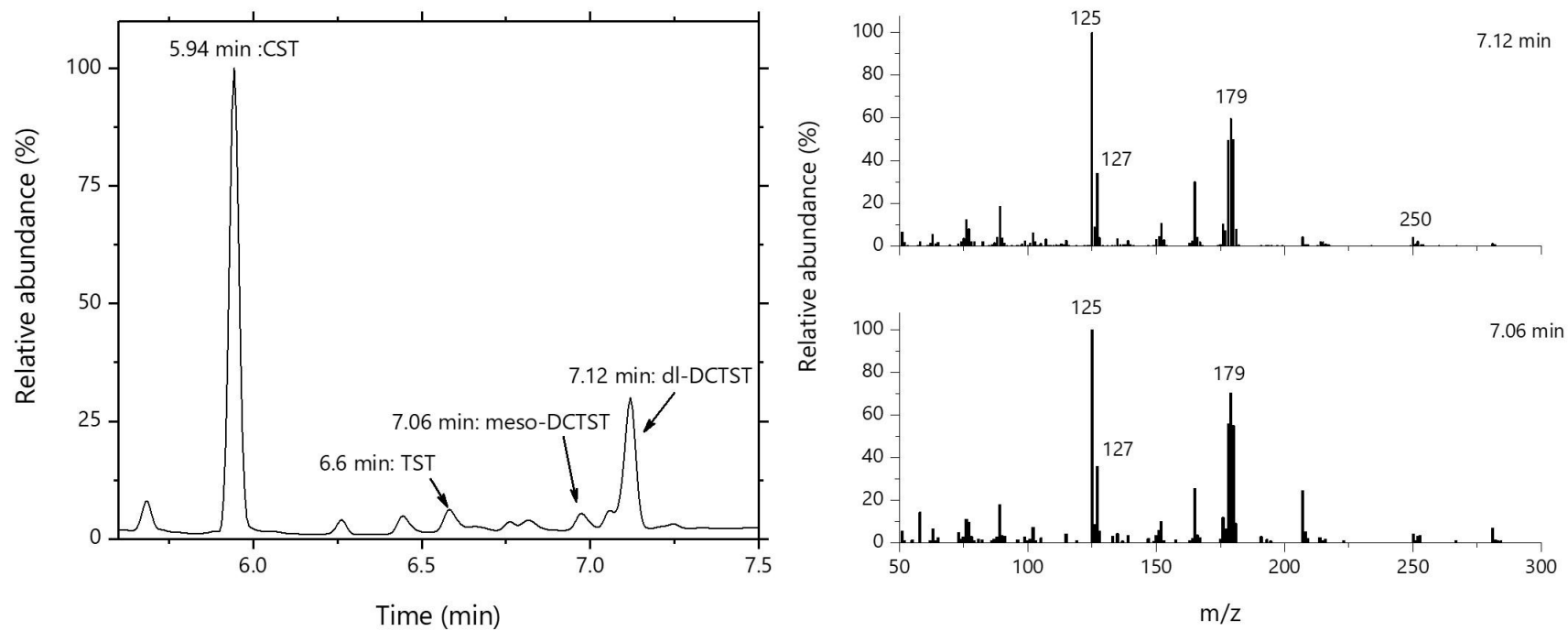
Figure 4.14. CST and dechlorinated derivatives chromatographic signals (left) with its respective MS spectrum (right), obtained from recovery rate experiment with sampling duration of 15 min. Numbers and arrows within the MS spectrum indicate the representative m/z

4.2.3. Summary

A method for sampling halogens in volcanic exhaust gases was devised using syringe filters impregnated with two previously tested coatings (TST and CST) and octenol instead of diffusion separators. The main aspects of the method are:

(1) Coated filters show better removal efficiency for chlorine gas at low coating rates compared to denuders.

(2) Cis-stilbene has a higher collection efficiency than TST and octenol, although the filters must be impregnated with an excess of it to allow for evaporation of the CST, since the open surface allows this process to occur.

(3) Sampling time depends on the amount of CST used; it can be estimated by the flow rate.

(4) Commercially available electronic sensors combined with a data acquisition unit prove to be useful on-line systems for monitoring the deposition performance of the different coatings at different sampling times and flow rates due to their high sensitivity in the low ppm range (0 - 0.75 ppm Cl_2).

(5) No isomerization of cis- to trans-stilbene was observed during sampling, so this does not affect field use for day or night measurements.

(6) Low recoveries despite high collection efficiency indicate evaporation of the coating during sampling.

4.3. Application of in-situ sampling techniques: Vulcano and Masaya case of study

4.3.1. Volcano settings

4.3.1.1. Vulcano

Vulcano Island (38.404° N, 14.962° E) is southernmost island of the Aeolian Island Arc, generated by the subduction of the Ionian plate beneath the European plate beneath the Tyrrhenian Sea. This volcano is the exposed summit of a volcanic edifice that rises up to the maximum height of 499 m.a.s.l., at Monte Aria (Inguaggiato et al., 2018). The island comprises four main volcanic structures: Southern Vulcano, Lentia Mountains, La Fossa Crater and Vulcanello (Figure 4.15). The volcano has been interpreted as a volcanic arc in a convergent tectonic setting composed exclusively of volcanic and epivolcanic rocks, with a high level in K_2O (Keller, 1980). La Fossa crater (391 m.a.s.l) was formed in early pre-historic times, in a 2.5 Km wide caldera characterized by the presence of at least five distinct crater rims and by a strong, diffuse alteration of the outcropping rocks due to a very active hydrothermal system. Since its last eruption in 1888 – 1890, the volcano has remained in a fumarolic state of activity, with some documented periods of unrest (Baubron et al., 1990; Paonita et al., 2013; Selva et al., 2020). A new period of volcanic unrest started in 2021 and is still ongoing.
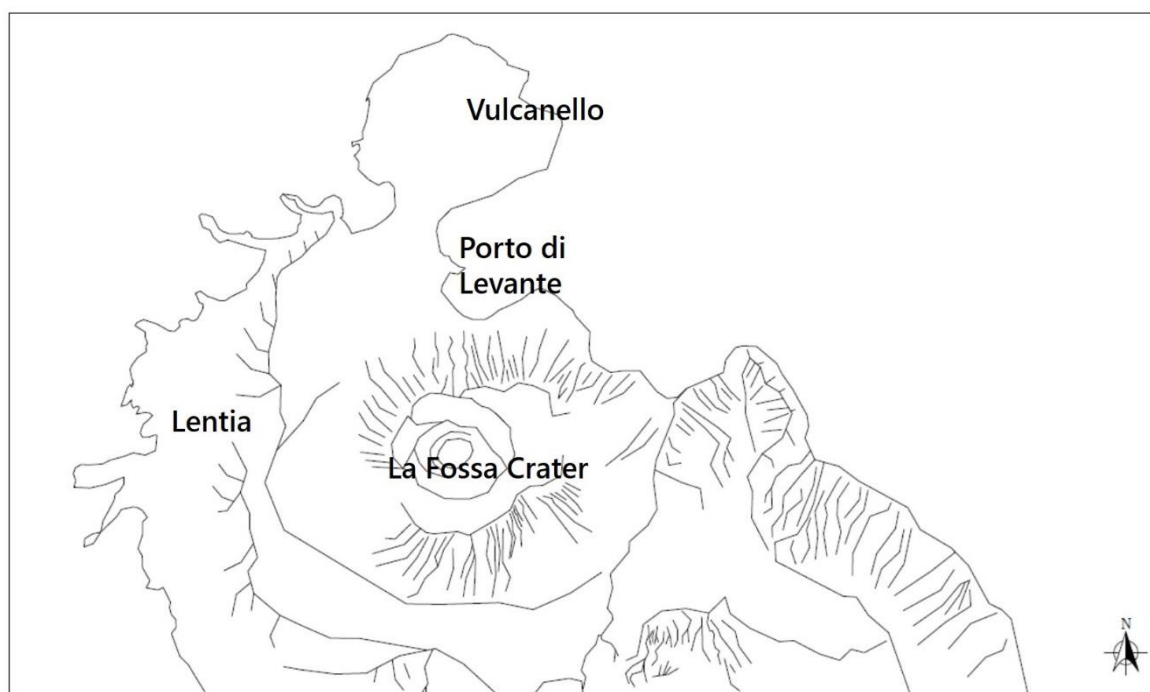

Figure 4.15. Vulcano Island main for structures: La Fossa, Vulcanello, Lentia and southern Vulcano.

4.3.1.2 Masaya

Masaya volcano is located in southwestern Nicaragua (11.984° N, 86.161° W), 20 – 25 Km southeast of the capital city, Managua. This is a persistently active basaltic shield volcano and caldera complex, that is composed of the summit Masaya caldera (~ 11.5 × 6.0 Km) and numerous pit craters: Nindirí, Santiago, San Fernando and San Pedro (Figure 4.16). The complex was formed by a sequence of explosive eruptions (Plinian and ignimbrite) and by repeated passive collapse due to underground magma withdrawal (Walker et al., 1993) and references therein). (Viramonte and Incer-Barquero, 2008)have described the complex as a caldera with elevation of 650 m.a.s.l, with a floor that rises to a maximum of 550 m.a.s.l at the rim of Santiago crater with an average of 264 m elsewhere. Masaya is one of 18 distinct volcanic centers that make up the Nicaraguan portion of the Central American Volcanic Arc (CAVA), which is formed as a result of the subduction of the Cocos Plate beneath the Caribbean Plate, along the Mesoamerican trench (Stoiber and Carr, 1973; Williams-Jones, 2001). Prolonged episodes of passive degassing and oscillations in the level of the magma column are characteristic of activity at Santiago crater, the currently active crater formed in 1859. Behavior in the historic period has been predominantly passive with repeated episodes of lava lake formation, strong degassing and subsequent quiescence (Aiuppa et al., 2018; Duffell et al., 2003; Walker et al., 1993). Due to the presence of the active lava lake that sometimes overflowed the crater, the volcano has been called the "Mouth of Hell" since the period of America's conquest (Viramonte and Incer-Barquero, 2008); and references therein).
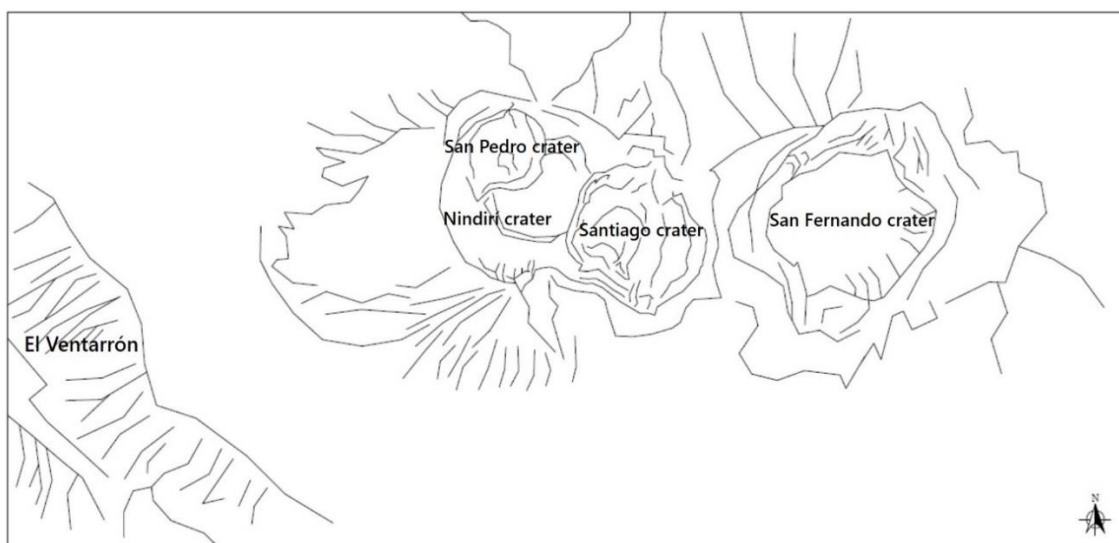

Figure 4.16. Schematic map showing the El Ventarrón Caldera and Masaya volcanic complex.

4.3.2. In-situ measurements

In-situ measurements were carried out during three different surveys: (1) between 22 – 24 January 2019 at Masaya volcano, Nicaragua; (2) between 24 – 26 September 2019; and (3) between 11 – 14 October 2020 at Vulcano Island, Italy. Table 4.6 summarizes an overview of the measurement places and meteorological data. The sampling was performed on days with generally good weather conditions (no rain and only gentle wind).
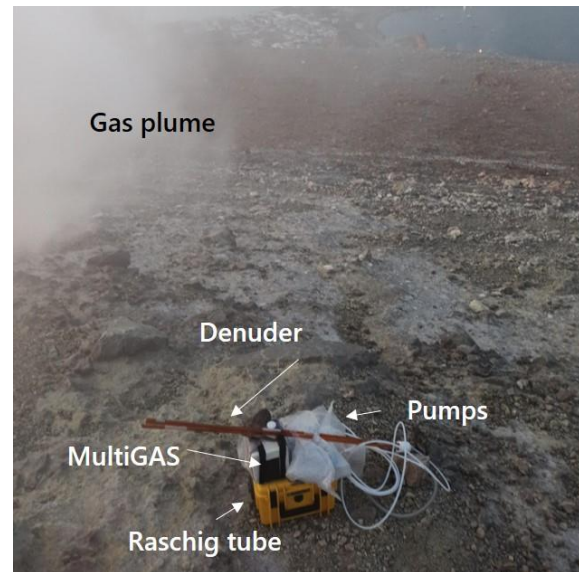
Figure 4.17. Instrumentation applied for the measurement of different gas species.

4.3.2.1. Sampling sites: Masaya

Figure 4.18 shows the four sampling locations at Masaya volcano at different distances from the active Santiago crater. The volcano was in a quiescent state with continuous plume degassing. The lava lake at Santiago pit crater appeared with minor incandesce with respect to reported in previous years (2015 – 2017). Samples were taken simultaneously at two sampling sites (Santiago – Pole and Nindirí or Santiago – Pole and Los Vientos). The duration time of each measurement was ~ 1h. An additional measurement was performed on the January 23rd at Cerro Ventarrón located ~ 2.5 km from Santiago rim.

Figure 4.18. Sampling sites at Masaya volcano complex: (A) Santiago rim – Pole, (B) Ninidirí rim, (C) Los Vientos, and (D) Cerro Ventarrón.

4.3.2.2. Sampling sites: Vulcano

Different sampling sites were selected around La Fossa Crater fumarole field choosing high emission vents and avoiding the cross-passing of tourists (Figure 4.19). Sampling time varied between 1 – 3 h depending on the emission state of the fumaroles. The first survey was characterized for good weather conditions (sunny and low wind speeds), while the second was characterized for cloudy weather with precipitations between the measurements, usually overnight. During the 2020 campaign an additional measurement was performed at night (Table 4.6). In both field campaigns, Vulcano was in quiescent state with degassing activity of variable intensity from several fumarolic vents located in the area of La Fossa crater.
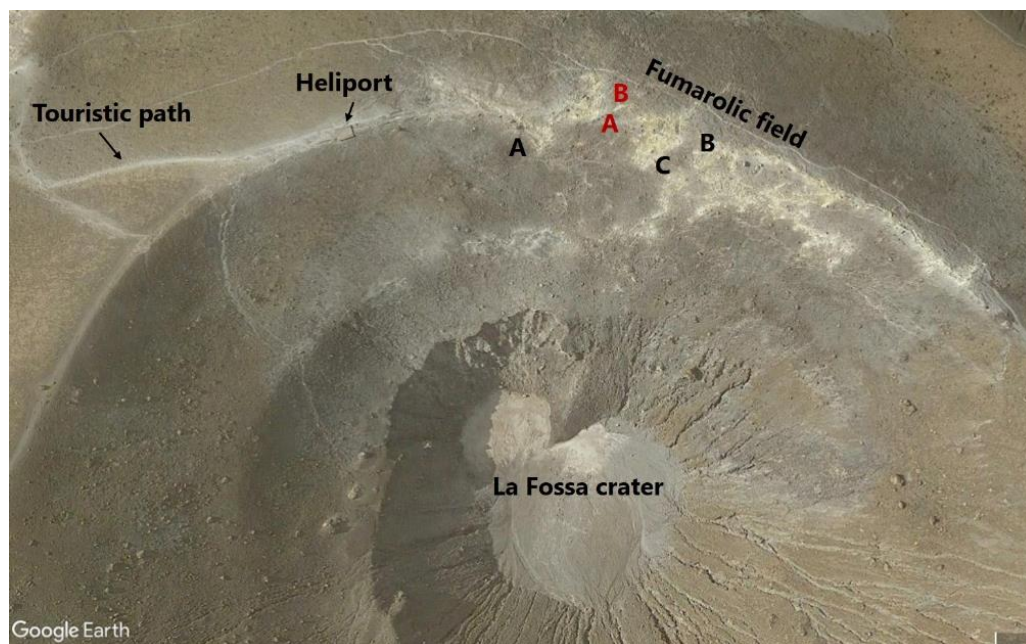
Figure 4.19. Location of sampling sites at La Fossa Crater. Black letters denote sampling sites during the 2019 survey, while red letters indicate sampling sites in 2020.

4.3.3. CO_2/SO_2 molar ratios

Masaya volcano concentrations ranged from 0.5 to 20.5 ppmv SO_2 and from 0.9 to 28.3 ppmv CO_2, whereas at Vulcano these gases ranged between 0.9 – 177.8 ppmv SO_2 and from 398.6 to 11357.7 ppmv CO_2. Table 4.7 lists mean and standard deviation of the CO_2/SO_2 molar ratios obtained using the RatioCalc software.

Figure 4.20a illustrates the temporal variation of CO_2/SO_2 molar ratios using published data taken prior and following the formation of the lava lake at Santiago crater pit (Moor et al., 2017b, Rüdiger et al., 2018). During our survey, the lava lake was still present although we

Table 4.6. Daily weather conditions and sampling time recorded during the field campaigns at Masaya and La Fossa crater.

Date	Place	Wind speed (m/s)	T (°C)	Relative Humidity (%)	P (mbar)	Sampling time (min)*	Distance to the main vent (m)
Masaya							
22/01/2019	Santiago rim/ Pole	10.0	25.0	65.0	949.0	66	0
22/01/2019	Nindirí rim	n.a**	26.2	n.a	929.0	60	400
23/01/2019	Santiago rim/ Pole	10.0	26.0	55.0	949.0	66	0
23/01/2019	Nindirí rim	n.a	25.0	n.a	928.0	60	400
23/01/2019	Cerro Ventarrón	n.a	33.9	n.a	931.0	142	2,400
24/01/2019	Santiago rim/ Pole	n.a	30.0	n.a	922.0	64	0
24/01/2019	Los Vientos	9.0	32.0	n.a	922.0	64	250
Vulcano							
24/09/2019	Fumarole A	5.2	26.3	66.5	982.2	179.1	2
25/09/2019	Fumarole B	2.8	24.6	70.0	982.9	120.2	2
26/09/2019	Fumarole C	2.9	24.2	71.8	984.0	89.4	1
11/10/2020	Fumarole A	n.a	21.0	65.0	n.a	180.1	2
11/10/2020	Fumarole B -night	n.a	18.5	77.5	n.a	122.3	1
12/10/2020	Fumarole B	n.a	17.0	69.0	n.a	181.1	1
14/10/2020	Fumarole B	n.a	22.0	n.a	n.a	60	1

* Sampling time for Raschig tube and denuders, **n.a.: not available

observed less incandescence with respect to the reported before (Figure 4.20b). The decrease on the activity of the lava lake is evident on our CO_2/SO_2 ratios, with a C-poorer signature (6.6 ± 1.2) than the one during the "rebirth of the lava lake" period reported by (Aiuppa et al., 2018) in November – December 2015 (12.2 ± 6.3). Here, the authors suggested an increase in the supply of CO_2 from a shallow magma body. Since there was a decrease in the lava lake activity, our results are consistent with that suggestion, having compositions similar to the ones preceding and following the lake formation (Table 4.8). Aiuppa et al. (2017) presented a CO_2/S compilation for arc volcanoes, appointing Masaya with C-rich signature in the range of ~ 2.7 – 4, which are ratios with values below the presented here. However, their estimation corresponds to a larger period of time (1998 – 2006) including also even lower lava lake activity, while our result reflects less than a week in 2019, considering our observations still in good agreement with the characteristic C-rich signature of this volcano.
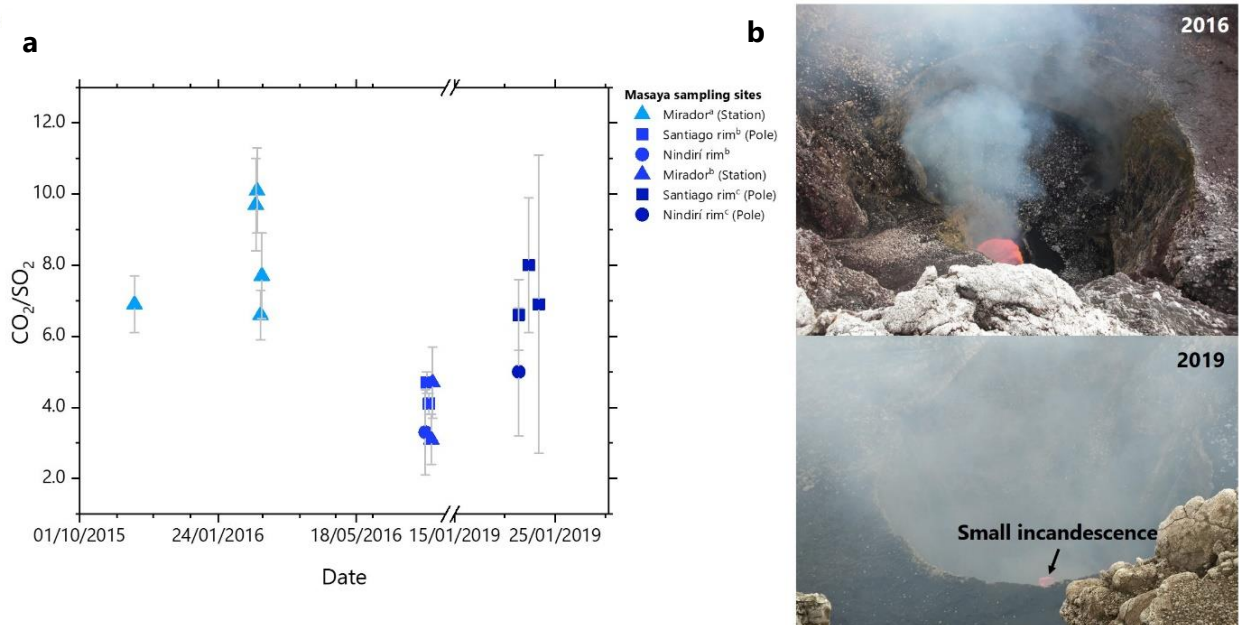

Figure 4.20. a) Comparison of CO2/SO2 ratios of Masaya's volcanic plume at different sampling sites obtained by MultiGAS instrument. Gas data source: ^{a}de Moor et al., 2017; ^{b}Rüdiger et al., 2018; ^{c}This work. (b) Picture of states of lava lake in 2016 and in 2019 by N. Bobrowski and X. Gutiérrez, respectively.

Table 4.7. CO_2/SO_2 molar ratios and SO2 peak concentrations acquired with MultiGAS method.

Date	Place	SO₂ Max (ppmv)	CO₂/SO₂
Masaya			
22/01/2019	Santiago rim – Pole	10.4	6.6 ± 0.7
22/01/2019	Nindirí rim	20.5	5.0 ± 1.8
23/01/2019	Santiago rim – Pole	15.3	8.0 ± 1.6
24/01/2019	Santiago rim – Pole	8.1	6.9 ± 3.5
	Average	**13.6 ± 5.5**	**6.6 ± 1.2**
Vulcano			
24/09/2019	Fumarole A	177.8	18.0 ± 0.6
25/09/2019	Fumarole B	94.6	19.4 ± 2.3
26/09/2019	Fumarole C	177.8	18.6 ± 0.4
11/10/2020	Fumarole A	110.1	16.6 ± 1.8
11/10/2020	Fumarole B-night	110.1	16.4 ± 1.5
12/10/2020	Fumarole B	45.8	19.9 ± 0.6
14/10/2020	Fumarole B	22.9	23.2 ± 2.9
Average		**105.6 ± 59.2**	**18.9 ± 2.3**

Table 4.8. CO_2/SO_2 molar ratios detected at Masaya volcanic plume between 2015 - 2019.

Sampling dates	Lava lake period	Mean CO₂/SO₂	Reference
05/03/2014 – 01/09/2014	P	6.3 ± 3.1	Aiuppa et al., 2018
04/03/2015 – 28/05/2015	P	4.9 ± 2.0	
16/11/2015	P	6.9 ± 0.8	(Moor et al., 2017a)
15/11/2015 – 10/12/2015	LF	12.2 ± 6.3	Aiuppa et al., 2018
22/02/2016 – 28/03/2016	F	5.4 ± 2.1	
25/02/2016 – 21/07/2016	F	7.0 ± 2.8	(Moor et al., 2017a)
14/07/2016 – 20/07/2016	F	3.6 ± 0.6	Aiuppa et al., 2018
19/07/2016 – 01/03/2017	F	5.5 ± 1.9	Rüdiger et al., 2018

P: prior, LF: lava lake formation, F: following

For Vulcano, temporal variation of the CO₂/SO₂ molar ratios at La Fossa crater fumaroles is shown in Figure 4.21. Our measurements are within each other's confidence intervals (2019: 18.7 ± 0.7, 2020: 20.4 ± 2.2). However, these are in disagreement with previously reported data

acquired by FTIR and MultiGAS devices. Moreover, our 2020 results differ from the one reported by the local Observatory for the similar period. Nevertheless, these discrepancies might be due to the sampling site, since La Fossa is known for hosting fumaroles with different emission rates and temperatures, which influences the composition of the degassed emissions. Aiuppa et al. (2005) already described the chemical heterogeneity of the fumarolic field with $CO_2/(SO_2+H_2S)$ ratios ranging from 10 – 131 (35.0 ± 21.0). These values represent composition from the rim and inner crater fumaroles together. Furthermore, the author classify composition according to the temperature of the fumaroles: (a) close-to-boiling fumaroles with a S-poor composition ($CO_2/(SO_2+H_2S) \geq 50$) at the inner crater, and (b) under-saturated fumaroles with T > 130° C ($CO_2/(SO_2+H_2S) \sim 20$ to 30) at the rim. Our measurements were performed at Vulcano's rim with molar ratios ranging from 16.4 – 23.2 (18.9 ± 2.3), agreeing with composition range just described. Following Aiuppa et al. (2017), Vulcano has a CO_2-rich composition (mean CO_2/SO_2: 9.2 ± 4.4). The authors estimated the mean C/S_t ratio using 20 years of measurements performed by direct sampling, mostly at high-temperature fumaroles. This could be the reason of discrepancy with our results, since our ratios are estimated in a shorter period of time using a MultiGAS instrument, which measures only SO_2. Nevertheless, our results are still within the group of arc volcanoes with C-richer composition (CO_2/SO_2 > 4.0).

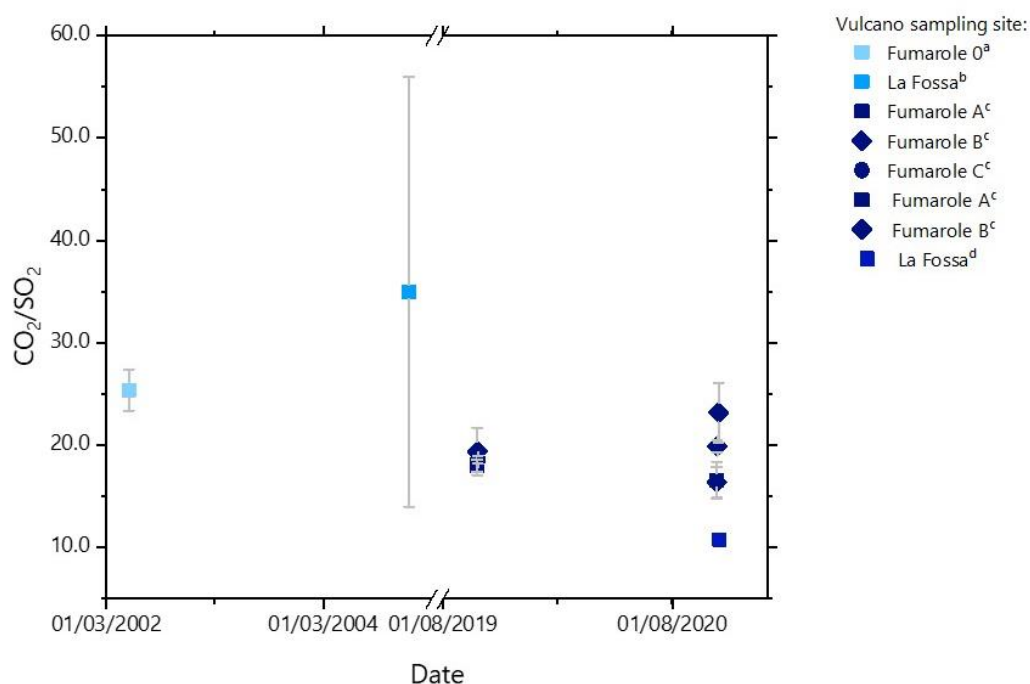*Figure 4.21. Temporal CO2/SO2 variation at Vulcano, Italy using FTIR (squares) and MultiGAS (diamonds) instruments. Gas data source: a (Aiuppa et al. 2004); b (Aiuppa 2005b); cThis work; dINGV-report, October 2020.*

4.3.4. Carbon and halogen to sulfur ratios (C/S and X/S)

Analysis obtained from the Raschig Tube samples were processed to correct for blank effects (atmospheric contribution) according to Wittmer et al. (2014), by substracting the amount of analyte in the blank ($C_{b,i}$) from the amount of analyte in the sample (C_i): $C_{analyte} = C_i - C_{b,i}$. Results of the analyzed samples using the RT are summarized in Table 4.9, calculated according to Wittmer et al. (2014). Molar mixing ratios (CO_2/S and X/S, where X = F, Cl, Br, I) were obtained and summarized on Table 4.10. Larger errors are encountered within the CO_2 concentrations obtained from the RT samples, evidencing perhaps systematics errors on the titration performed, which led to higher ratios than the acquired by MultiGAS.

Comparison of halogen-to-sulfur molar ratios obtained from measurements performed at Masaya in 2016 (Rüdiger et al., 2021) and our estimations are presented in Figure 4.22. The samples were taken at the same spots and using the same sampling method (RT) in each study. Rüdiger et al. (2021) presented F/S ratios of 0.077 ± 0.019 at Santiago's crater and 0.079 ± 0.005 at Nindirí rim, and Cl/S of 0.69 ± 0.04 and 0.92 ± 0.28, respectively. Our results are in agreement with these ones obtaining F/S of 0.04 ± 0.03 at the crater and 0.05 ± 0.01 at Nindirí rim, whereas Cl/S ratios are 0.6 ± 0.09 and 0.7 ± 0.09, respectively. However, Br/S mean value in 2016 (7.4 ± 1.7) × 10^{-4} is higher than our 2019 estimation ((1.4 ± 1.4) × 10^{-4}), although in the same order of magnitude as well as previous studies (~ 10^{-4}) performed with filter packs at Masaya (Oppenheimer et al., 2006; Witt et al., 2008). Higher discrepancies are encountered with I/S with a value of one order of magnitude lower ((2.56 ± 2.25) × 10^{-6}) than the 2006 (2.0 × 10^{-5}) and 2016 (4.6 × 10^{-5}) observations (Rüdiger et al., 2021, Witt et al., 2008), but within those measured at Etna (4.0 – 6.7 × 10^{-6}). However, this decrease in the Br/S and I/S ratios might be related to Masaya's state of activity at the time of the surveys (different stages of magma degassing).

Table 4.9. Concentration (± error) of detected volcanic gases by RT in the gas plume of Masaya and Vulcano, calculated from the molar concentrations of each analyte and the sampled air volume.

Date	Place	CO_2 (ppm)	S(ppm)	F(ppm)	Cl (ppm)	Br(ppt)	I (ppt)
Masaya							
22/01/2019	Santiago rim/ Pole	157.2 ± 26.7	7.4 ± 1.3	0.4 ± 0.07	3.6 ± 0.6	551.9 ± 93.8	0.6 ± 0.1
22/01/2019	Nindirí rim	350.8 ± 59.6	3.9 ± 0.7	0.2 ± 0.04	2.4 ± 0.4	942.9 ± 160.3	37.8 ± 6.4
23/01/2019	Santiago rim/ Pole	184.9 ± 31.4	6.8 ± 1.2	0.4 ± 0.06	3.8 ± 0.6	181.4 ± 30.8	8.6 ± 1.5
23/01/2019	Nindirí rim	152.2 ± 25.9	3.2 ± 0.5	0.1 ± 0.03	2.3 ± 0.4	n.a	n.a
23/01/2019	Cerro Ventarrón	241.0 ± 41.0	n.a	n.a	0.4 ± 0.1	821.5 ± 139.6	4.2 ± 0.7
24/01/2019	Santiago rim/ Pole	223.2 ± 37.9	6.8 ± 1.1	n.a	4.5 ± 0.8	1254.1 ± 213.2	31.0 ± 5.3
24/01/2019	Los Vientos	259.3 ± 44.1	5.1 ± 0.9	0.2 ± 0.03	2.7 ± 0.5	620.3 ± 105.4	12.1 ± 2.1
Vulcano							
24/09/2019	Fumarole A	642.6 ± 109.2	14.3 ± 2.4	0.3 ± 0.1	2.4 ± 0.4	n.a	n.a
25/09/2019	Fumarole B	980.7 ± 166.7	8.6 ± 1.5	0.2 ± 0.03	0.9 ± 0.2	n.a	n.a
26/09/2019	Fumarole C	1449.5 ± 246.4	11.5 ± 2.0	0.2 ± 0.04	1.2 ± 0.2	n.a	n.a
11/10/2020	Fumarole A	579.4 ± 98.5	16.1 ± 2.7	0.04 ± 0.01	0.5 ± 0.1	n.a	n.a
11/10/2020	Fumarole B -night	596.3 ± 101.4	12.6 ± 2.1	0.2 ± 0.03	2.6 ± 0.4	n.a	n.a
12/10/2020	Fumarole B	281.5 ± 47.9	6.8 ± 1.2	0.1 ± 0.02	1.7 ± 0.3	n.a	n.a
14/10/2020	Fumarole B	500.0 ± 85.0	5.9 ± 1.0	0.3 ± 0.2	1.7 ± 0.3	n.a	n.a

n.a: not available

Table 4.10. Molar Ratios (± error) of species obtained by RT.

| Date	Place	CO_2/S	F/S	Cl/S	Br/S × 10^{-4}	I/S × 10^{-6}	Cl/F
Masaya							
22/01/2019	Santiago rim/ Pole	35.3 ± 8.5	0.1 ± 0.01	0.5 ± 0.1	1.3 ± 0.2	5.1 ± 1.2	8.8 ± 2.1
22/01/2019	Nindirí rim	39.9 ± 9.6	0.1 ± 0.01	0.6 ± 0.1	1.4 ± 0.3	0.2 ± 0.03	9.8 ± 2.4
23/01/2019	Santiago rim/ Pole	35.5 ± 8.5	0.1 ± 0.01	0.6 ± 0.1	1.2 ± 0.3	0.6 ± 0.1	9.9 ± 2.4
23/01/2019	Nindirí rim	48.1 ± 11.6	0.05 ± 0.01	0.7 ± 0.2	n.a	n.a	15.5 ± 3.7
24/01/2019	Santiago rim/ Pole	33.1 ± 7.9	n.a	0.7 ± 0.2	1.9 ± 0.4	4.6 ± 1.1	n.a
24/01/2019	Los Vientos	50.6 ± 12.2	0.03 ± 0.01	0.5 ± 0.1	1.2 ± 0.3	2.4 ± 0.06	16.9 ± 4.1
Vulcano							
24/09/2019	Fumarole A	642.6 ± 109.2	0.02 ± 0.01	0.2 ± 0.04	n.a	n.a	8.7 ± 1.8
25/09/2019	Fumarole B	980.7 ± 166.7	0.02 ± 0.01	0.1 ± 0.02	n.a	n.a	5.0 ± 1.0
26/09/2019	Fumarole C	1449.5 ± 246.4	0.02 ± 0.01	0.1 ± 0.02	n.a	n.a	5.0 ± 1.0
11/10/2020	Fumarole A	579.4 ± 98.5	0.03 ± 0.001	0.03 ± 0.01	n.a	n.a	10.2 ± 2.2
11/10/2020	Fumarole B -night	596.3 ± 101.4	0.01 ± 0.01	0.2 ± 0.04	n.a	n.a	14.1 ± 3.0
12/10/2020	Fumarole B	281.5 ± 47.9	0.02 ± 0.01	8.7 ± 0.3	n.a	n.a	16.0 ± 3.4
14/10/2020	Fumarole B	500.0 ± 85.0	0.03 ± 0.01	17.7 ± 0.3	n.a	n.a	8.4 ± 1.8

b.d.l: below detection limit

n.a: not available
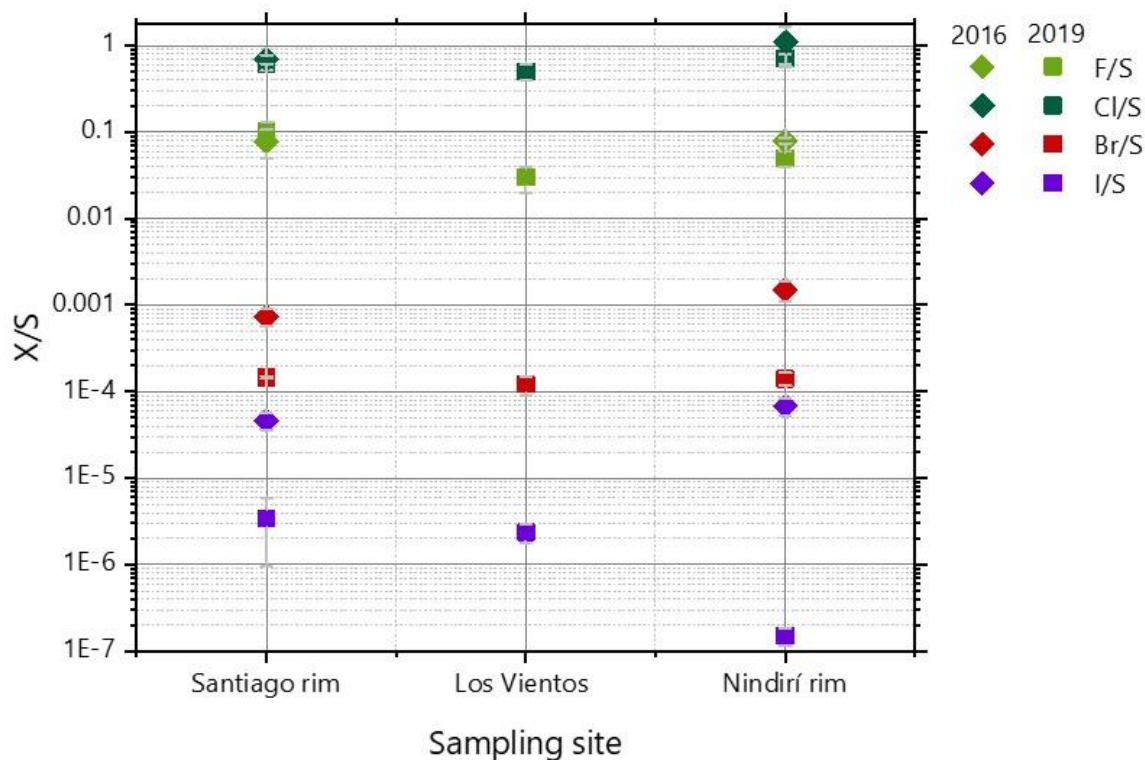
Figure 4.22. Halogen-to-sulfur molar ratios (X/S, where X = F, Cl, Br, I) measured at different sampling sites at Masaya volcano in 2016 (diamonds – Rüdiger et al., 2021) and 2019 (squares – this work).

Mean molar Cl/S and F/S ratios were 0.2 ± 0.1 and 0.02 ± 0.1, respectively, at La Fossa crater, Vulcano, Italy. These are similar to those measured in 2016 with values of 0.1 ± 0.02 and 0.08 ± 0.01. However, a large discrepancy is observed with measurements performed in 2002 by means of filter packs and FTIR. Moreover, those measurements are not within each confidence interval even though the authors stated good agreement between their sampling methods due to the fact that their estimations are in the same order of magnitude. However, those measurements were performed at fumarole 0 (T = 340 °C) with a sampling duration of 30 minutes. This are different settings from our sampling conditions, since we didn't sample on the same fumarole in each survey. Also, our results evidence an increase in the Cl/S ratios in between campaigns of around 2 times more than the previous year. Figure 4.23 shows the Cl/S ratios as a function of the sampled air volume for each measurement performed. All ratios agree well within each survey, with exception of samples at fumaroles A. However, the plot evidence these deviations are not related to the sampled air volume but possibly due to the different variations on the sulfur concentration as a result of intermittent emissions in fumarole A, for which the sampling site was changed to B where the emissions were almost constant.
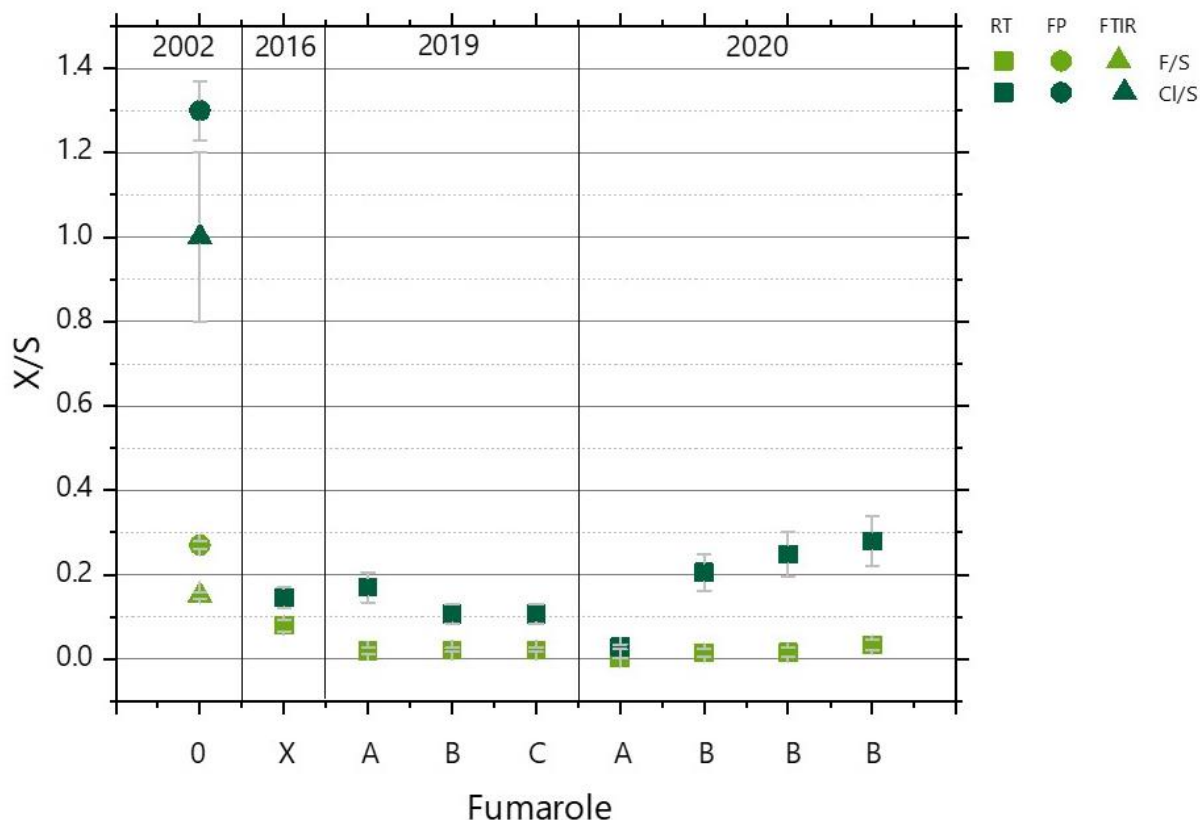
Figure 4.23. Temporal variation of halogen-to-sulfur molar ratios (X/S, where X = F, Cl, Br, I) measured at different fumaroles in La Fossa crater by means of Raschig tube (RT), filter packs (FP) and FTIR.

4.3.5. Reactive halogens species (RHS)

4.3.5.1. Day-time measurements

Here we present a second set of RHS data for Masaya and the first one for Vulcano Island, obtained by the denuder technique. In both cases, the concentrations are in the ppt level (Table 4.11), representing << 1% of the total halogen composition obtained from the RT samples. Molar ratios of RHS to total halogen and total sulfur were obtained using the denuder values against the RT concentrations. Figure 4.24 shows RHS ratios as a function of the distance from the vent, matching the tendency observed by Rüdiger et al. (2021), where the RHS ratios increased with the distance, evidencing the halogen speciation as a function of plume age. Vulcano's RHS ratios are similar to the ones taken at Santiago rim, with values in the range of ~10^{-6}. This behaviour match model predictions at near vent conditions (e.g., crater rim, fumaroles), where only small quantities of RHS are produced (Gerlach, 2004; Martin et al., 2006). Samples further distance from the vent were collected only at Masaya as shown in Figure 4.24. Our results are two and one order of magnitude lower than the samples taken in

2016 for chlorine and bromine, respectively (Table 4.12). This is probably due to the already mentioned decrease of activity of the lava lake. Warnach et al. (2019) indicated that when magma composition doesn't change, high BrO/SO_2 ratios are associated with degassing from magma at shallow depths. This is consistent with the elevated shallow magma circulation described by Aiuppa et al., (2018), that was considered as a new batch of gas-rich magma that culminated with the formation and growth of the lava lake at Santiago crater. Dinger et al. (2021) indicated an annual cyclicity in the analysed BrO/SO_2 time series (2014 – 2020) with amplitudes between $1.4 - 2.5 \times 10^{-5}$, with a maximum in early March. However, here we suggest that the discrepancy between the 2016 and the 2019 measurements, is not related to seasonal changes but rather related to the activity of the volcano since our measurements were conducted more than a year later after the peak activity of the lava lake, where the decrease in the magma feeding of the shallow system was lower (Figure 4.22 and Figure 4.24). In addition, the same study estimated the BrO fluxes emitted in the period of high activity of the lava lake (72 ± 18 Kg d^{-1}, Nov 2015 – Mar 2018) and the following period (56 ± 18 Kg d^{-1}, Jun 2018 – March 2020), supporting the decrease of emissions during the period of our measurements.

4.3.5.2. Night-time measurement

Collection of RHS during night time was achieved at Vulcano in 2020 (Table 4.11). These measurements have values similar to the more concentrated samples from 2019, for both bromine and chlorine. Rüdiger et al. (2021) presented night-time measurements at Masaya, also finding similar values for bromine as those measured during day-time. Although, there are model simulations at night-time, only BrO/SO_2 evolution has been published (Roberts et al., 2009, Surl et al., 2021). However, overnight production of BrO ceases and the remaining reactive bromine (BrX) is converted to other RHS (e.g., Br_2, BrCl, HOBr) via hydrolysis of $BrONO_2$ and HOBr, and by reaction with HCl. Futhermore, the recent study presented for Masaya volcano, gives a similar explanation for the active chlorine considering the reactions that can take place during night-time. Here, the authors suggests that the remaining Cl atoms produced during the day are recombined to form Cl_2, increasing its amount during night since it cannot be photolyzed, validating the similar amounts of reactive chlorine obtained with the denuder technique.

Table 4.11. Concentrations and molar mixing ratios of RHS found in analysed samples by GC-MS and comparison with total chlorine and total sulfur (RT).

Date	Location	Reactive halogens		BrX/Br	ClX/Cl × 10⁻⁵	BrX/S × 10⁻⁵	ClX/S× 10⁻⁶
		BrX (ppt)	ClX (ppt)				
Masaya							
22.01.2019	Santiago rim/ Pole	21.1 ± 3.6	b.l.d	0.02 ± 0.01	n.a	0.3 ± 0.1	n.a
22.01.2019	Nindirí rim	18.4 ± 3.1	27.3 ± 2.3	0.03 ± 0.01	1.1 ± 0.2	0.5 ± 0.1	0.7 ± 0.1
23.01.2019	Santiago rim/ Pole	27.9 ± 4.7	59.3 ± 6.8	0.03 ± 0.01	1.6 ± 0.3	0.4 ± 0.1	0.9 ± 0.2
23.01.2019	Nindirí rim	7.5 ± 1.3	b.l.d	n.a	n.a	0.2 ± 0.05	n.a
23.01.2019	Cerro Ventarrón	b.l.d	b.l.d	n.a	n.a	n.a	n.a
24.01.2019	Santiago rim/ Pole	19.2 ± 3.3	18.2 ± 3.1	0.02 ± 0.004	0.4 ± 0.1	0.3 ± 0.1	0.3 ± 0.006
24.01.2019	Los Vientos	9.8 ± 1.7	b.l.d	0.02 ± 0.005	n.a	0.2 ± 0.05	n.a
Vulcano							
24/09/2019	Fumarole A	32.6 ± 2.2	39.4 ± 1.8	n.a	1.6 ± 2.9	0.2 ± 0.04	0.3 ± 0.05
25/09/2019	Fumarole B	28.9 ± 1.6	7.9 ± 0.4	n.a	8.6 ± 1.5	0.3 ± 0.06	0.09 ± 0.02
26/09/2019	Fumarole C	b.l.d	9.7 ± 0.5	n.a	0.8 ± 0.1	n.a	0.08 ± 0.02
11/10/2020	Fumarole A	b.l.d	b.l.d	n.a	n.a	n.a	n.a
11/10/2020	Fumarole B -night	31.5 ± 1.8	24.9 ± 1.4	n.a	0.9 ± 0.2	0.3 ± 0.05	0.2 ± 0.04
12/10/2020	Fumarole B	15.5 ± 1.8	3.0 ± 0.4	n.a	0.2 ± 0.04	0.2 ± 0.04	0.04 ± 0.001
14/10/2020	Fumarole B	78.8 ± 4.4	16.0 ± 0.7	n.a	1.0 ± 0.2	1.3 ± 0.2	2.7 ± 0.5

b.d.l: below detection limit

n.a: not available

Table 4.12. Comparison of mean molar ratios of RHS to total halogen and total sulfur from samples taken at ground in Masaya volcano.

RHS	Rüdiger et al. (2021)			This work		
	Santiago rim	Nindirí rim	Ventarrón	Santiago rim	Nindirí rim	Ventarrón
ClX/S× 10⁻⁶	210 ± 40	1600 ± 900	n.a	2.7 ± 0.06	6.94 ± 1.32	n.a
ClX/Cl × 10⁻⁶	27.0 ± 7.0	1100 ± 300	n.a	4.07 ± 0.98	11.4 ± 2.16	n.a
BrX/S × 10⁻⁵	13.0 ± 6.0	50 ± 34	n.a	2.4 ± 0.5	3.53 ± 1.62	n.a
BrX/Br	0.2 ± 0.1	0.67 ± 0.05	0.76 ± 0.26	0.02 ± 0.004	0.03 ± 0.01	n.a

n.a: not available
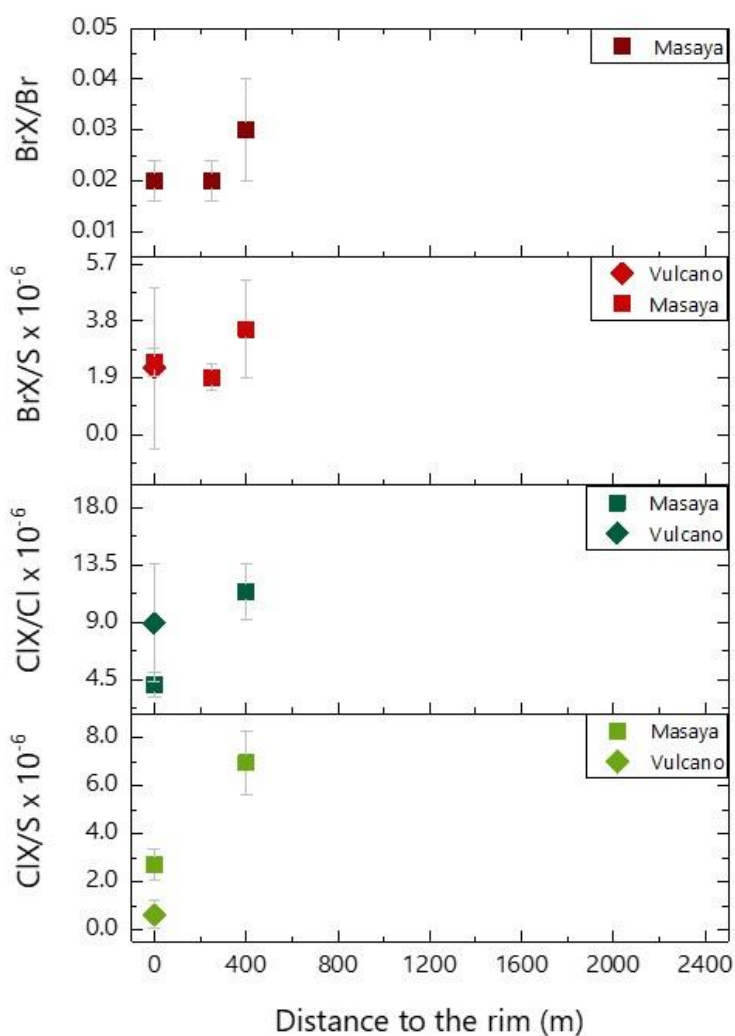
Figure 4.24. Reactive halogen species (RHS) molar ratios with respect to the distance from the main vent.

4.3.6. Summary

The chemical composition of volcanic gases at Masaya volcano, Nicaragua and Vulcano, Italy; is evaluated by three different in-situ sampling techniques: MultiGAS, Raschig tube and diffusion denuder in order to obtained major gases compositions (CO_2 and S) and traceable gases (Cl, F, Br and I). Our results confirm that both Masaya and Vulcano have a C-rich composition with mean CO_2/SO_2 molar ratios of 6.6 ± 1.2 and 18.9 ± 2.3, respectively. These values also display the signature of their respective arc segments (continental arc and island arc, respectively). Aiuppa et al. (2018) stated that CAVA volcanism has a mean CO_2/SO_2 molar ratio of 2.0 ± 1.0, with Nicaragua's compositions being richer due to C extraction by fluids formed along a "wet" slab and/or subduction of a substantial section of marine carbonates, while Italy has a mean CO_2/SO_2 molar ratio of 7.6 ± 1.4, with island arc contributing with additionally crustal CO_2. Also, we report total halogen compositions with their corresponding halogen to sulfur ratios, showing different variations according to the sampling site, especially in fumarole samples, where the gas plume was not always continuous and/or wind direction changed its path. Furthermore, we determine the sum of reactive bromine and chlorine species separately by means of the denuder technique, increasing the dataset for Masaya and extending to Vulcano. This data shows the speciation of halogens with respect to the distance to the emission vent as predicted by models (von Glasow, 2010; Roberts et al., 2014; Surl et al., 2021), and confirmed by field measurements (Rüdiger et al., 2021). Additionally, we present results obtained from a measurement performed during night-time. This data supports the suggestion made with the study at Masaya (Rüdiger et al., 2021), that evidence the continuation of halogen speciation during night via heterogeneous reactions.

4.4. Geochemical characterization of Santa Ana and San Miguel by means of real-time measurements

4.4.1. Volcano settings

4.4.1.1. Santa Ana

Santa Ana volcano (13.853° N, 89.630° W), also known as Ilamatepec, is the highest volcano in El Salvador (2,381 m.a.s.l), located at 40 Km west from the capital city San Salvador (population > 1.7 million) and 15 Km from Santa Ana city (population > 550,000). This active stratovolcano is part of the Santa Ana-Izalco-Coatepeque volcanic complex located at the intersection of the NW-SE regional fault system and the southern boundary of the Central American Graben (Meyer-Abbich, 1956). On its northeast flank lies Coatepeque caldera, an elliptical depression of 6.5 × 10.5 Km; and on its southern-southeast flanks, Izalco volcano and further numerous older cinder cones and explosion craters are found in the surroundings (Figure 4.25). The edifice consists of a large hydrothermal vent with four concentric craters in its summit, the largest one with a radius of 1.5 Km, and the innermost one with a radius of 0.5 Km. The later crater formed after the 1,904 eruption and host a small (~ 200 m diameter) acidic lake and an adjacent fumarole field on the western crater wall (Bernard et al., 2004; Laiolo et al., 2017).
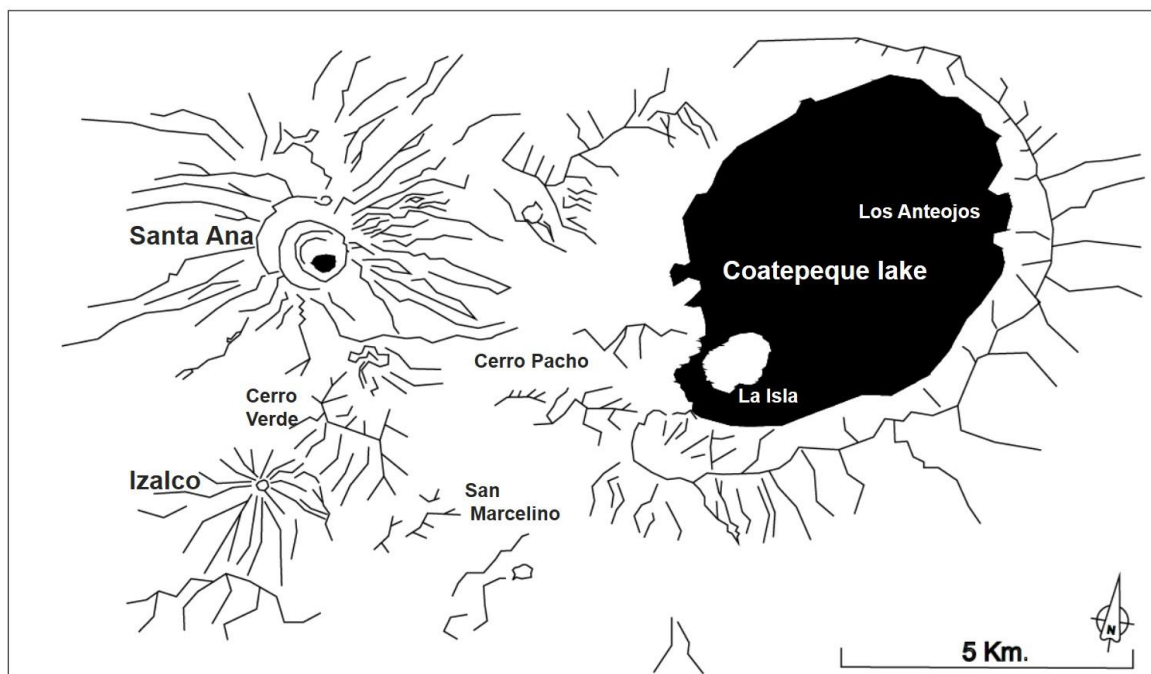

Figure 4.25. Geological map with the major volcano-structural features of the Santa Ana-Izalco-Coatepeque volcanic complex.

4.4.1.2. San Miguel

San Miguel volcano, locally named Chaparrastique, is an active volcano located at the eastern part of El Salvador (13. 434° N, 88.269° W). It rises 2,310 m.a.s.l in the proximity (~ 11 Km) of the communities of San Miguel, El Tránsito, San Rafael Oriente, and San Jorge (Major et al., 2001). It lies on the eastern segment of the Central Graben of the country, crossed by the regional NW-SE fault system (Bonforte et al., 2016). Its northern flank reaches the river San Esteban, whereas the western flank is truncated against the Ojo de Agua (Cerro El Limbo) and Chinameca (Cerro El Pacayal) volcanoes (Chesner et al., 2004) (Figure 4.26).

This stratovolcano has a symmetrical cone shape with steep upper slopes (> 40 degrees). The edifice consists of two major cones, the ancestral one at the east of the summit, and a younger one produced by the collapse of the ancestral cone with a central crater of ~ 900 m in diameter and several adventive cones (Escobar, 2003).
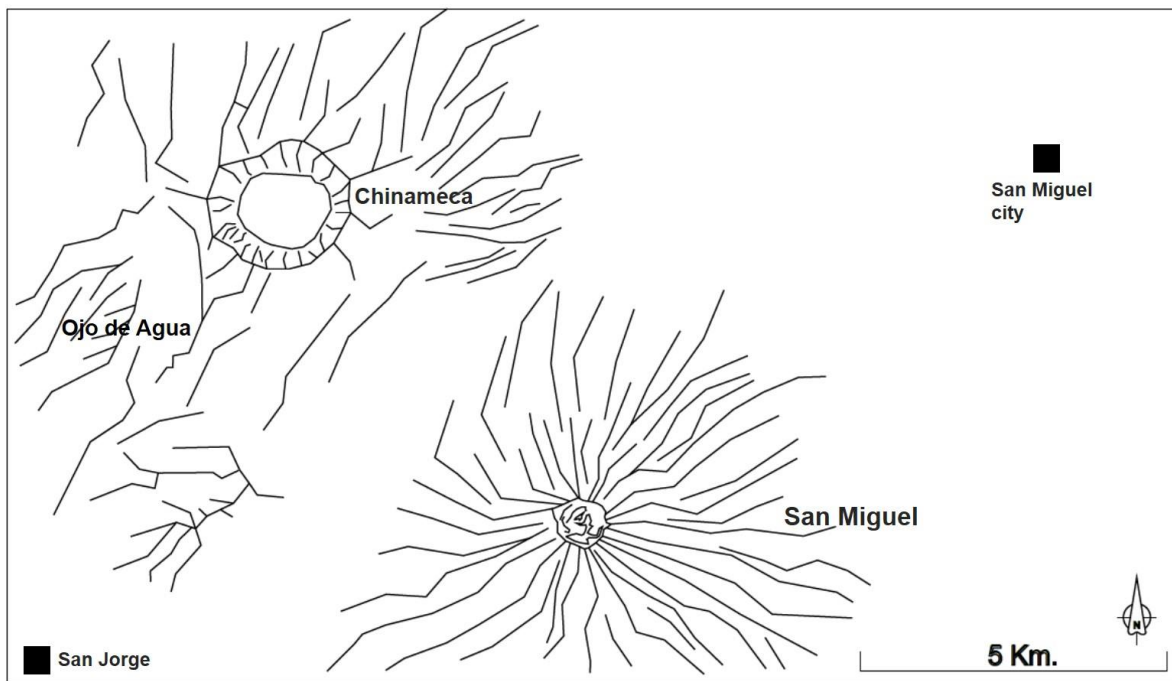

Figure 4.26. Structural map of San Miguel volcano and its surroundings. Black filled squares indicate important cities around the volcano.

4.4.2. Sampling sites

The composition of gases emitted by Santa Ana and San Miguel volcanoes was investigated using both remote-sensing and in-situ techniques (MultiGAS, Rashig tube and denuder). The location for in-situ sampling was chosen according to accessibility and dominant wind direction to achieve measurements of the fumarole gases at the craters of each volcano (Figure 4.27), using the techniques described in section 3.1. Measurements were done during regular monitoring of the local observatory and during field campaigns for this research: (1) between January 29th – February 7th 2019; and (2) between December 2nd – 7th 2020. Remote sensing measurements were performed by the DOAS stations described in section 3.2.1.
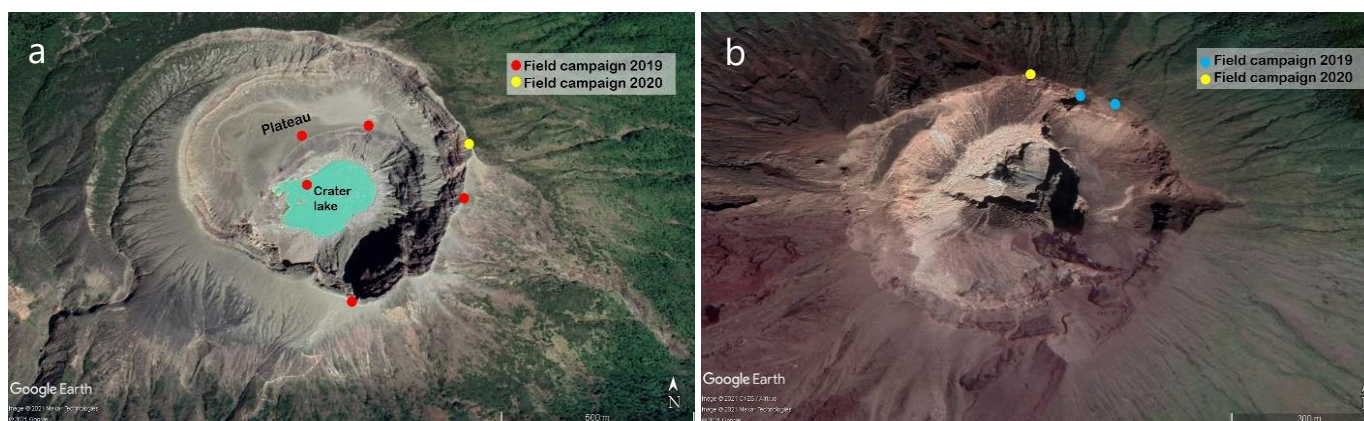
Figure 4.27. In-situ sampling sites at (a) Santa Ana, and (b) San Miguel during the 2019 and 2020 surveys.

4.4.3. DOAS data evaluation
4.4.3.1. SO$_2$ and BrO SCDs

Here we present a description of the SO$_2$ and BrO SCD's retrieved from the NOVAC stations at Santa Ana and San Miguel volcanoes, with its respective limit of detection (LOD), which were calculated as 2 times the fit error. Santa Ana has 97.3 % of the total SO$_2$ SCD's are above the LOD whilst San Miguel has 78.0 % of its data that pass this limit. In the case of the BrO SCDs less than 5 % of the total measurements are above this parameter for each volcano. Our results evidence relatively low SO$_2$ emissions in comparison to high emitting volcanoes (e.g., Etna, Nyiragongo, Cotopaxi, Masaya) that present SO$_2$ SCDs > 2 × 10^{18} molecules cm^{-2} (Bobrowski et al., 2015; Bobrowski and Giuffrida, 2012; Dinger et al., 2018; Dinger et al., 2021).

Table 4.13. SO₂ and BrO SCDs in the gas plume of Santa Ana and San Miguel volcanoes between 2008 – 2020.

Volcano	SO₂ SCD ($\times 10^{17}$ molecules cm⁻²)				BrO SCD ($\times 10^{13}$ molecules cm⁻²)				Total days
	Mean	SD	Max	LOD	Mean	SD	Max	LOD	
Santa Ana	1.04	0.43	4.92	0.49	-2.49	1.52	7.06	3.0	1213
San Miguel	1.33	1.04	13.1	0.70	0.049	1.93	13.08	3.76	635
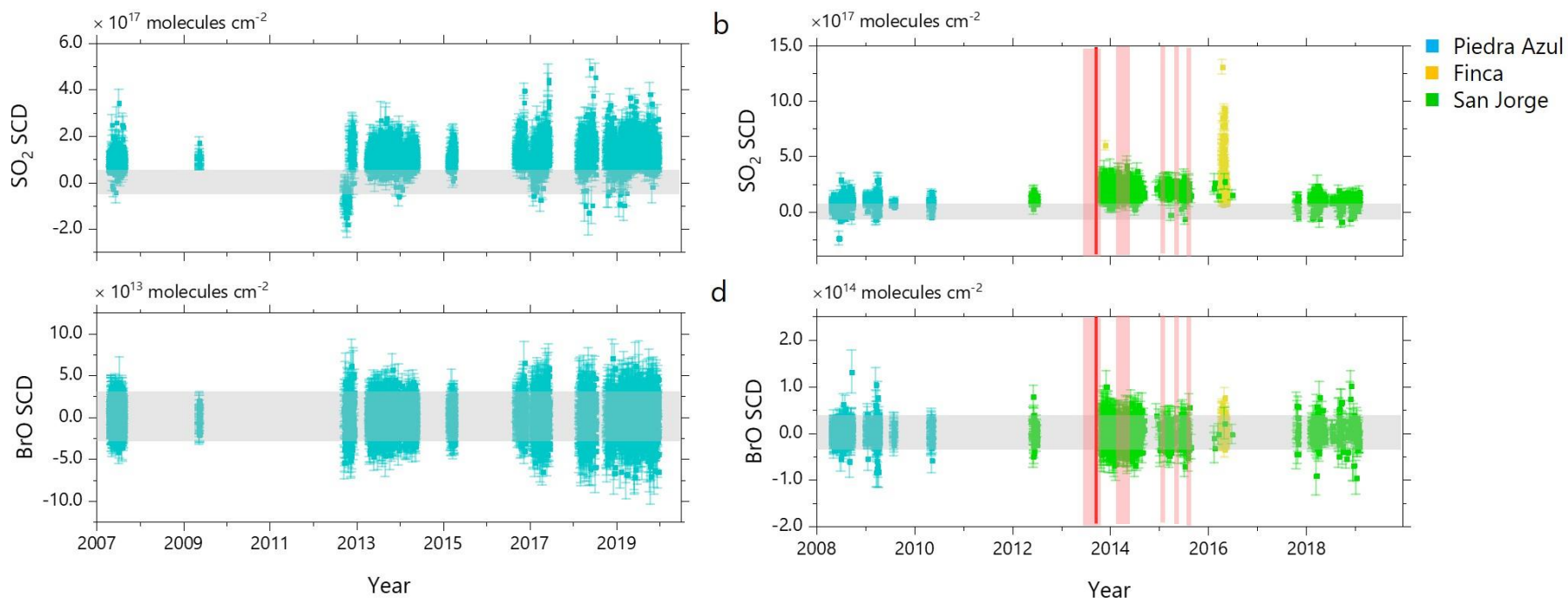
Figure 4.28. Time series of SCD's of SO₂ and BrO for Santa Ana (a and c) and San Miguel (b and d). NOVAC stations are indicated by different colors. Gray shadow indicates the limit of detection (LOD), reddish shadow indicates periods of increase of activity and explosions, and red line indicates eruption.

75

4.4.3.2. SO$_2$ emission fluxes

Daily SO$_2$ fluxes were calculated using the daily SO$_2$ SCDs of each volcano and assuming a fixed plume height. The daily average SO$_2$ flux for Santa Ana is of 546.7 ± 276.6 t/d with a maximum of 3,905.9 t/d in January 2009 and a minimum of 10.6 t/d in July 2009. San Miguel has a daily average of 1,028.5 ± 331.7 SO$_2$ t/d with a maximum of 2,789.8 t/d in April 2009, and a minimum of 11.1 t/d in September 2012. During San Miguel's evaluation period, an eruption was registered on December 29th 2013. Here we divided the long-term series in three-time intervals according to this major event (Figure 4.29): (1) before the unrest of the volcano, between July 2008 – September 2012, with an average value of 511.0 ± 258.7 t/d, (2) the period following the eruption, where minor explosion were reported by the local Observatory, between February 2014 – September 2016, with mean SO$_2$ rates of 1,173.2 ± 311.3 t/d, and (3) the low activity period, between October 2017 – April 2019, with an average of 935.2 ± 451.2 t/d Figures 3.6 and 3.7 show the wind rose corresponding to the long-term period of data acquisition, illustrating the prevalence of the wind direction to the NE-SE with a mean wind speed of 5.8 ± 2.1 m/s (± 37 %) for Santa Ana, and prevalence of wind direction to the N-ESE with 6.1 ± 2.0 m/s (± 33 %) for San Miguel.

Arellano et al. (2021) presented a compilation of SO$_2$ fluxes obtained from the same NOVAC stations for a 12-year period between 2005- 2017. The calculation of the fluxes was done using the NOVAC Post-Processing-Program (Galle et al., 2010) and wind speed downloaded from the ERA-Interim re-analysis database. An average of 169.5 ± 48.7 SO$_2$ t/d was reported for Santa Ana volcano, corresponding to 22 days between June 2008 and September 2009. From this data, emission rates of 12 days were extracted to match with observations within our dataset, obtaining a new mean value of 183.7 ± 50.6 t/d. Our average flux for these 12 days is 441.0 ± 351.5 t/d, being ~ 2.5 times higher due to differences in the meteorological data used (Annex) but still within each other's confidence interval. In the case of San Miguel, an average of 1,945.1 ± 533.5 SO$_2$ t/d was reported as the mean value for the period of 2005 – 2017, calculated with 4 days that correspond to the last 2 days of December 2013 and 2 days of February 2014 (Arellano et al., 2021). To compare with our estimations, we re-calculated their emission rate with the two dates presented for February 2014 (1,136.2 ± 381.9 t/d), because the December 2013 data were not available to us. Our results show a mean SO$_2$ emission rate of 1,233.1 ± 186.7t/d, which is in agreement with the re-calculated estimation from the NOVAC inventory. Our comparison demonstrates general consistency of the calculated SO$_2$ fluxes, indicating the validity of both post-processing methods.

Table 4.14. SO₂ in the gas plume of Santa Ana and San Miguel volcanoes between 2008 – 2020.

Volcano	SO₂ fluxes (t d⁻¹)				Total days	Wind speed (m s⁻¹)		Wind direction (°)	
	Mean	SD	Min	Max		Mean	SD	Mean	SD
Santa Ana	413.9	331.1	10. 1	5,002.0	1,638	5.8	2.1	96.5	41.4
San Miguel	761.5	564.2	10.0	4,147.0	623	6.1	2.0	95.5	45.2
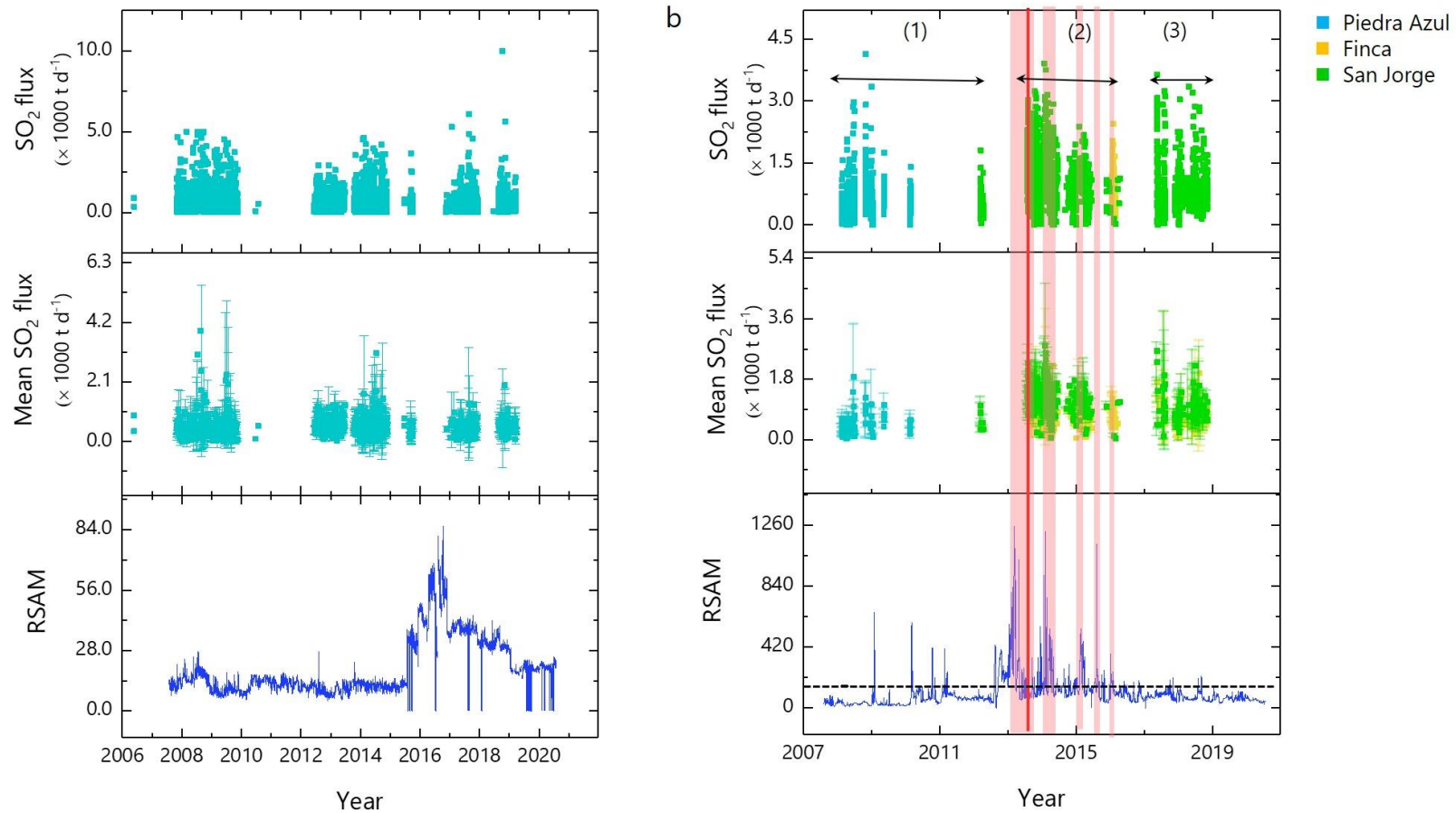
Figure 4.29. Temporal variation of SO2 fluxes and RSAM of (a) Santa Ana and (b) San Miguel volcanoes. Red line indicates eruption, red shadow points out periods of increase of activity, black dash line shows the RSAM threshold.

4.4.3.2.1.   Comparison of SO$_2$ fluxes with seismic data

Real-time Seismic-Amplitude Measurement – RSAM (Endo and Murray, 1991), is the average signal size over a given period of time (10 minutes) acquired by the seismic network of the local Observatory. For both volcanoes, the Observatory has assigned 150 RSAM units as the threshold, data above this value represent an anomaly. Figure 4.29 shows the temporal variation of SO$_2$ fluxes and RSAM, evidencing the quiescent degassing of Santa Ana volcano, even when an increase in the seismic data is observed between 2016 – 2018, since these values are still at background level. Nonetheless, San Miguel volcano's seismic data show different periods in which RSAM values were above the threshold, matching events or preceding stages in which the volcano increased its activity with SO$_2$ rates > 1000 t/d, indicating the good agreement between the seismic data and the SO$_2$ fluxes.

4.4.4. Molar carbon, hydrogen and water to sulfur ratios (X/SO$_2$)

The recorded sets of data from the MultiGAS instruments were post-processed using RatioCalc program (Tamburello, 2015). Following Aiuppa et al. (2018), the obtained ratios reported here have a maximum SO$_2$ concentration above a 3 ppmv, and high correlations (R^2 > 0.6) between co-acquired gases (Table 4.15).

Figure 4.30a shows the molar X/SO$_2$ time series for both volcanoes. Variations up to a factor of 5 were observed for Santa Ana's CO$_2$/SO$_2$ ratios, ranging from 2.1 to 10.1, while San Miguel ratios range only between 5.2 to 9.2, which indicate a C-richer composition than the average of the CAVA arc-segment (2.0 ± 1.1) reported by Aiuppa et al. (2017) (Figure 4.31). To check these variabilities, scattered plots of molar gas ratios against the SO$_2$ peak concentration measured during the corresponding temporal window were produced (Figure 4.30b). At SO$_2$ concentrations below 15 ppmv, the CO$_2$/SO$_2$ are scattered for both volcanoes. However, Santa Ana's CO$_2$/SO$_2$ meet values in the range between 2.1 to 3.3 at more concentrated plume conditions, behaving within the CAVA and the global arc gas (~ 2.5) signature (Aiuppa et al., 2017). A similar behavior is observed with the H$_2$O/SO$_2$ (Figure 4.30c), where low ratios are obtained in denser plumes (SO$_2$ peak concentrations > 15 ppmv). Additionally, different trends were observed upon sampling site. For example, at Santa Ana's outer rim the estimated CO$_2$/SO$_2$ ratios ranged from 2.9 – 10.1 (mean: 4.8 ± 2.37), while over Santa Ana's crater lake, a smaller range is observed (2.1 - 3.7, mean: 2.9 ± 0.8). The measurements are more prone to error as the distance to the SO$_2$ emission source

(the lake) and the sampling site increased (0 Km for flights over the lake, ~ 0.2 Km for the plateau and ~0.5 Km for the rim). The same applies for San Miguel where the mean CO_2/SO_2 obtained is 7.2 ± 2.7 for the rim, while 9.2 ± 4.7 is observed at the plateau, at ~0.4 Km and ~ 0.25 Km from the summit, respectively. These values are higher than the one presented by Granieri et al. (2014) for San Miguel volcano, as seen in Figure 4.30, where the author hypothesized the obtained low CO_2/SO_2 as a consequence of the high SO_2 emissions (416 – 1,136 t/d) recorded during their survey (January – February 2014), whereas our estimations were done during quiescent period, with SO_2 outputs in the range of 173 – 547 t/d.

H_2/SO_2 ratios obtained for Santa Ana vary between 0.4 and 0.5 (0.47 ± 0.05), with no difference between sites, a different behavior than the presented by (Hasselle et al., 2019), reporting large differences between sites (lake: 0.42 ± 0.11, and plateau: 2.39 ± 0.27), that was attributed to an additional contribution of H_2 by diffuse degassing. However, at the end of their study (May – June 2018), lower H_2/SO_2 ratios were found with daily averages ranging from 0.37 – 0.39 at Santa Ana's plateau. Our results are in agreement with those last observations, suggesting the decrease and/or stop of this additional gas supply since 2018. San Miguel provided no data for this gas because no correlation or anti-correlation between H_2 and SO_2 was achieved (Annex). Also, H_2S/SO_2 ratios were determined and show the same mean value (0.1 ± 0.03) for both volcanoes, for which these observations are considered as SO_2 interference signal due to low H_2S concentrations.

Table 4.15. Gas mixing ratios observed at Santa Ana and San Miguel volcanoes, using the portable MultiGAS devices.

Date	Instrument	Place	SO_2 max (ppmv)	CO_2/SO_2	H_2S/SO_2	H_2/SO_2	H_2O/SO_2
Santa Ana							
29.01.2019	SN	Plateau	33.6	2.5 ± 0.4	0.1 ± 0.02	0.4 ± 0.08	
30.01.2019	SN	Plateau	23.7	3.2 ± 0.6	0.1 ± 0.02	0.5 ± 0.1	56.4 ± 12.4
30.01.2019	PT	Plateau	12.5	5.1 ± 0.3	b.l.d		
30.01.2019	SK	Lake (dron flight 1)	16.3	3.0 ± 1.5	b.l.d		
31.01.2019	SN	Plateau	12.0	6.2 ± 2.0	0.1 ± 0.02	0.5 ± 0.2	83.2 ± 29.3
31.01.2019	PT	Plateau	10.8	5.7 ± 0.7	b.l.d		
31.01.2019	SK	Lake (dron flight 1)	17.3	2.1 ± 1.6	b.l.d		

Cont. Table 4.15

Date	Instrument	Place	SO₂ max (ppmv)	CO₂/SO₂	H₂S/SO₂	H₂/SO₂	H₂O/SO₂
Santa Ana							
31.01.2019	SK	Lake (dron flight 3)	19.6	3.7 ± 1.4	b.l.d		
08.08.2019	SN	Crater rim	4.6	10.1 ± 5.9	0.2 ± 0.04		42.9 ± 22.3
24.10.2019	SN	Crater rim	3.0		0.1 ± 0.05		
17.12.2019	SN	Crater rim	12.7	3.8 ± 1.7	0.1 ± 0.04	0.4 ± 0.2	67.7 ± 33.9
23.01.2020	SN	Crater rim	15.8	2.9 ± 1.7	0.2 ± 0.05		41.8 ± 19.1
30.09.2020	SN	Crater rim	11.0	6.7 ± 2.9	0.1 ± 0.04	0.5 ± 0.1	163.4 ± 64.2
03.12.2020	SN	Crater rim	7.9	4.4 ± 1.9	0.1 ± 0.03		176.9 ± 86.8
		Average		**4.6 ± 2.2**	**0.14 ± 0.03**	**0.47 ± 0.05**	**90.3 ± 56.5**
San Miguel							
13.07.2018	SN	Plateau	3.5	9.2 ± 4.7	0.1 ± 0.04		
06.02.2019	SN	Crater rim	5.3	7.0 ± 2.1	0.1 ± 0.02		140.5 ± 42.2
07.02.2019	SN	Crater rim	5.7	5.2 ± 1.5	0.1 ± 0.02		70.5 ± 29.5
27.03.2019	SN	Crater rim	6.1	8.3 ± 3.2	0.2 ± 0.04		97.6 ± 32.9
		Average		**7.4 ± 1.8**	**0.1 ± 0.04**		**102.9 ± 35.3**
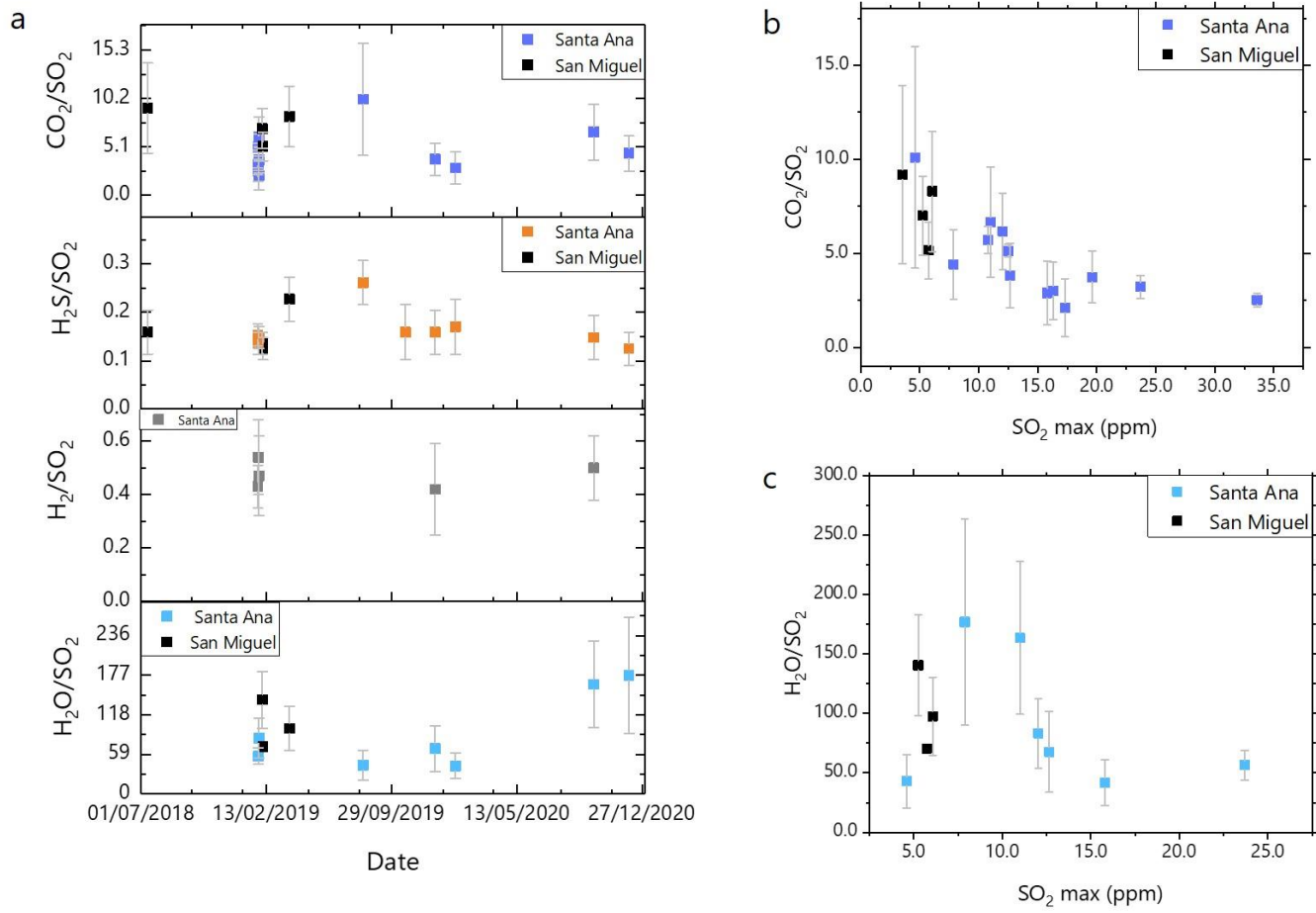
Figure 4.30. (a) Time series of carbon, hydrogen sulfide, hydrogen and water to sulfur molar ratios for Santa Ana and San Miguel corresponding to the 2018 – 2020 time period. (b) and (c) are the CO_2/SO_2 and H_2O/SO_2 versus the peak SO_2 concentration (maximum concentration within each evaluation window)
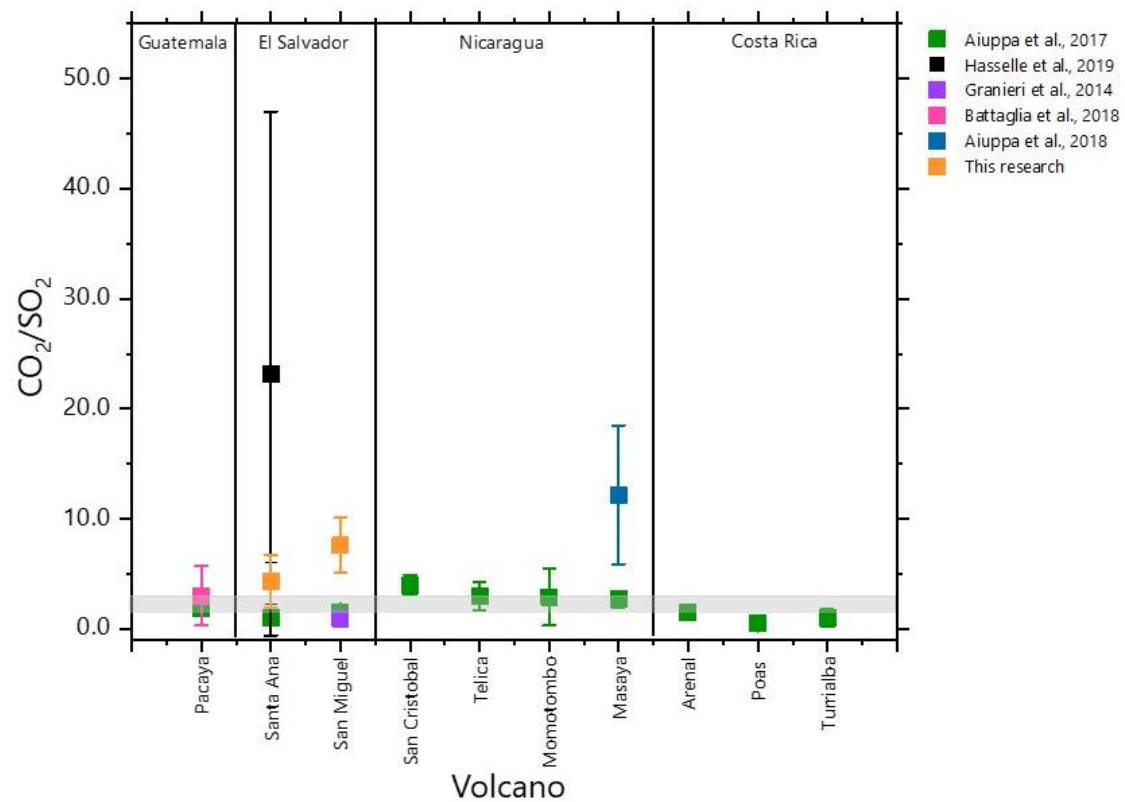
Figure 4.31. Comparison of published CO2/SO2 molar ratios of volcanoes belonging to the CAVA arc segment and the ones obtained in this work. Gray shadow indicates the CO2/St signature assigned to the arc (Aiuppa et al., 2017).

4.4.5. Total halogen to sulfur ratios (Y/S)

Analysis obtained from the Raschig Tube samples were processed and corrected for blank effects. Here Y represents the halogens encountered in the samples (Y = Cl, Br, I). Table 4.16 summarizes the concentration of volcanic gases in the air, while Table 4.17 shows the obtained halogen to sulfur molar ratios for each volcano. Figure 4.32a show the total halogen to sulfur ratios with variations upon sampling site. The mean Y/S ratios for Santa Ana's rim are 0.2 ± 0.3 for fluorine, 1.1 ± 1.0 for chlorine and $(2.7 \pm 5.1) \times 10^{-4}$ for bromine; while for the plateau only Cl/S was detected with a value of 0.1 ± 0.02. Large variations are observed for Br even though all samples belong to the rim, with differences of ~ 1 order of magnitude. However, these discrepancies are evident after performing the blank correction, thus implying a possible contamination of the blank. At San Miguel's rim Cl, Br and I were detected within its plume with mean Y/S ratios of 1.0 ± 0.08 for chlorine, $(5.2 \pm 1.0) \times 10^{-4}$ for bromine and $(1.8 \pm 0.63) \times 10^{-5}$ for iodine. No F/S was obtained since sulfur was below the limit of detection for that specific sample (Table 4.17). Figure 4.32b shows the Y/S obtained during the two field campaigns. No large variations are observed between the surveys, evidencing the quiescent state of the volcano.

3.1.1. Reactive halogens species (RHS)

Reactive bromine and chlorine (BrX, ClX) were determined only on few days, since most of the samples were below the limits of detections and quantitation (LOD_{Cl2} = 0.18 ng and LOQ_{Cl2} = 0.5 ng, and LOD_{Br2} = 0.13 ng and LOQ_{Br2} =0.4 ng). The results for these samples are shown in Table 4.18, along with the reactive to total halogen and total sulfur ratios in (mol/mol). The uncertainties were calculated by the Gaussian error propagation using 5 % error for the sampled volume and 10 % for the measured analyte amounts. These are the first measurements of RHS performed in both volcanoes. Santa Ana's RHS ranged from 1.1 – 9.1 ppt BrX and from 3.6 – 35.3 ppt ClX, whereas San Miguel's samples only detected ClX (1.2 – 1.7 ppt). This data represents less than 1 % of the total chlorine composition obtained from the RT samples with exception of one sample at Santa Ana's crater rim for ClX.

Several studies suggest halogen activation within the volcanic plume as a function of the distance to the crater (e.g., von Glasow, 2010; Bobrowski et al., 2012; Roberts et al., 2014; Theys et al., 2016; Surl et al., 2021). My results sit within this behavior (Figure 4.33), showing low ratios when nearer to the emission vent and increasing when further away from it. For example, BrX/S increases from $(0.21 \pm 0.04) \times 10^{-5}$, at

Table 4.16. Concentrations (± error) of detected elements in the plume of Santa Ana and San Miguel volcanoes using the alkaline trap method.

Date	Place	F (ppm)	Cl (ppm)	S (ppm)	Br (ppt)	I (ppt)	CO_2 (ppm)
Santa Ana							
29.01.2019	Rim	b.d.l	0.3 ± 0.04	0.5 ± 0.1	19.9 ± 3.4	b.d.l	54.1 ± 9.2
30.01.2019	Rim	b.d.l	0.1 ± 0.03	0.2 ± 0.04	1.55 ± 0.3	b.d.l	107.5 ± 18.3
30.01.2019	Plateau	b.d.l	0.4 ± 0.06	3.0 ± 0.5	b.d.l	b.d.l	136.1 ± 23.1
31.01.2019	Rim	b.d.l	0.2 ± 0.03	0.1 ± 0.01	b.d.l	b.d.l	114.6 ± 19.5
31.01.2019	Plateau	b.d.l	0.5 ± 0.1	4.9 ± 0.8	8.3 ± 1.4	b.d.l	163.0 ± 27.7
02.12.2020	Rim	0.1 ± 0.01	0.3 ± 0.04	0.2 ± 0.03	b.d.l	b.d.l	153.6 ± 26.1
03.12.2020	Rim	0.006 ± 0.0001	0.2 ± 0.04	1.2 ± 0.2	14.38	b.d.l	289.5 ± 49.2
San Miguel							
05.02.2019	Rim	b.d.l	0.8 ± 0.1	b.d.l	555.8 ± 94.5	b.d.l	192.8 ± 32.8
06.02.2019	Rim	b.d.l	1.5 ± 0.3	1.5 ± 0.3	696.1 ± 118.3	34.0 ± 5.8	154.4 ±26.3
07.02.2019	Rim	b.d.l	1.4 ± 0.2	1.3 ± 0.2	770.7 ± 131.0	17.0 ± 2.9	130.2 ± 22.1
08.12.2020	Rim	0.001 ± 0.0002	b.d.l	b.d.l	b.d.l	b.d.l	737.9 ± 125.4
09.12.2020	Rim	b.d.l	b.d.l	b.d.l	b.d.l	b.d.l	414.6 ± 70.5

b.d.l: below detection limit

Table 4.17. Molar ratios (± error) estimated from data in Table 4.16.

| Date	Place	F/S	Cl/S	Br/S × 10^{-5}	I/S × 10^{-6}	CO_2/S
Santa Ana						
29.01.2019	Rim	n.a	0.5 ± 0.1	4.3 ± 1.0	n.a	116.1 ± 27.9
30.01.2019	Rim	n.a	0.6 ± 0.1	0.62 ± 0.15	n.a	430.7 ± 103.5
30.01.2019	Plateau	n.a	0.1 ± 0.03	n.a	n.a	46.0 ± 11.0
31.01.2019	Rim	n.a	2.6 ± 0.6	11.9 ± 2.9	n.a	1630.7 ± 392.0
31.01.2019	Plateau	n.a	0.1 ± 0.02	n.a	n.a	33.3 ± 8.0
02.12.2020	Rim	0.5 ± 0.1	1.5 ± 0.4	n.a	n.a	889.7 ± 216.3
03.12.2020	Rim	0.0005 ± 0.0001	0.2 ± 0.05	1.17 ± 0.28	n.a	235.7 ± 56.7
San Miguel						
06.02.2019	Rim	n.a	0.9 ± 0.2	45.1 ± 10.9	2.2 ± 0.5	100.2 ± 24.1
07.02.2019	Rim	n.a	1.1 ± 0.3	59.2 ± 14.2	13.1 ± 3.1	100.0 ± 24.0

n.a: not available
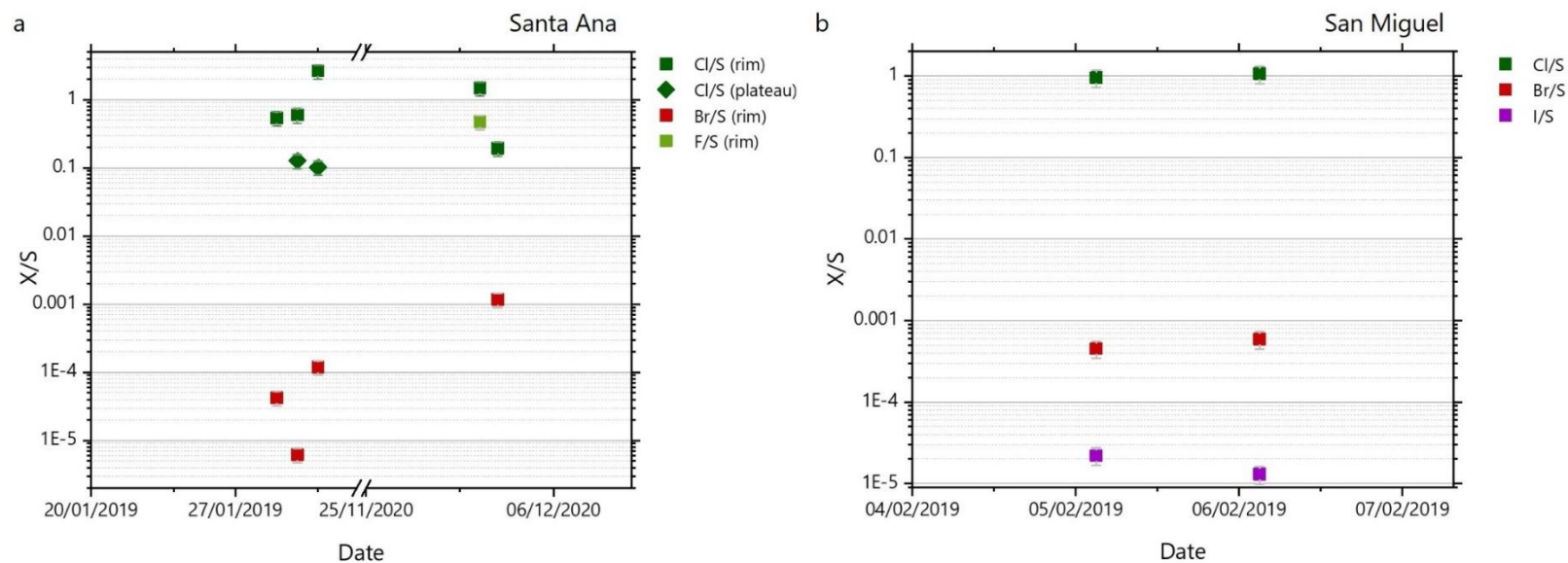
Figure 4.32. Halogen-to-sulfur molar ratios (X/S, where X = F, Cl, Br, I) measured at different sampling sites at Santa Ana volcano (left) and at San Miguel's rim (right).

Table 4.18. Molar mixing ratios of reactive halogens, obtained from denuders, to total halogens and total sulfur, obtained at different sampling sites.

Date	Location	Distance to the vent (m)	Reactive halogens		BrX/Br	BrX/S × 10^{-5}	ClX/Cl × 10^{-5}	ClX/S× 10^{-5}
			BrX (ppt)	ClX (ppt)				
Santa Ana								
29.01.2019	Rim	480	9.1 ± 1.5	b.l.d	0.46 ± 0.11	1.95 ± 0.46	n.a	n.a
30.01.2019	Plateau	230	6.3 ± 0.8	3.6. ± 0.1	n.a	0.21 ± 0.04	0.95 ± 0.16	0.12 ± 0.02
31.01.2019	Rim	370	1.1 ± 0.2	35.3. ± 2.5	0.13 ± 0.03	1.6 ± 0.4	19.0 ± 3.5	50.3 ± 9.25
31.01.2019	Plateau	260	2.0 ± 0.3	b.l.d	n.a	0.04 ± 0.004	n.a	n.a
02.12.2020	Rim	570	3.1 ± 0.5	b.l.d	n.a	1.8 ± 0.4	n.a	n.a
San Miguel								
05.02.2019	Rim	366	b.l.d	1.2 ± 0.2	n.a	n.a	0.14 ± 0.03	n.a
07.12.2019	Rim	430	b.l.d	1.7 ± 0.3	n.a	n.a	0.12 ± 0.03	0.13 ± 0.03

b.l.d: below limit of detection

n.a: not available

Santa Ana's plateau, to $(1.8 \pm 0.4) \times 10^{-5}$ at the crater rim, while BrX/Br increases from 0.13 ± 0.03 to 0.46 ± 0.11. Same tendency applies for ClX, with ClX/S increasing from $(0.12 \pm 0.02) \times 10^{-5}$ at Santa Ana's plateau, to $(50.3 \pm 9.25) \times 10^{-5}$ at its rim, whereas ClX/Cl rises from $(0.95 \pm 0.16) \times 10^{-5}$ to $(19.0 \pm 3.5) \times 10^{-5}$ from plateau to rim. In the case of San Miguel volcano, sampling was performed only at its crater rim due to accessibility to the plateau and fumaroles. However, it is observed that at San Miguel's plume, lower RHS concentration was found with RHS molar ratios similar to Santa Ana's plateau.
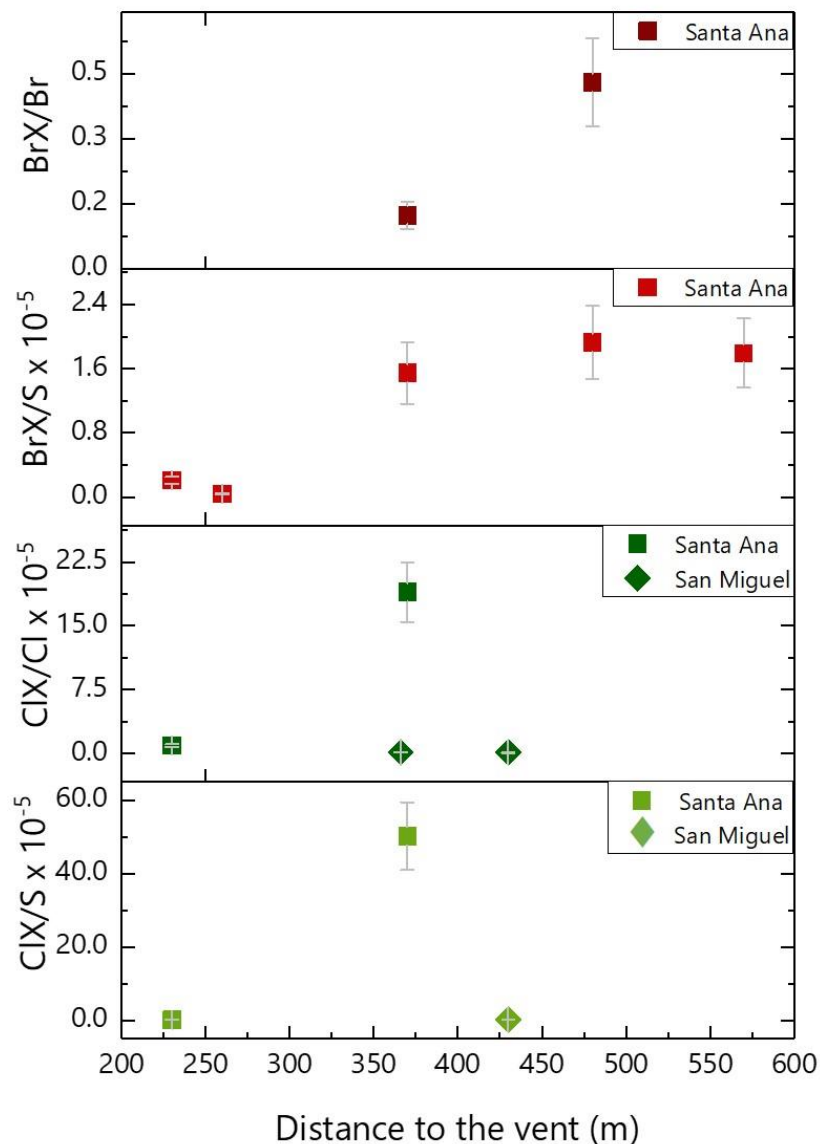
Figure 4.33. RHS molar ratios estimated from the concentrations detected at Santa Ana and San Miguel's craters.

4.4.6. Summary

Here we present a historical long-time series of SO_2 emission rates for Santa Ana and San Miguel which is more complete than the ones presented before, which refer to periods of 1 – 2 years (Rodriguez et al., 2004; Bernard et al., 2004; Cartagena et al., 2004; Pérez et al., 2006; Olmos et al., 2007) or 10 – 12 years, but considering only few month (Aiuppa et al. 2018; Arellano et al., 2021). We obtained a daily average of 626.2 ± 457.7 t/d (average ± 1σ) for San Miguel and 375.6 ± 320.0 t/d for Santa Ana. This data was recorded by the NOVAC stations installed SW downwind the craters of each volcano. Most of the data was acquired during quiescent period, with exception of the Vulcanian eruption and minor explosion events marked in Figure 4.29 at San Miguel, where peak SO_2 fluxes of 2,769.8 t/d and 2,624.6 t/d were observed.

The remote sensing data was complemented with in-situ sampling performed during field campaigns between 2019 -2020, with the aim to further characterize the chemical signature of the gas plumes at Santa Ana and San Miguel. In general, both volcanoes show a C-richer composition (CO_2/SO_2 > 4.0) relative to their arc segment (Figure 4.31). When the CO_2/SO_2 were acquired at more concentrated plume conditions (SO_2 > 15 ppm), a C-poor composition is observed meeting values in the range between 2.1 to 3.3, behaving within the CAVA and the global arc gas (~ 2.5) signature.

We also report total halogen fraction of the discharged gases with their corresponding halogen to sulfur ratios, showing variations upon sampling site, specifically for the case of Santa Ana because we were able to perform measurements at different distances from the emission vent.

At San Miguel the estimated halogen to sulfur ratios have mean values of 1.0 ± 0.2, (5.2 ± 1.3) × 10^{-4} and (1.8 ± 0.4) × 10^{-5}, for HCl/SO_2, HBr/SO_2 and HI/SO_2, respectively, and at Santa Ana we found average values of HCl/SO_2, HF/SO_2 and HBr/SO_2 of 0.8 ± 0.2, 0.2 ± 0.1, (4.7 ± 1.7) × 10^{-5}, respectively. Additionally, I present the first measurements of RHS (sum of reactive bromine and chlorine species) made at this two El Salvadorean volcanoes by means of the denuder technique. The data shows the halogen speciation with respect to the distance to the emission vent, thus obtaining higher concentrations of RHS when further away from it, following model predictions (von Glasow, 2010; Bobrowski et al., 2012; Roberts et al., 2014) with RHS to sulfur ratios in the range of 10^{-5}. These field observations will contribute to the enlargement of

measurements of RHS, corresponding to low-emitter volcanoes, and to further understand the halogen speciation within volcanic plumes.

5. Conclusions and outlook

Two different sampling mediums to collect dihalogen molecules in volcanic environments were tested, glass denuders and syringe filters. Cis- and trans-stilbene were used as in-situ derivatizing agents for the selective speciation of Br_2, Cl_2 and BrCl. Cis-stilbene showed to be suitable for sampling the three differents halogen species tested (Br_2, Cl_2 and BrCl), as reaction with this coating produce the corresponding dihalogenated derivatives determinable by GC-MS. This approach was proven to be successfully identify dihalogens. However, quantification was not possible due to very low yields when denuder were applied as sampling units. Moreover, coated syringe filters show better efficiency for chlorine gas than the diffusion denuders using cis-stilbene. However, the syringe filters must be coated with an excess of the reagent, as the low recoveries indicate evaporation during sampling, which means only identification of the dechlorinated derivative was possible.

As halogens are mainly emitted by volcanoes as halogen halides (HCl, HBr), a suitable gas source for these species with oxidation state of -1 should be included in future laboratory experiments, since the HCl permeation gas source used in this research didn't achieve a stable output rate. Future work should also include the search for additional coatings that can further discriminate between species (e.g., Br_2, BrCl) but are also suitable for species with oxidation state -1 (HCl, HBr) and possibly even halogen radicals.

In-situ measurements at several arc volcanoes - Masaya, Vulcano, Santa Ana and San Miguel - were performed using Raschig tubes, MultiGAS systems, and TMB (trimethoxybenzene)-coated denuders. Acid gases (CO_2, SO_2, HCl, HF, HBr, HI) were collected with the Raschig tubes and subsequently analyzed with IC and ICP-MS. The MultiGAS instruments recorded two major volcanic gas species CO_2 and SO_2 concentrations, which were post-processed to obtain CO_2/SO_2 mole ratios. The CO_2 and SO_2 values that were used to complete the characterization of the individual volcanic plumes investigated and their ratio was used to put the data set in context compared with previously published data and discuss the variation between volcanoes and for individual volcanoes over time, with changes in the compositions upon emission vent (fumarole – Vulcano, Santa Ana and San Miguel, lava lake – Masaya, crater lake – Santa Ana), as well as the state of activity the volcano (quiescent degassing, eruption).

Using the TMB-coated denuders and GC-MS analysis, the sum of the RHSs of bromine and chlorine were determined. First measurements of this type were made for Vulcano, Santa Ana, and San Miguel, while further results were added to the already existing Masaya data set. Each dataset allows us to extend (Masaya, Vulcano) and fully characterize (Santa Ana and San Miguel) the chemical composition of the emitted gases from each volcano.

Future work related to this dataset should include their application in the validation of chemistry box modelling (e.g., CAABA/MECCA) to test whether the field observations can be reproduced by the model simulations as well as to improve the current understanding of halogen chemistry in volcanic plumes.

Spectroscopic analysis of DOAS data from Santa Ana and San Miguel volcanoes in El Salvador, collected by DOAS stations there since 2006 and 2008, respectively, was also performed as part of the dissertation presented. Post-processing for these two NOVAC stations was based on the code developed by Dinger et al. (2021), which provides SO_2 and BrO SCDs as output. When wind information is available, the code also produces SO_2 emission rates. The data obtained provide evidence of fluctuations in activity from San Miguel, where an eruptive event occurred in late 2013. These datasets are used to update the amounts of gas emitted from these volcanoes. Future work with the DOAS data could include using local wind conditions instead of model-based data to calculate even more reliable SO_2 fluxes.

In summary, this work has demonstrated the usefulness of combining different in-situ measurement techniques in the study of volcanic gases to identify different activity states of volcanoes between field campaigns. For example, variation in the gas composition of Masaya's plume was observed between observations made in 2016 at the peak of activity of its crater lava lake, and the observation made during our field campaign in 2019, when the lava lake was almost disappearing. Also, at San Miguel volcano, the long-term SO_2 emission rates allow to identify three-time intervals surrounding the eruption of December 2013. The application of the recently developed in-situ derivatization techniques in combination with GC-MS was also useful to validate the halogen speciation predicted by models.

6. References

Aiuppa, A.; Burton, M.; Murè, F.; Inguaggiato, S. (2004): Intercomparison of volcanic gas monitoring methodologies performed on Vulcano Island, Italy. In *Geophys. Res. Lett.* 31 (2). DOI: 10.1029/2003GL018651.

Aiuppa, A.; Federico, C.; Franco, A.; Giudice, G.; Gurrieri, S.; Inguaggiato, S. et al. (2005a): Emission of bromine and iodine from Mount Etna volcano. In *Geochem. Geophys. Geosyst.* 6 (8), n/a-n/a. DOI: 10.1029/2005GC000965.

Aiuppa, A. (2005b): Chemical mapping of a fumarolic field: La Fossa Crater, Vulcano Island (Aeolian Islands, Italy). In *Geophys. Res. Lett.* 32 (13). DOI: 10.1029/2005GL023207.

Aiuppa, A.; Baker, D. R.; Webster, J. D. (2009): Halogens in volcanic systems. In *Chemical Geology* 263 (1-4), pp. 1–18. DOI: 10.1016/j.chemgeo.2008.10.005.

Aiuppa, A. (2015): Volcanic-gas monitoring. In Schmidt, A.,Kirsten E. Fristad, Linda T. Elkins-Tanton (Eds.): Volcanism and Global Environmental Change. Cambridge: Cambridge University Press, pp. 81–96.

Aiuppa, A.; Fischer, T. P.; Plank, T.; Robidoux, P.; Di Napoli, R. (2017): Along-arc, inter-arc and arc-to-arc variations in volcanic gas CO 2 /S T ratios reveal dual source of carbon in arc volcanism. In *Earth-Science Reviews* 168, pp. 24–47. DOI: 10.1016/j.earscirev.2017.03.005.

Aiuppa, A.; Moor, J. M. de; Arellano, S.; Coppola, D.; Francofonte, V.; Galle, B. et al. (2018): Tracking Formation of a Lava Lake From Ground and Space: Masaya Volcano (Nicaragua), 2014-2017. In *Geochem. Geophys. Geosyst.* 19 (2), pp. 496–515. DOI: 10.1002/2017GC007227.

Al-hassan, M. I. (1989): Conversion of Stilbene to trisubstituted Olefins. In *Synthetic Communications* 19 (3-4), pp. 463–472. DOI: 10.1080/00397918908050687.

Ali, Z.; Paul Thomas, C.L; Alder, J.F. (1989): Denuder Tubes for Sampling of Gaseous Species. In *Analyst* 114, pp. 759–769.

Alphasense Ltd (2014, November): Alphasense Application Note AAN 201-06 NDIR: Gas concentration Calculation Overview. Retrieved from https://www.alphasense.com/downloads/application-notes/

Alphasense Ltd (Issue 12): Alphasense Application Note AAN How electrochemical Gas sensors Work. Retrieved from https://www.alphasense.com/downloads/application-notes/

Amburgey-Peters, J. C.; Haynes, L. W. (2005): The Addition of Bromine to 1,2-Diphenylethene. In *J. Chem. Educ.* 82 (7), p. 1051. DOI: 10.1021/ed082p1051.

Andres, R. J.; Kasgnoc, A. D. (1998): A time-averaged inventory of subaerial volcanic sulfur emissions. In *Jourbal of Geophysical Research* 103 (D19), 25,251–25,26.

Arellano, S.; Galle, B.; Apaza, F.; Avard, G.; Barrington, C.; Bobrowski, N. et al. (2021): Synoptic analysis of a decade of daily measurements of SO2 emission in the troposphere from volcanoes of the global ground-based Network for Observation of Volcanic and Atmospheric Change. In *Earth Syst. Sci. Data* 13 (3), pp. 1167–1188. DOI: 10.5194/essd-13-1167-2021.

Battaglia, A.; Bitetto, M.; Aiuppa, A.; Rizzo, A.L.; Chigna, G.; Watson, I. M.; et al. (2018): The magmatic gas signature of Pacaya Volcano, with implications for the volcanic CO2 flux from Guatemala. In *Geochemistry,Geophysics, Geosystems*, 19. https://doi.org/10.1002/2017GC007238

Baubron, J. C.; Allard, P.; Toutain, J. P. (1990): Diffuse volcanic emissions of carbon dioxide from Vulcano Island, Italy. In *Nature* 344 (6261), pp. 51–53. DOI: 10.1038/344051a0.

Bernard, A.; Escobar, C.D.; Mazot, A.; Gutierrez, R.E. (2004): The acid volcanic lake of Santa Ana volcano, El Salvador. In *Natural Hazards in El Salvador*, William I. Rose, Julian J. Bommer, Dina L. López, Michael J. Carr, Jon J. Major

Berrisford, P.; Dee D.; Poli, P.; Brugge, R.; Fielding, K.; Fuentes, M. et al. (2011): ERA-40 Project Report Series.

Bluth, G.J.S.; Rose, W.I.; Sprod, I.E.; Krueger, A. (1997): Stratospheric loading of sulfur from explosive volcanic eruptions. In *Journal of Geology* 105, pp. 671 - 683.

Bobrowski (2003): Detection of bromine monoxide in a volcanic plume. In *Nature* 423 (6937), pp. 273–276. DOI: 10.1038/nature01638.

Bobrowski, N.; Glasow, R. von; Aiuppa, A.; Inguaggiato, S.; Louban, I.; Ibrahim, O. W.; Platt, U. (2007): Reactive halogen chemistry in volcanic plumes. In *J. Geophys. Res.* 112 (D6). DOI: 10.1029/2006JD007206.

Bobrowski, N.; Giuffrida, G. (2012): Bromine monoxide / sulphur dioxide ratios in relation to volcanological observations at Mt. Etna 2006–2009. In *Solid Earth* 3 (2), pp. 433–445. DOI: 10.5194/se-3-433-2012.

Bobrowski, N.; Glasow, R. von; Giuffrida, G. B.; Tedesco, D.; Aiuppa, A.; Yalire, M. et al. (2015): Gas emission strength and evolution of the molar ratio of BrO/SO2 in the plume of Nyiragongo in comparison to Etna. In *J. Geophys. Res. Atmos.* 120 (1), pp. 277–291. DOI: 10.1002/2013JD021069.

Bonforte, A.; Hernandez, D.A.; Gutiérrez, E.; Handal. L.; Polío, C.; Rapisarda, S.; Scarlato, P. (2016): The unrest of the SAn Miguel volcano (EL Salvador, Central America): installation of the monitoring network and observed volcano-tectonic ground deformation. In *Nat. Hazards Earth Syst. Sci.*, 16, pp.1755–1769.

Buckles, R. E.; Bader J. M.; Thurmaier, R. J. (1962): Stereospecificity of the Addition of Bromine to cis- and trans-Stilbene[1]. In *Journal of Organic Chemistry* 27, pp. 4523–4527. Available online at doi.org/10.1021/jo01059a097.

Carey, F.A.; Sundberg, R.J. (2008): Advanced Organic Chemistry, Part B: Reactions and Synthesis. 5th Ed. Springer, pp. 298 - 301.

Cartagena, R.; olmos, R.; López, D.L.; Soriano, T.; Barahona, F.; Hernández, P.A.; Pérez, N.: (2004): Diffuse soil degassing of carbon dioxide, radon and mercury at San Miguel volcano, El Salvador. In *Natural Hazards in El Salvador*, William I. Rose, Julian J. Bommer, Dina L. López, Michael J. Carr, Jon J. Major.

Cicerone R. (1987): Changes in stratospheric ozone. In *Science*, 237, pp. 35 - 42.

Chesner, C.A.; Pullinger, C.R.; Escobar, C.D. (2004): Physical and chemical evolution of San Miguel volcano, El Salvador. In *Natural Hazards in El Salvador*, William I. Rose, Julian J. Bommer, Dina L. López, Michael J. Carr, Jon J. Major.

Colvin, A.; Rose, W.I.; Varekamp, J.C.; Palma, J.L.; Escobar, D.; Gutierrez, E.; Montalvo, F.; Maclean, A. (2013): Crater lake evolution at Santa Ana Volcano (El Salvador) following the 2005 eruption. In Rose, W.I.; Palma, J.L.; Delgado Granados, H.; Varley, N., eds., Understanding Open-Vent Volcanism and Related Hazards: Geological Society of America Special Paper 498, p. 23–43, doi:10.1130/2013.2498(02).

Costa, F.; Widiwijayanti, C.; Nang, T. Z. W.; Fajiculay, E.; Espinosa-Ortega, T.; Newhall, C. (2019): WOVOdat – the global volcano unrest database aimed at improving eruption forecasts. In *DPM* 28 (6), pp. 738–751. DOI: 10.1108/DPM-09-2019-0301.

Cristol, S. J.; Bly, R. S. Jr. (1960): Mechanisms of Elimination Reactions. XXI. The Alkaline Dehydrochlorination of meso- and dl-Stilbene Dichlorides[1]. In *Journal of Organic Chemistry* 82.

Delmelle, P.; Stix, J.; Baxter, P.; Garcia-Alvarez, J.; Barquero, J. (2002): Atmospheric dispersion, environmental effects and potential health hazard associated with the low-altitude gas plume of Masaya volcano, Nicaragua. In *Bull Volcanol* 64 (6), pp. 423–434. DOI: 10.1007/s00445-002-0221-6.

Dinger, F.; Bobrowski, N.; Warnach, S.; Bredemeyer, S.; Hidalgo, S.; Arellano, S. et al. (2018): Periodicity in the BrO∕SO$_2$ molar ratios in the volcanic gas plume of Cotopaxi and its correlation with the Earth tides during the eruption in 2015. In *Solid Earth* 9 (2), pp. 247–266. DOI: 10.5194/se-9-247-2018.

Dinger, F.; Kleinbek, T.; Dörner, S.; Bobrowski, N.; Platt, U.; Wagner, T. et al. (2021): SO$_2$ and BrO emissions of Masaya volcano from 2014 to 2020. In *Atmos. Chem. Phys.* 21 (12), pp. 9367–9404. DOI: 10.5194/acp-21-9367-2021.

Duffell, H. J.; Oppenheimer, C.; Pyle, D. M.; Galle, B.; McGonigle, A. J.S; Burton, M. R. (2003): Changes in gas composition prior to a minor explosive eruption at Masaya volcano, Nicaragua. In *Journal of Volcanology and Geothermal Research* 126 (3-4), pp. 327–339. DOI: 10.1016/S0377-0273(03)00156-2.

Endo, E. T.; Murray, T. (1991): Real-time Seismic Amplitude Measurement (RSAM): a volcano monitoring and prediction tool. In *Bull Volcanol* 53 (7), pp. 533–545. DOI: 10.1007/BF00298154.

Escobar, C.D. (2003): San Miguel Volcano and its Volcanic Hazards, El Salvador, Central America (Master of Science thesis). Michigan Technological University.

Finnigan, R. E. (1994): Quadrupole mass spectrometers. In Analytical chemistry, 66, pp. 969A-975A, doi:10.1021/ac00091a002.

Freundt, A.; Grevemeyer, I.; Rabbel, W.; Hansteen, T. H.; Hensen, C.; Wehrmann, H. et al. (2014): Volatile (H2O, CO2, Cl, S) budget of the Central American subduction zone. In *Int J Earth Sci (Geol Rundsch)* 103 (7), pp. 2101–2127. DOI: 10.1007/s00531-014-1001-1.

Galle, B.; Johansson, M.; Rivera, C.; Zhang, Y.; Kihlman, M.; Kern, C. et al. (2010): Network for Observation of Volcanic and Atmospheric Change (NOVAC)—A global network for volcanic gas monitoring: Network layout and instrument description. In *J. Geophys. Res.* 115 (D5). DOI: 10.1029/2009JD011823.

Geil, B. (2021): Methodenentwicklung zur Halogenbestimmung von Vulkanischen Systemen mittels Basischer Fallen und Diffusionsabscheidern/Entwicklung einer Permeablen Chlorgasquelle (Master thesis). Johannes Gutenberg Universität Mainz.

Gerlach, T. M. (2004): Volcanic sources of tropospheric ozone-depleting trace gases. In *Geochem. Geophys. Geosyst.* 5 (9), n/a-n/a. DOI: 10.1029/2004GC000747.

Giggenbach, W. F. (1975): A simple method for the collection and analysis of volcanic gas samples. In *Bull Volcanol* 39 (1), pp. 132–145. DOI: 10.1007/BF02596953.

Giggenbach, W.F. (1987): Redox processes governing the chemistry of fumarolic gas discharges from White Island, New Zealand. In *Applied Geochemistry*, 2. pp. 143 - 161.

Giggenbach, W. F. (1996): Chemical composition of volcanic gases. In *Monitoring and Mitigation of Volcano Hazards*. Scarpa/Tilling (eds).

Glasow, R. von (2010): Atmospheric chemistry in volcanic plumes. In *Proceedings of the National Academy of Sciences of the United States of America* 107 (15), pp. 6594–6599. DOI: 10.1073/pnas.0913164107.

Gonnermann, H. M.; Manga, M.; Fagents, S. A. (2013): Dynamics of magma ascent in the volcanic conduit. In Tracy K. P. Gregg, Rosaly M. C. Lopes, Sarah A. Fagents (Eds.): Modeling Volcanic Processes. Cambridge: Cambridge University Press, pp. 55–84.

Granieri, D.; Salerno, G.; Liuzzo, M.; La Spina, A.; Giuffrida, G.; Caltabiano, T. et al. (2015): Emission of gas and atmospheric dispersion of SO 2 during the December 2013 eruption at San Miguel volcano (El Salvador, Central America). In *Geophys. Res. Lett.* 42 (14), pp. 5847–5854. DOI: 10.1002/2015GL064660.

Gutmann, A. (2015): Entwicklung von Diffusionsabscheidern zur quantitativen Bestimmung von Bromwasserstoff aus vulkanischen Systemen mittels einer GC-MS-Methode (Diplomarbeit). Johannes Gutenberg Universität Mainz.

Gutmann, A.; Bobrowski, N.; Roberts, T.J.; Rüdiger, J.; Hoffmann, T. (2018): Advances in Bromine Speciation in Volcanic Plumes. In *Front. Earth Sci.* 6 (213). doi: 10.3389/feart.2018.00213

Halmer, M. M.; Schmincke, H.-U.; Graf, H.-F. (2002): The annual volcanic gas input into the atmosphere, in particular into the stratosphere: a global data set for the past 100 years. In *Journal of Volcanology and Geothermal Research* 115 (3-4), pp. 511–528. DOI: 10.1016/S0377-0273(01)00318-3.

Hasselle, N.; Montalvo, F.; Rouwet, D.; Battaglia, A.; Bitetto, M.; Escobar, D. et al. (2019): The crater lake of Ilamatepec (Santa Ana) volcano, El Salvador: insights into lake gas composition and implications for monitoring. In *Bull Volcanol* 81 (11). DOI: 10.1007/s00445-019-1331-8.

Huang, R.; Hoffmann, T. (2008): A denuder-impinger system with in situ derivatization followed by gas chromatography-mass spectrometry for the determination of gaseous iodine-containing halogen species. In *Journal of chromatography. A* 1210 (2), pp. 135–141. DOI: 10.1016/j.chroma.2008.08.003.

Huygen, C. (1963): The sampling of hydrogen fluoride in air with impregnated filter paper. In *Analytica Chimica Acta* 29, pp. 448–452.

Inguaggiato, S.; Diliberto, I. S.; Federico, C.; Paonita, A.; Vita, F. (2018): Review of the evolution of geochemical monitoring, networks and methodologies applied to the volcanoes of the Aeolian Arc (Italy). In *Earth-Science Reviews* 176, pp. 241–276. DOI: 10.1016/j.earscirev.2017.09.006.

Jourdain, L.; Roberts, T.J.; Pirre, M.; Josse, B. (2016): Modeling the reactive halogen plume from Ambrym and its impact on the troposphere with the CCATT-BRAMS mesoscale model. In *Atmos. Chem. Phys.*, 16, pp. 12099–12125. doi:10.5194/acp-16-12099-2016.

Karbach, N. (2021): Charakterisierung verschiedener Denuderbeschichtungen und ihre Fähigkeit zur Absorption von gasförmigem Chlor im ppm Bereich in Luft (Bachelor thesis). Johannes Gutenberg Universität Mainz.

Kaupp, G.; Matthies, D. (1987): Organische Gas-Festkörper-Reaktionen mit Stilbenen, Chalkonen und Enamiden. In *Chem. Ber.* 120 (11), pp. 1897–1903. DOI: 10.1002/cber.19871201120.

Kaupp, G.; Kuse, A. (1998): 100% Yield in 300 Gas-Solid Reactions Covering 22 Reaction Types: A Benign Option for Industrial Solid-State Production. In *Molecular Crystals and Liquid Crystals Science and Technology. Section A. Molecular Crystals and Liquid Crystals* 313 (1), pp. 361–366. DOI: 10.1080/10587259808044300.

Kaupp, G. (2017): "Organic Solid-State Reactions" in: Encyclopedia of Physical Organic Chemistry Online.

Keller, J. (1980): The-island-of-vulcano_compress 36 (1), pp. 369–414.

Kern, C.; Sihler, H.; Vogel, L.; Rivera, C.; Herrera, M.; Platt, U. (2009): Halogen oxide measurements at Masaya Volcano, Nicaragua using active long path differential optical absorption spectroscopy. In *Bull Volcanol,* 71. pp. 659–670. DOI 10.1007/s00445-008-0252-8.

Kloskowski, A.; Pilarczyk, M.; Namieśnik, J. (2002): Denudation—a convenient method of isolation and enrichment of analytes. In Critical reviews in analytical chemistry, 32, pp. 301–335.

Kutterolf, S.; Hansteen, T. H.; Freundt, A.; Wehrmann, H.; Appel, K.; Krüger, K.; Pérez, W. (2015): Bromine and chlorine emissions from Plinian eruptions along the Central American Volcanic Arc: From source to atmosphere. In *Earth and Planetary Science Letters* 429, pp. 234–246. DOI: 10.1016/j.epsl.2015.07.064.

Laiolo, M.; Coppola, D.; Barahona, F.; Benitez, J. E.; Cigolini, C.; Escobar, D. et al. (2017): Evidences of volcanic unrest on high-temperature fumaroles by satellite thermal monitoring: The case of Santa Ana volcano, El Salvador. In *Journa of Volcanolgy and Geothermal Research* 340, pp. 170–179.

Lee, S.; Kang, N.; Park, M.; Hwang, J. Y.; Yun, S. H.; Jeong, H. Y. (2018): A review on volcanic gas compositions related to volcanic activities and non-volcanological effects. In *Geosci J* 22 (1), pp. 183–197. DOI: 10.1007/s12303-017-0056-y.

Lübcke, P.; Bobrowski, N.; Arellano, S.; Galle, B.; Garzón, G.; Vogel, L.; Platt, U. (2014): BrO/SO_2 molar ratios from scanning DOAS measurements in the NOVAC network. In *Solid Earth* 5 (1), pp. 409–424. DOI: 10.5194/se-5-409-2014.

Major, J.J.; Schilling, S.P.; Pullinger, C.R.; Escobar, C.D:; Chesner, C.A.; Howell, M.M. (2001): Lahar-Hazard Zonation for San Miguel volcano, El Salvador. In U.S. Geological Survey Open file report 01-395.

Martin, R. S.; Mather, T. A.; Pyle, D. M. (2006): High-temperature mixtures of magmatic and atmospheric gases. In *Geochem. Geophys. Geosyst.* 7 (4). DOI: 10.1029/2005GC001186.

Mather, T, A. (2015): Volcanoes and the environment: Lessons for understanding Earth's past and future from studies of present-day volcanic emissions. In *Journal of Volcanology and Geothermal Research* 304, pp. 160–179. DOI: 10.1016/j.jvolgeores.2015.08.016.

McCormick, M.; Thomason, L.; Trepte, C. (1995): Atmospheric effects of the Mt Pinatubo eruption. In *Nature* 373, pp. 399–404. https://doi.org/10.1038/373399a0

Menyailov, I. A. (1975): Prediction of eruptions using changes in composition of volcanic gases. In *B. Volcanol.*, 39, 112–125.

Meyer-Abbich, H. (1956): Anales Servicio Geologico Nacional. In *Anales del Servicio Geologico Nacional*.

Ministry of Environment and Natural Resources (2013, December 31st): Informe Especial - Erupción del Volcán Chaparastique, San Miguel. Retrieved from https://www.snet.gob.sv/ver/vulcanologia/informes+especiales/informe+tecnico/

Moor, J. M. de; Kern, C.; Avard, G.; Muller, C.; Aiuppa, A.; Saballos, A. et al. (2017a): A New Sulfur and Carbon Degassing Inventory for the Southern Central American Volcanic Arc: The Importance of Accurate Time-Series Data Sets and Possible Tectonic Processes Responsible for Temporal Variations in Arc-Scale Volatile Emissions. In *Geochem. Geophys. Geosyst.* 18 (12), pp. 4437–4468. DOI: 10.1002/2017GC007141.

Moor, J. M. de; Kern, C.; Avard, G.; Muller, C.; Aiuppa, A.; Saballos, A. et al. (2017b): A New Sulfur and Carbon Degassing Inventory for the Southern Central American Volcanic Arc: The Importance of Accurate Time-Series Data Sets and Possible Tectonic Processes Responsible for Temporal Variations in Arc-Scale Volatile Emissions. In *Geochem. Geophys. Geosyst.* 18 (12), pp. 4437–4468. DOI: 10.1002/2017GC007141.

Noguchi, K. and Kamiya, H. (1963): Prediction of volcanic eruption by measuring the chemical composition and amounts of gases. In *B. Volcanol.*, 26, 367–378.

Olmos, R.; Barrancos, J.; Rivera, C.; Barahona, F.; López, D. L.; Henriquez, B. et al. (2007): Anomalous Emissions of SO2 During the Recent Eruption of Santa Ana Volcano, El Salvador, Central America. In *Pure appl. geophys.* 164 (12), pp. 2489–2506. DOI: 10.1007/s00024-007-0276-6.

Oppenheimer, C.; Tsanev, V. I.; Braban, C. F.; Cox, R. A.; Adams, J.W.; Aiuppa, A. et al. (2006): BrO formation in volcanic plumes. In *Geochimica et Cosmochimica Acta* 70 (12), pp. 2935–2941. DOI: 10.1016/j.gca.2006.04.001.

Oppenheimer, C.; Scaillet, B.; Martin; R.S. (2011): Sulfur Degassing From Volcanoes: Source Conditions, Surveillance, Plume Chemistry and Earth System Impacts. In *Reviews in Mineralogy and Geochemistry, Mineralogical Society*, 73, pp.363-421. 10.2138/rmg.2011.73.13

Paonita, A.; Federico, C.; Bonfanti, P.; Capasso, G.; Inguaggiato, S.; Italiano, F. et al. (2013): The episodic and abrupt geochemical changes at La Fossa fumaroles (Vulcano Island, Italy) and related constraints on the dynamics, structure, and compositions of the magmatic system. In *Geochimica et Cosmochimica Acta* 120, pp. 158–178. DOI: 10.1016/j.gca.2013.06.015.

Pérez, N.M.; Hernández, P.A.; Padrón, E.; Cartagena, R.; Olmos, R.; Barahona, F.; Melián, G.; Salazar, P.; López, D.L. (2006): Anomalous diffuse CO2 emissions prior to the January 2002 Short-Term unrest at San Miguel volcano, El Salvador, Central America. In *Pure appl. geophys.* 163, pp. 883–896.

Platt, U.; Stutz, J. (2008): Differential Optical Absorption Spectroscopy. Principles and Applications. Springer.

Platt, U. Bobrowski, N. (2015): Quantification of volcanic reactive halogen emissions. In Volcanism and Global Environmental Change. Cambridge: Cambridge University Press, pp. 115–132.

Pyle, D. M.; Mather, T. A.; Biggs, J. (2013): Remote sensing of volcanoes and volcanic processes: integrating observation and modelling – introduction. In *Geological Society, London, Special Publications* 380 (1), pp. 1–13. DOI: 10.1144/SP380.14.

Roberts, T. J.; Braban, C. F.; Martin, R. S.; Oppenheimer, C.; Adams, J. W.; Cox, R. A. et al. (2009): Modelling reactive halogen formation and ozone depletion in volcanic plumes. In *Chemical Geology* 263 (1-4), pp. 151–163. DOI: 10.1016/j.chemgeo.2008.11.012.

Roberts, T. J.; Braban, C. F.; Oppenheimer, C.; Martin, R. S.; Freshwater, R. A.; Dawson, D. H. et al. (2012): Electrochemical sensing of volcanic gases. In *Chemical Geology* 332-333, pp. 74–91. DOI: 10.1016/j.chemgeo.2012.08.027.

Roberts, T. J.; Martin, R. S.; Jourdain, L. (2014): Reactive bromine chemistry in Mount Etna's volcanic plume: the influence of total Br, high-temperature processing, aerosol loading and plume–air mixing. In *Atmos. Chem. Phys.* 14 (20), pp. 11201–11219. DOI: 10.5194/acp-14-11201-2014.

Roberts, T. J.; Lurton, T.; Giudice, G.; Liuzzo, M.; Aiuppa, A.; Coltelli, M. et al. (2017): Validation of a novel Multi-Gas sensor for volcanic HCl alongside H2S and SO2 at Mt. Etna. In *Bulletin of volcanology* 79 (5), p. 36. DOI: 10.1007/s00445-017-1114-z.

Robock, A. (2000): Volcanic eruptions and climate. In *Earth in Space*, 12 (7), pp. 9-10.

Robock, A.; Oppenheimer, C. (2003): Volcanism and the Earth's Atmosphere. Washington, D. C.: American Geophysical Union (Geophysical Monograph Series).

Rodríguez, L.A.; Watson, I. M.; Rose, W. I.; Branan, Y. K.; Bluth, G.J.S.; Chigna, G. et al. (2004): SO2 emissions to the atmosphere from active volcanoes in Guatemala and El Salvador, 1999–2002. In *Journal of Volcanology and Geothermal Research* 138 (3-4), pp. 325–344. DOI: 10.1016/j.jvolgeores.2004.07.008.

Rouwet, D.; Hidalgo, S.; Joseph, E. P.; González-Ilama, G. (2019): Fluid Geochemistry and Volcanic Unrest: Dissolving the Haze in Time and Space. In Joachim Gottsmann, Jürgen Neuberg, Bettina Scheu (Eds.): Volcanic Unrest. Cham: Springer International Publishing (Advances in Volcanology), pp. 221–239.

Rüdiger, J.; Bobrowski, N.; Liotta, M.; Hoffmann, T. (2017): Development and application of a sampling method for the determination of reactive halogen species in volcanic gas emissions. In *Analytical and bioanalytical chemistry* 409 (25), pp. 5975–5985. DOI: 10.1007/s00216-017-0525-1.

Rüdiger, J.; Tirpitz, J.; Moor, J. M. de; Bobrowski, N.; Gutmann, A.; Liuzzo, M. et al. (2018): Implementation of electrochemical, optical and denuder-based sensors and sampling techniques on UAV for volcanic gas measurements: examples from Masaya, Turrialba and Stromboli volcanoes. In *Atmos. Meas. Tech.* 11 (4), pp. 2441–2457. DOI: 10.5194/amt-11-2441-2018.

Rüdiger, J.; Gutmann, A.; Bobrowski, N.; Liotta, M.; Moor, J. M. de; Sander, R. et al. (2021): Halogen activation in the plume of Masaya volcano: field observations and box model investigations. In *Atmos. Chem. Phys.* 21 (5), pp. 3371–3393. DOI: 10.5194/acp-21-3371-2021.

Schönhardt, A.; Richter, A.; Theys, N.; Burrows, J. P. (2017): Space-based observation of volcanic iodine monoxide. In *Atmos. Chem. Phys.* 17 (7), pp. 4857–4870. DOI: 10.5194/acp-17-4857-2017.

Sehring, J. (2016): Charakterisierung einer Diffusionsabscheider-Beschichtung zur selektiven Derivatisierung von Interhalogenverbindungen (Bachelorarbeit). Johannes Gutenberg Universität Mainz.

Selva, J.; Bonadonna, C.; Branca, S.; Astis, G. de; Gambino, S.; Paonita, A. et al. (2020): Multiple hazards and paths to eruptions: A review of the volcanic system of Vulcano (Aeolian Islands, Italy). In *Earth-Science Reviews* 207, p. 103186. DOI: 10.1016/j.earscirev.2020.103186.

Shinohara, H. (2005): A new technique to estimate volcanic gas composition: plume measurements with a portable multi-sensor system. In *Journal of Volcanology and Geothermal Research* 143 (4), pp. 319–333. DOI: 10.1016/j.jvolgeores.2004.12.004.Shinohara, H.; Aiuppa, A.; Giudice, G.; Gurrieri, S.; Liuzzo, M. (2008): Variation of H2O/CO2 and CO2 /SO2 ratios of volcanic gases discharged by continuous degassing of Mount Etna volcano, Italy. In *J. Geophys. Res.* 113 (B9). DOI: 10.1029/2007JB005185.

Shinohara, H. (2008): Excess degassing from volcanoes and its role on eruptive and intrusive activity. In *Rev. Geophys.* 46 (4). DOI: 10.1029/2007RG000244.

Sparks et al. (2012): Monitoring volcanoes. In *Science (New York, N.Y.)* 335 (6074), pp. 1310–1311. DOI: 10.1126/science.1220225.

Staunton-Sykes, J.; Aubry, T. J.; Shin, Y. M.; Weber, J.; Marshall, L. R.; Luke Abraham, N. et al. (2021): Co-emission of volcanic sulfur and halogens amplifies volcanic effective radiative forcing. In *Atmos. Chem. Phys.* 21 (11), pp. 9009–9029. DOI: 10.5194/acp-21-9009-2021.

Stoiber, R.E. & Carr, M.J. (1973): Quaternary volcanic and tectonic segmentations of Central America. In *Bull Volcanol* 37 (3), pp. 304–325.

Surl, L.; Roberts, T.; Bekki, S. (2021): Observation and modelling of ozone-destructive halogen chemistry in a passively degassing volcanic plume. In *Atmos. Chem. Phys.* 21 (16), pp. 12413–12441. DOI: 10.5194/acp-21-12413-2021.

Symonds et al. (1994): VOLCANIC-GAS STUDIES: METHODS, RESULTS, AND APPLICATIONS. In *Volatiles in Magmas*, edited by Michael R. Carroll and John R. Holloway, Berlin, Boston: De Gruyter, 2018, pp. 1-66. https://doi.org/10.1515/9781501509674-007

Symonds R.B., Gerlach T.M. & Reed M.H (2001): Magmatic gas scrubbing: implications for volcano monitoring. In *Journal of Volcanology and Geothermal Research* 108, pp. 303–341.

Tabazadeh, A. and Turco, R.P. (1993): Stratospheric Chlorine Injection by Volcanic Eruptions: HCl Scavenging and Implications for Ozone 260, pp. 1082–1086.

Tamburello, G. (2015): Ratiocalc: Software for processing data from multicomponent volcanic gas analyzers. In *Computers & Geosciences* 82, pp. 63–67. DOI: 10.1016/j.cageo.2015.05.004.

Tanaka, K.; Shiraishi, R. & Toda, F. (1999): A new method for stereoselective bromination of stilbene and chalcone in a water suspension medium. In *The Royal Society of Chemistry* 1, pp. 3069–3070.

Textor, C. (2003): Injection of gases into the stratosphere by explosive volcanic eruptions. In *J. Geophys. Res.* 108 (D19). DOI: 10.1029/2002JD002987.

Theys, N.; De Smedt, I.; Van Roozendael, M.; Froidevaux, L.; Clarisse, L.; Hendrick, F. (2014): First satellite detection of volcanic OClO after the eruption of Puyehue-Cordón Caulle. In *Geophys. Res. Lett.*, 41. pp. 667–672. doi:10.1002/2013GL058416.

Timmreck, C. (2012): Modeling the climatic effects of large explosive volcanic eruptions. In *WIREs Clim Change* 3 (6), pp. 545–564. DOI: 10.1002/wcc.192.

Tsai Lee, C.S.; Mathai, I.M.; Miller, S.I. (1970): Stereoselectivity and dehalogenation mechanisms. The elimintion reactions of meso- and dl-stilbene dibromides with iodide in methanol. In *J. Am. Chem. Soc.*, 92, 15, pp. 4602-4609. DOI: 10.1021/ja00718a022

Viramonte, J.G.; Incer-Barquero, J. (2008a): Masaya, the "Mouth of Hell", Nicaragua: Volcanological interpretation of the myths, legends and anecdotes. In *Journal of Volcanology and Geothermal Research* 176 (3), pp. 419–426. DOI: 10.1016/j.jvolgeores.2008.01.038.

Walker, J. A.; Williams, S.N., Kalamarides, R.I. & Feigenson, M:D. (1993): Shallow open-system evolution of basaltic magma beneath a subduction zone volcano: the Masaya Caldera Complex, Nicaragua. In *Journal of Volcanology and Geothermal Research* 56, pp. 379–400.

Wallace, P.J.; Anderson, A.; Davis, A.M. (1999): Gradients in H2O, CO2 and exsolved gas in a large-volume silicic magma system: Interpreting the record preserved in melt inclusions from the Bishop Tuff. In *Journal of Geophysical Research: Solid Earth*, 104, pp. 20097- 20122.

Wallace, P.J. (2003): From Mantle to Atmosphere: Magma Degassing, Explosive Eruptions, and Volcanic Volatile Budgets. In MELT INCLUSIONS IN VOLCANIC SYSTEMS: METHODS, APPLICATIONS AND PROBLEMS (B. De Vivo & R.J. Bodnar, Eds). Developments in Volcanology 5. Elsevier, Amsterdam, pp. 105-127.

Wallace, P. J. (2005): Volatiles in subduction zone magmas: concentrations and fluxes based on melt inclusion and volcanic gas data. In *Journal of Volcanology and Geothermal Research* 140 (1-3), pp. 217–240. DOI: 10.1016/j.jvolgeores.2004.07.023.

Warnach, S.; Bobrowski, N.; Hidalgo, S.; Arellano, S.; Sihler, H.; Dinger, F. et al. (2019): Variation of the BrO/SO2 Molar Ratio in the Plume of Tungurahua Volcano Between 2007 and 2017 and Its Relationship to Volcanic Activity. In *Front. Earth Sci.* 7. DOI: 10.3389/feart.2019.00132.

Williams-Jones, G. (2001): Integrated geophysical studies at Masaya volcano, Nicaragua. The Open University.

Witt, M. L. I.; Mather, T. A.; Pyle, D. M.; Aiuppa, A.; Bagnato, E.; Tsanev, V. I. (2008): Mercury and halogen emissions from Masaya and Telica volcanoes, Nicaragua. In *J. Geophys. Res.* 113 (B6). DOI: 10.1029/2007JB005401.

Wittmer, J.; Bobrowski, N.; Liotta, M.; Giuffrida, G.; Calabrese, S.; Platt, U. (2014): Active alkaline traps to determine acidic-gas ratios in volcanic plumes: Sampling techniques and

analytical methods. In *Geochem. Geophys. Geosyst.* 15 (7), pp. 2797–2820. DOI: 10.1002/2013GC005133.

7. Annex

7.1. Supplementary material from section 4.2
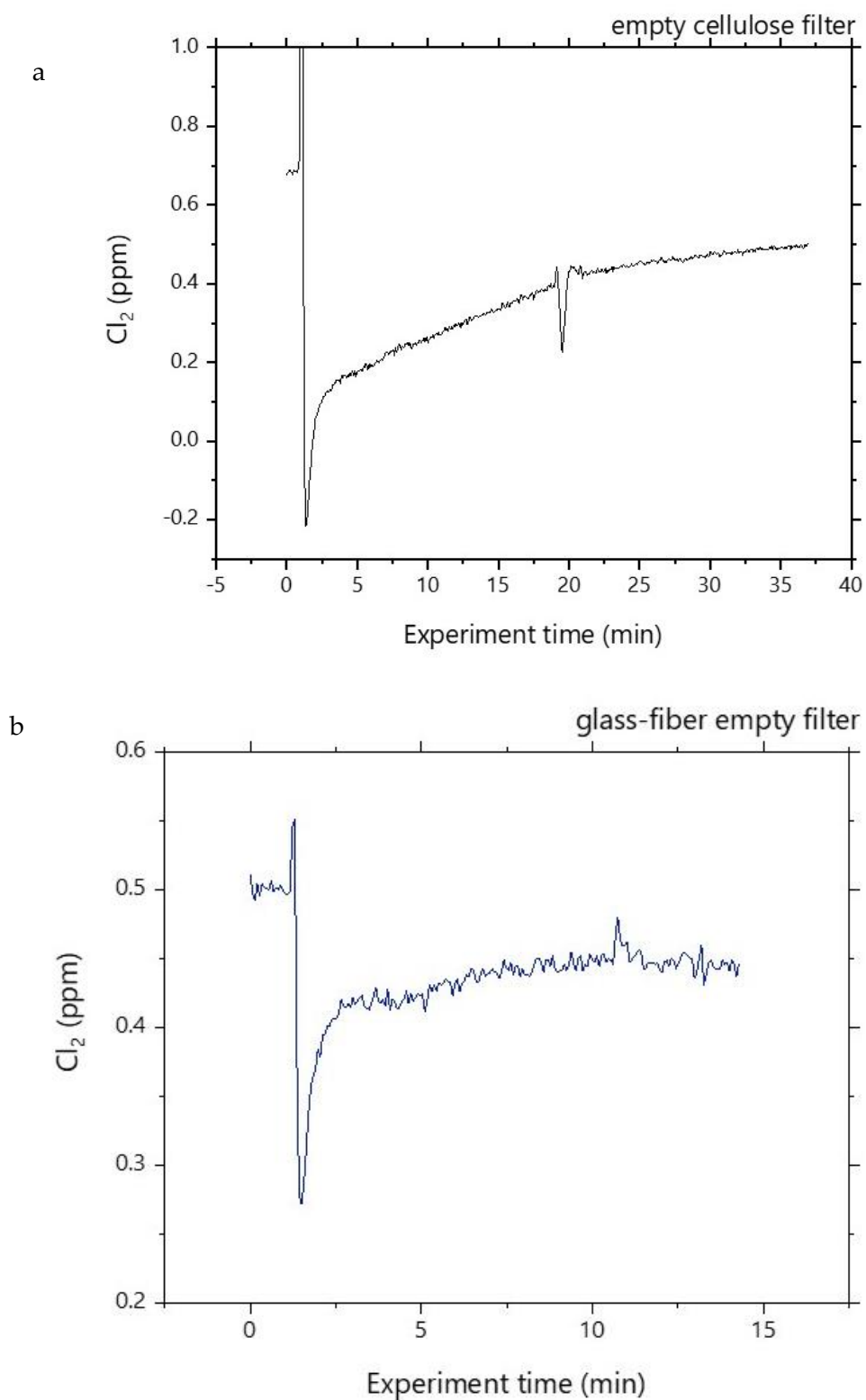
Figure S1. Comparison of absorption of Cl$_2$ of two different empty filters (a) cellulose and (b) glass-fiber
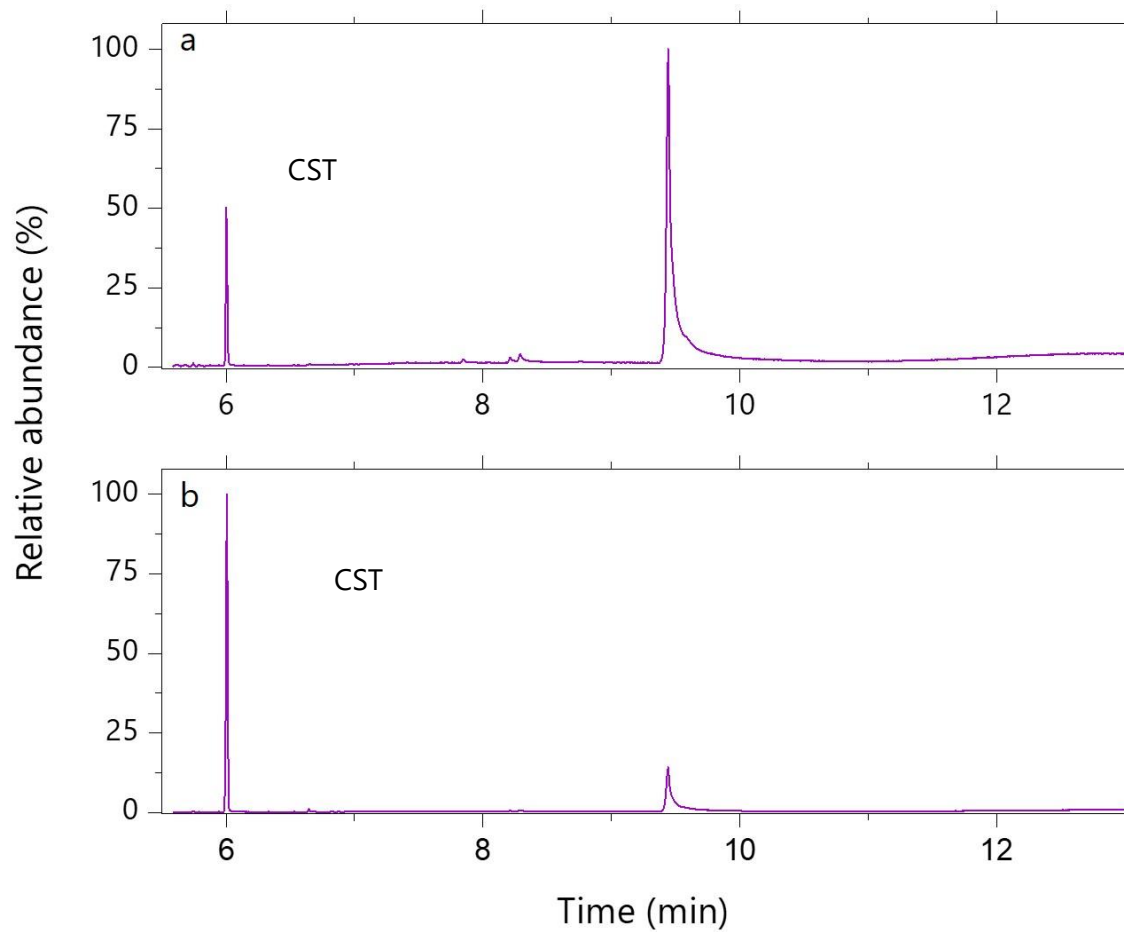
Figure S2. Chromatograms of CST-coated filters storage at (a) room-T and (b) -4 °C, for 1.5 days. And covered with aluminum foil. The chromatograms show the signal of CST at 6.0 minutes and an impurity at 9.8 minutes. There is no signal of the trans-isomer (6.5 min).

7.2. Supplementary material from section 4.3

Table S1. CO_2/SO_2 molar ratios obtained from Masaya volcano, Nicaragua using MultiGAS (SK)

Date	Sampling place	SO_2 max	CO_2/SO_2	error	R^2	Data points
22/01/2019	Pole	8.00	8.13	3.18	0.843	110
22/01/2019	Pole	5.48	8.75	3.05	0.822	128
22/01/2019	Pole	8.30	6.30	2.04	0.832	138
22/01/2019	Pole	6.52	7.15	1.80	0.907	137
22/01/2019	Pole	9.70	7.13	2.21	0.874	119
22/01/2019	Pole	4.93	6.06	3.61	0.722	110
22/01/2019	Pole	3.41	6.53	3.42	0.816	92
22/01/2019	Pole	4.92	6.68	3.93	0.812	92
22/01/2019	Pole	5.65	5.66	1.74	0.761	238
22/01/2019	Pole	5.95	5.40	4.02	0.913	91
22/01/2019	Pole	10.39	6.19	1.35	0.816	320
22/01/2019	Pole	6.34	5.38	1.44	0.828	238
22/01/2019	Nindiri	11.4	6.13	2.52	0.851	98
22/01/2019	Nindiri	4.16	7.88	4.53	0.883	60
22/01/2019	Nindiri	7.43	3.92	7.52	0.581	38
22/01/2019	Nindiri	8.38	5.44	7.52	0.753	60
22/01/2019	Nindiri	20.5	3.64	0.55	0.824	636
22/01/2019	Nindiri	12.87	3.73	2.01	0.755	103
22/01/2019	Nindiri	6.5	3.4	1.94	0.646	141
24/01/2019	Pole	5.80	8.28	2.68	0.686	334
24/01/2019	Pole	4.12	16.68	10.99	0.602	130
24/01/2019	Pole	6.45	4.68	1.88	0.603	296
24/01/2019	Pole	5.53	4.25	3.14	0.655	93
24/01/2019	Pole	5.64	4.85	2.76	0.630	149

24/01/2019	Pole	8.1	4.70	1.43	0.725	296
24/01/2019	Pole	7.49	6.00	3.03	0.684	149
24/01/2019	Pole	6.30	5.40	1.95	0.652	297
23/01/2019	Pole	10.20	8.82	4.48	0.684	
23/01/2019	Pole	5.80	11.16	4.35	0.826	
23/01/2019	Pole	8.80	9.82	5.21	0.810	
23/01/2019	Pole	8.46	7.22	2.21	0.854	
23/01/2019	Pole	7.64	7.53	2.97	0.838	
23/01/2019	Pole	8.00	7.96	2.74	0.705	
23/01/2019	Pole	10.06	5.91	1.67	0.761	
23/01/2019	Pole	15.33	5.77	1.12	0.737	
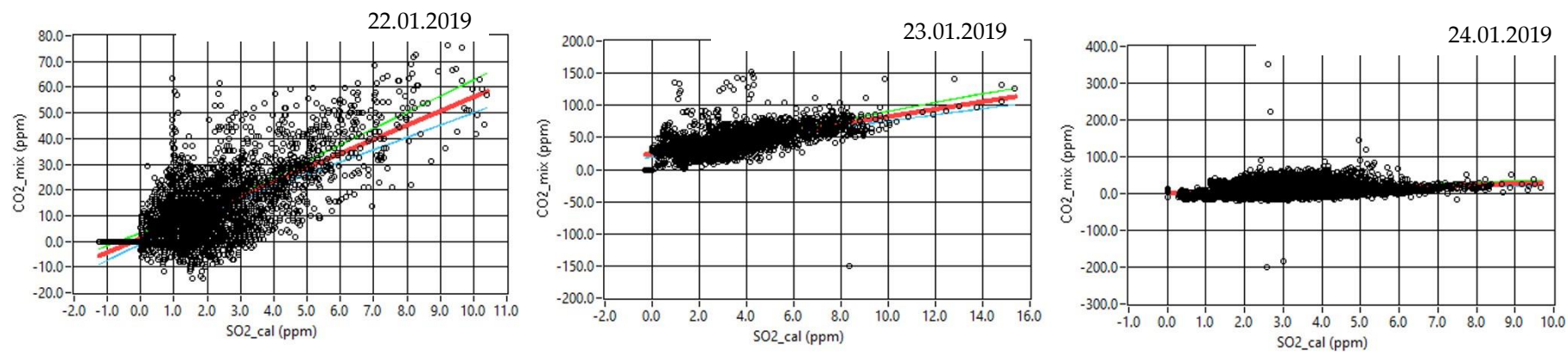
Figure S2. Scatter plot of CO_2 and SO_2 concentrations and the calculated best-fit line (red) obtained at Masaya using the RatioCalc program.

Table S2. CO_2/SO_2 molar ratios obtained from La Fossa crater, Vulcano, Italy using MultiGAS (SK)

Date	SO$_2$ max	CO$_2$/SO$_2$	error	R^2
9/24/2019	1023	15.45	5.24	0.675
9/24/2019	1023	15.7	4.06	0.727
9/24/2019	1023	14.85	3.6	0.708
9/24/2019	998.93	14.68	3.48	0.655
9/24/2019	1023	14.06	8.01	0.836
9/25/2019	458.8	2.47	0.31	0.83
9/25/2019	521.94	2.23	0.23	0.806
9/25/2019	564.7	2.2	0.35	0.702
9/25/2019	248.02	2.24	0..44	0.704
9/25/2019	257.97	2.16	0.36	0.717
9/25/2019	264.25	2.13	0.27	0.683
9/26/2019	1023	15.17	5.29	0.873
10/11/2020	786.2	2.2	0.04	0.934
10/11/2020	506	18.12	0.35	0.914
10/12/2020	341	2.51	0.08	0.905
10/14/2020	182.1	21.55	8.23	0.601
10/14/2020	188.94	22.35	6.4	0.517
10/14/2020	172.86	19.99	7.87	0.653
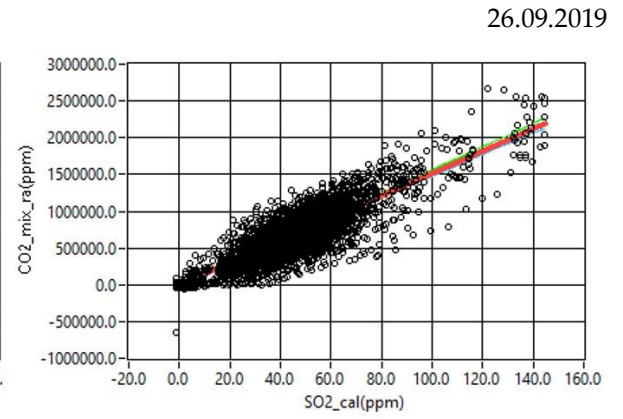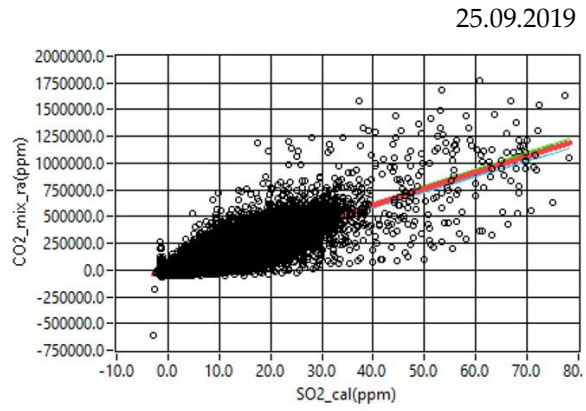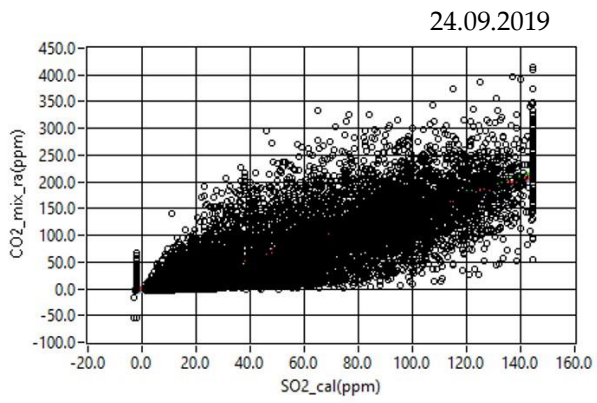
Figure S3. Scatter plot of CO₂ and SO₂ concentrations and the calculated best-fit line (red) obtained at Vulcano during field survey 2019.
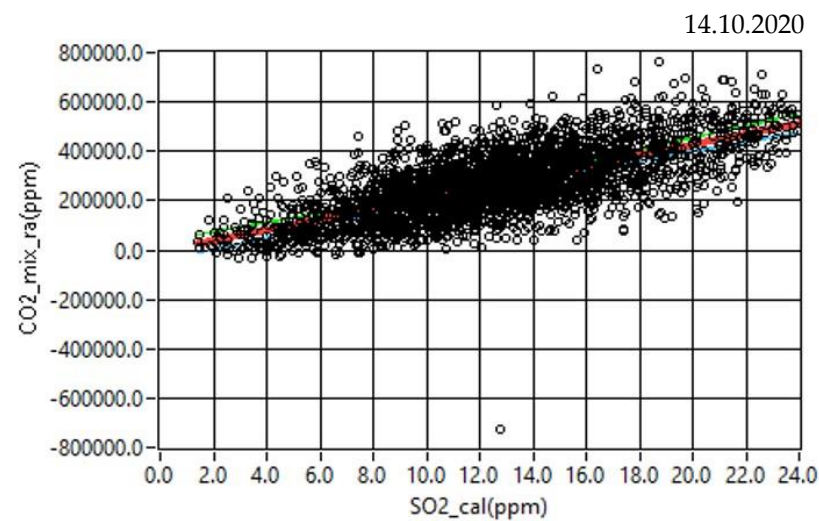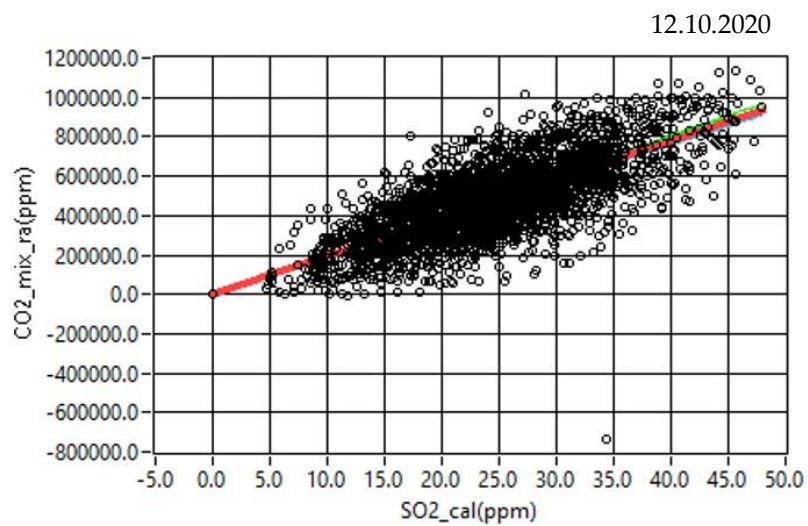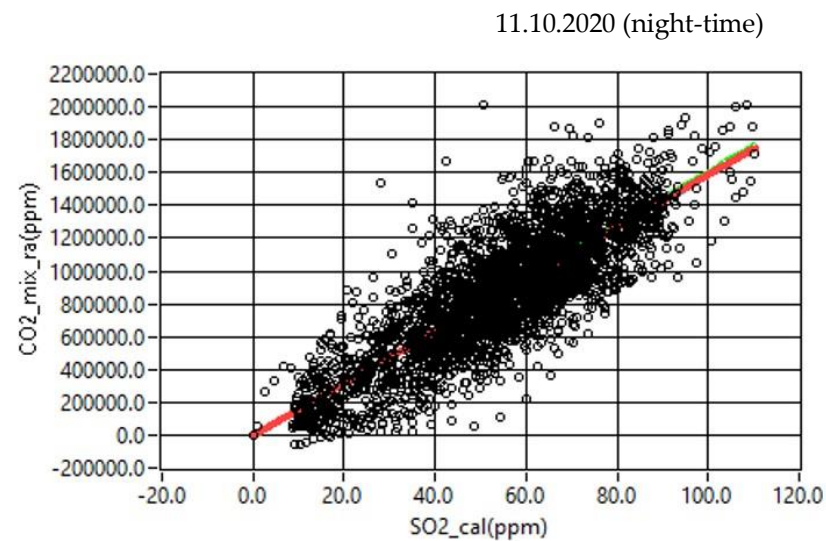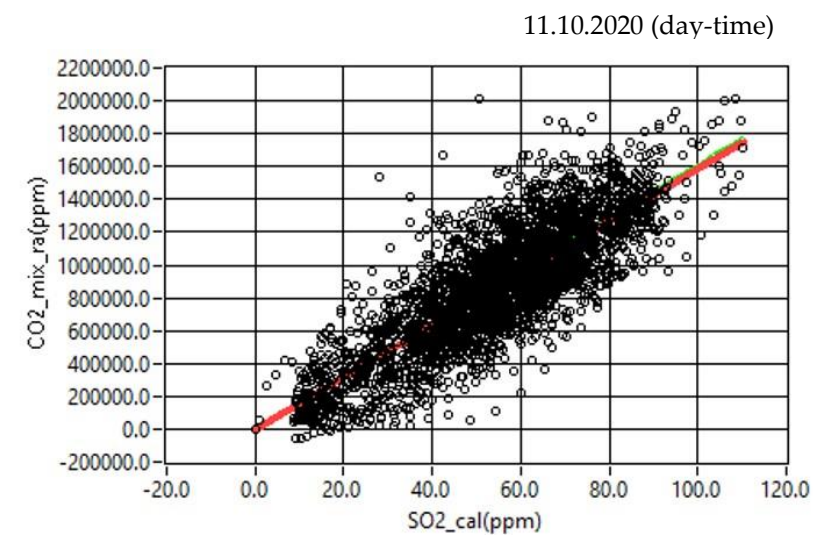
Figure S4. Scatter plot of CO_2 and SO_2 concentrations and the calculated best-fit line (red) obtained at Vulcano during field survey 2020.

7.3. Supplementary material from section 4.4

Table S3. CO_2/SO_2 molar ratios obtained from Santa Ana, El Salvador using MultiGAS (PT)

Date	Sampling site	SO_2 max	CO_2/SO_2	error	R^2	Data points
30/01/2019	SA plateau	11.90	5.34	0.32	0.719	417
30/01/2019	SA plateau	6.37	7.96	0.55	0.718	314
30/01/2019	SA plateau	12.22	5.59	0.39	0.904	121
30/01/2019	SA plateau	10.11	3.26	0.20	0.739	103
30/01/2019	SA plateau	9.26	3.90	0.44	0.752	357
30/01/2019	SA plateau	12.49	3.03	0.20	0.761	284
30/01/2019	SA plateau	4.90	9.35	1.14	0.631	202
30/01/2019	SA plateau	10.77	2.61	0.13	0.621	886
31/01/2019	SA plateau	6.76	5.16	0.90	0.709	101

30.01.2019

31.01.2019
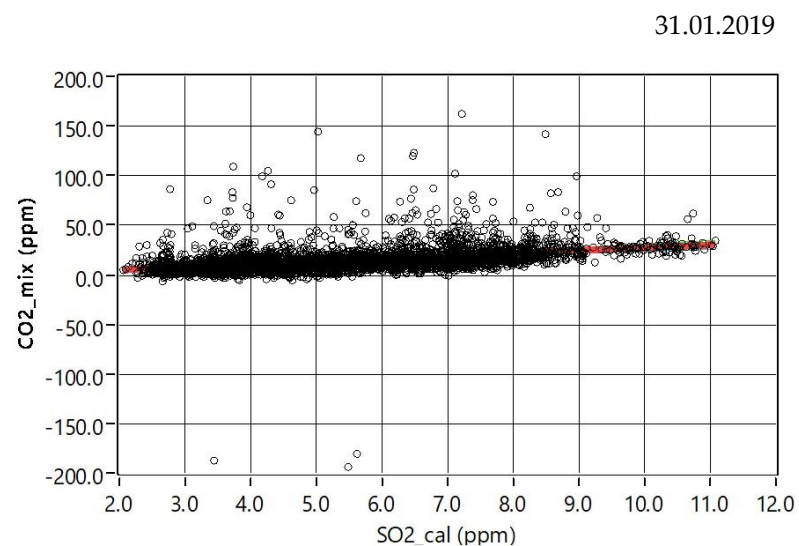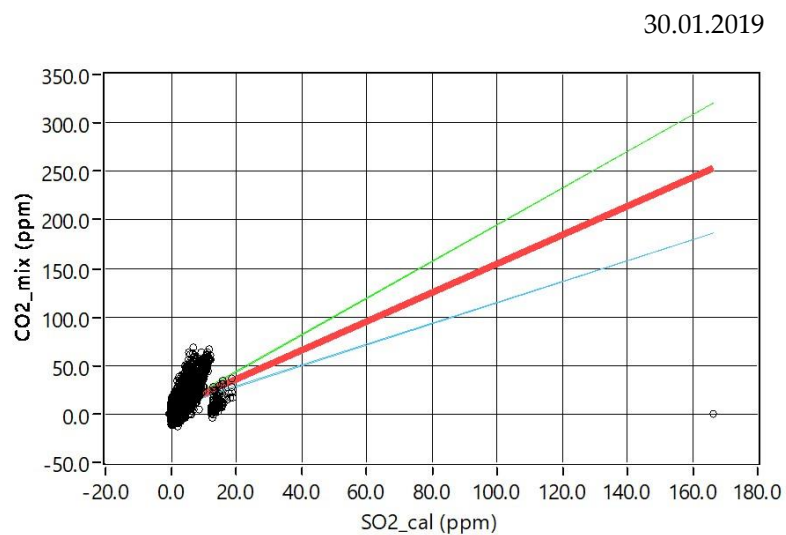
Figure S5. Scatter plot of CO_2 and SO_2 concentrations and the calculated best-fit line (red) obtained at Santa Ana during field survey 2019 using the PT device.

Table S4. CO_2/SO_2 molar ratios obtained during dron flights above crater lake at Santa Ana, El Salvador using MultiGAS (SK)

Date	Flight	SO₂ max	CO₂/SO₂	error	R²	Data points
30/01/2019	fligth 1	16.30	3.17	0.89	0.794	245
31/01/2019	fligth 1	17.30	2.10	1.55	0.638	405
31/01/2019	fligth 4	19.60	3.72	1.39	0.638	299
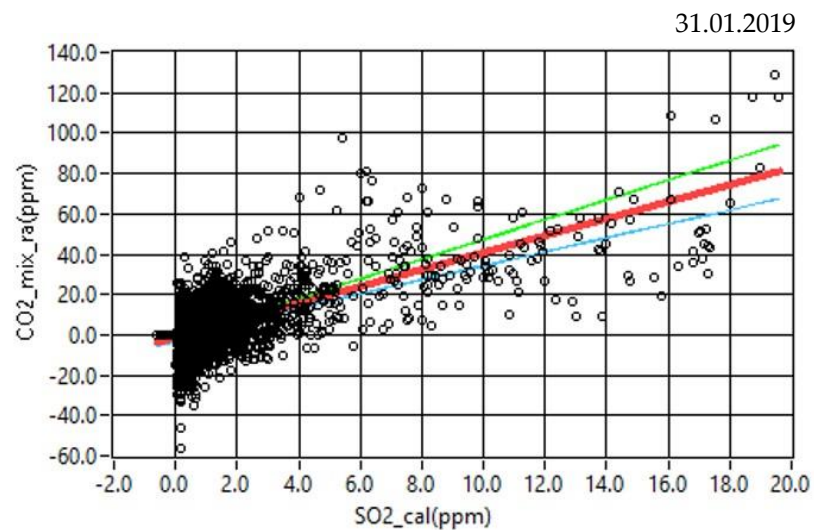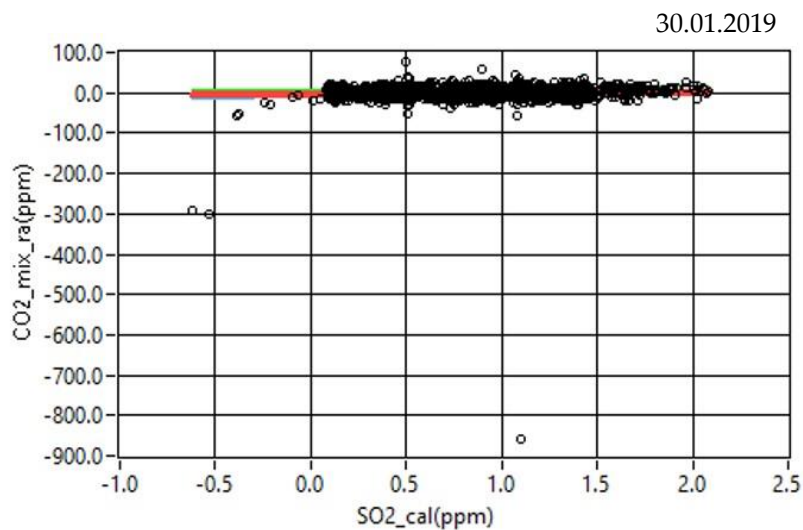
Figure S6. Scatter plot of CO_2 and SO_2 concentrations and the calculated best-fit line (red) obtained at Santa Ana during field survey 2019 using the SK device.

Table S5. CO₂, H₂S, H₂ and H₂O to SO₂ molar ratios obtained at Santa Ana, El Salvador with the SN instrument

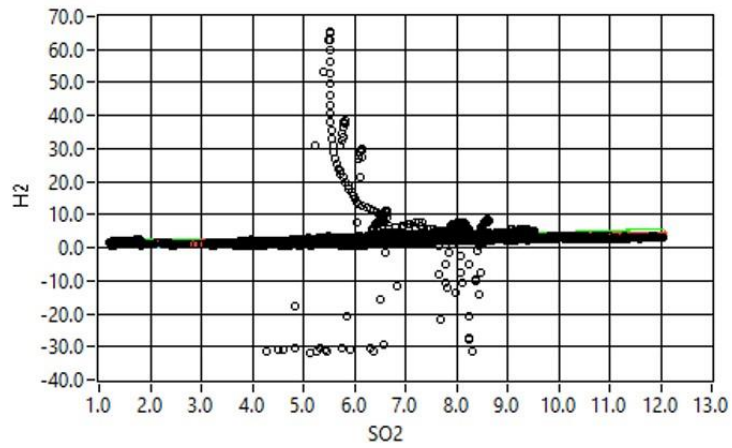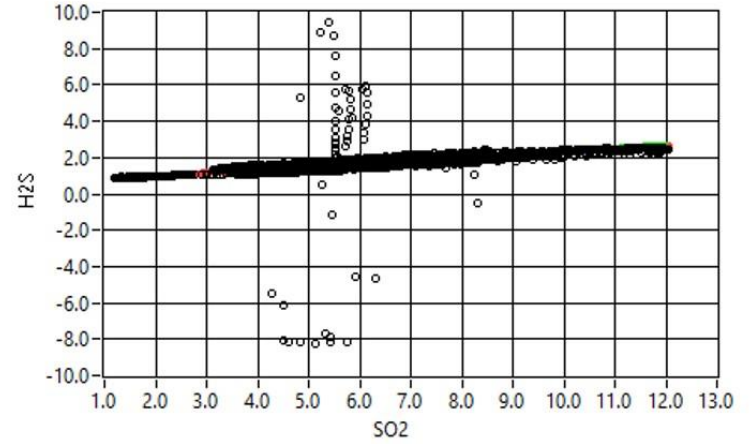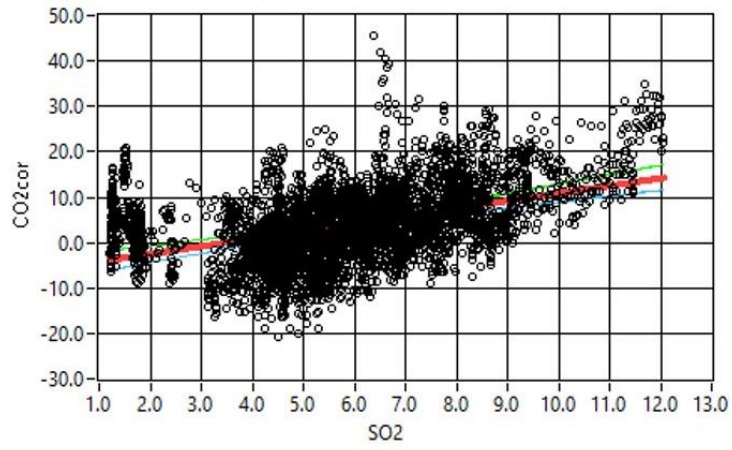| Date	Sampling place	SO_2 max	CO_2/SO_2	error	R^2	H_2S/SO_2	error	R^2	H_2/SO_2	error	R^2	H_2O/SO_2	error	R^2	Data points
29/01/2019	plateau	17.50	1.92	0.35	0.829	0.12	0.03	0.740							421
29/01/2019	plateau	32.15	2.39	0.29	0.869	0.13	0.02	0.828							688
29/01/2019	plateau	26.16	2.72	0.41	0.870	0.14	0.02	0.884							467
29/01/2019	plateau	25.56	3.05	0.54	0.852	0.13	0.02	0.911	0.44	0.08	0.860				385
29/01/2019	plateau	28.66	2.85	0.29	0.896	0.14	0.02	0.875	0.42	0.09	0.656				779
29/01/2019	plateau	33.57	2.20	0.20	0.914	0.14	0.01	0.926				80.09	8.21	0.897	742
30/01/2019	plateau	21.00	2.05	0.33	0.826	0.14	0.01	0.933	0.20	0.03	0.813	68.09	10.36	0.845	543
30/01/2019	plateau	11.80	4.00	0.75	0.835	0.12	0.03	0.781	0.80	0.27	0.617				397
30/01/2019	plateau	21.30	3.32	0.37	0.909	0.13	0.02	0.898	0.63	0.10	0.839	54.80	12.40	0.712	543
30/01/2019	plateau	8.41	3.69	1.40	0.634	0.13	0.03	0.811							291
30/01/2019	plateau	18.76	3.63	0.53	0.859	0.12	0.02	0.829	0.53	0.17	0.612	56.71	16.56	0.604	530
30/01/2019	plateau	19.75	3.00	0.56	0.744	0.12	0.02	0.821				45.96	10.31	0.671	662
30/01/2019	plateau	23.69	2.77	0.42	0.766	0.11	0.02	0.718							887
30/01/2019	plateau	6.99				0.12	0.04	0.789							225
31/01/2019	plateau	7.40	7.36	1.68	0.834	0.12	0.02	0.872				81.24	28.97	0.673	280
31/01/2019	plateau	12.04	2.52	0.61	0.694	0.15	0.01	0.976	0.23	0.01	0.725	44.53	13.01	0.611	515
31/01/2019	plateau	11.47	2.97	0.78	0.687	0.14	0.02	0.927	0.21	0.05	0.743	73.80	23.44	0.600	460
31/01/2019	plateau	9.53				0.14	0.02	0.855	0.72	0.18	0.740	107.09	20.11	0.836	392
31/01/2019	plateau	7.94	11.83	5.09	0.812	0.12	0.03	0.943	0.73	0.37	0.758	81.83	42.50	0.748	112
31/01/2019	plateau	11.69				0.13	0.03	0.865				110.98	47.75	0.646	224
08/08/2019	SA rim	4.60				0.19	0.04	0.908				50.92	21.71	0.661	215
08/08/2019	SA rim	3.93	10.10	5.90	0.756	0.28	0.05	0.973				34.91	22.96	0.709	92
24/10/2019	SA rim	3.04				0.14	0.05	0.740							199
17/12/2019	SA rim	10.60	1.96	1.50	0.658	0.17	0.07	0.875							88
17/12/2019	SA rim	8.40	3.97	1.37	0.663	0.15	0.02	0.912	0.57	0.18	0.706				308
17/12/2019	SA rim	12.65	3.88	1.25	0.857	0.14	0.03	0.912	0.39	0.17	0.768	69.71	28.36	0.789	136
17/12/2019	SA rim	10.63	4.28	1.04	0.842	0.15	0.02	0.938	0.33	0.09	0.800	70.52	50.52	0.378	240
17/12/2019	SA rim	9.01	3.75	1.80	0.765	0.12	0.04	0.851	0.41	0.26	0.646	61.28	22.91	0.844	117
17/12/2019	SA rim	5.22	4.97	3.32	0.668	0.12	0.06	0.801							103

Date	Type														
23/01/2020	SA rim	5.86	3.13	1.71	0.680	0.14	0.05	0.839				47.91	16.84	0.838	133
23/01/2020	SA rim	9.97	2.65	1.74	0.712	0.15	0.09	0.751							91
23/01/2020	SA rim	15.80				0.18	0.02	0.919				35.63	21.30	0.328	404
30/09/2020	SA rim	3.43				0.12	0.08	0.478							183
30/09/2020	SA rim	7.44	9.44	4.94	0.611	0.17	0.03	0.925				295.22	103.89	0.776	183
30/09/2020	SA rim	7.90	6.21	2.79	0.729	0.09	0.04	0.773							151
30/09/2020	SA rim	11.00	4.33	1.07	0.842	0.13	0.03	0.842	0.50	0.12	0.854	31.67	24.48	0.352	232
03/12/2020	SA rim					0.11	0.02	0.897				70.33	84.33	0.179	239
03/12/2020	SA rim	7.58	3.36	1.34	0.606	0.13	0.02	0.892				82.96	76.45	0.224	296
03/12/2020	SA rim	7.88	5.47	2.38	0.622	0.10	0.03	0.736	0.24	0.18	0.357	34.52	112.33	0.029	240
03/12/2020	SA rim					0.10	0.04	0.816	0.07	0.26	0.006	176.85	86.84	0.766	113

Figure S7 - 14. Set of scatter plots of CO₂, H₂S, H₂ and H₂O vs SO₂ concentrations and the calculated best-fit line (red) obtained at Santa Ana (2019 -2020) using the SN device.

29.01.2019
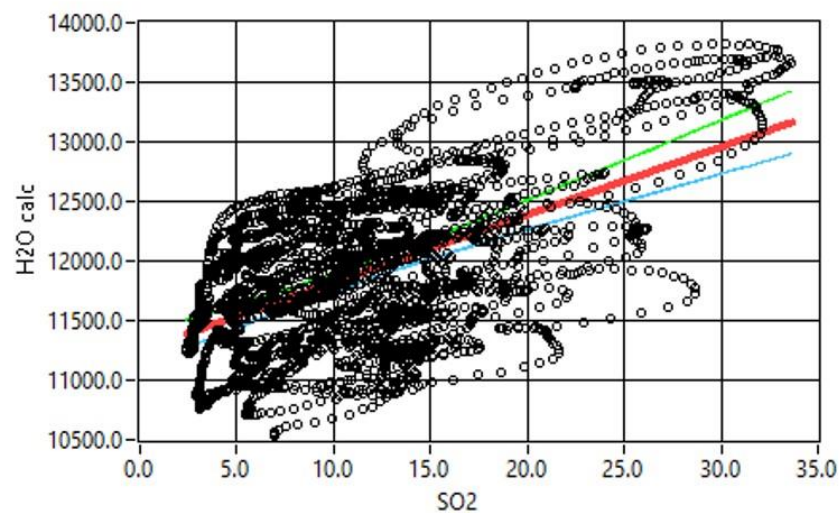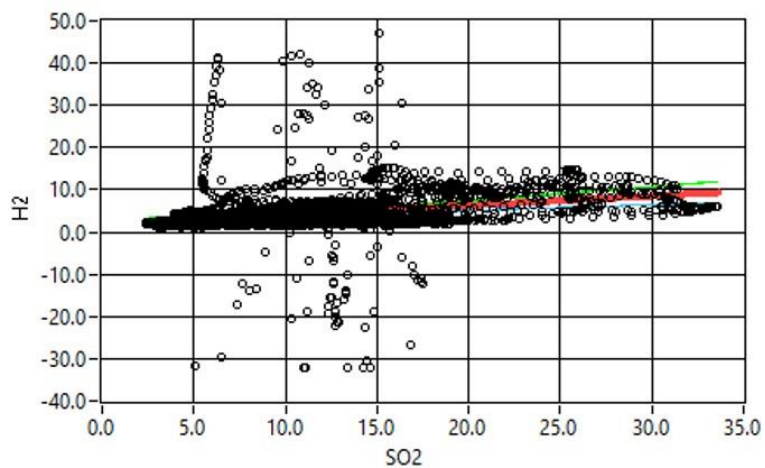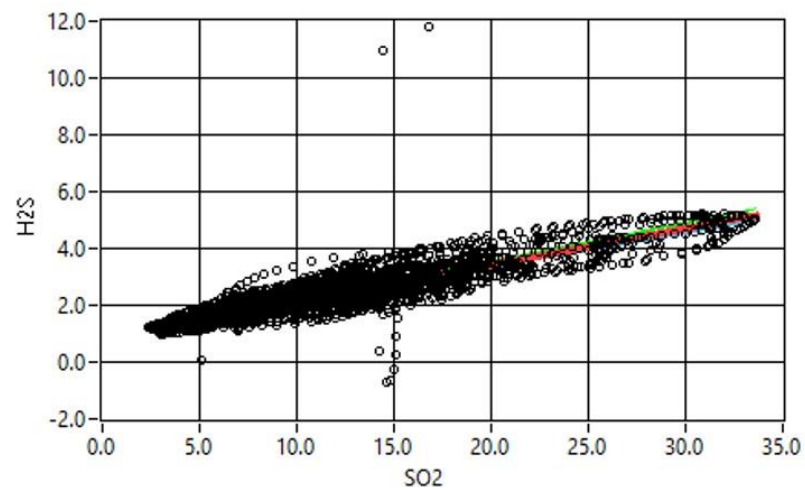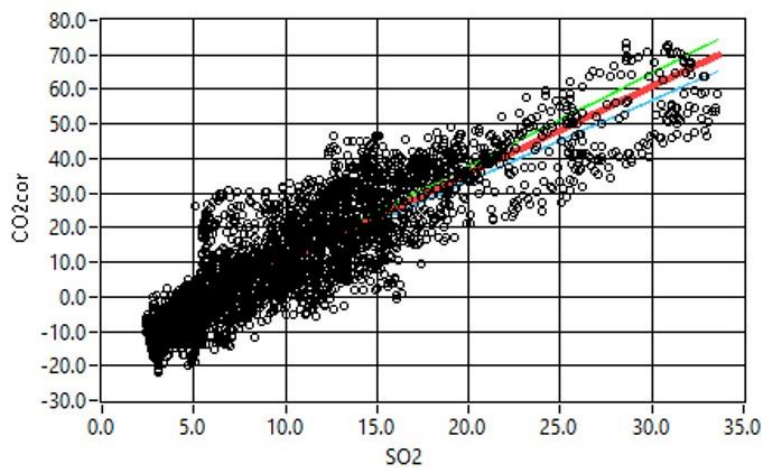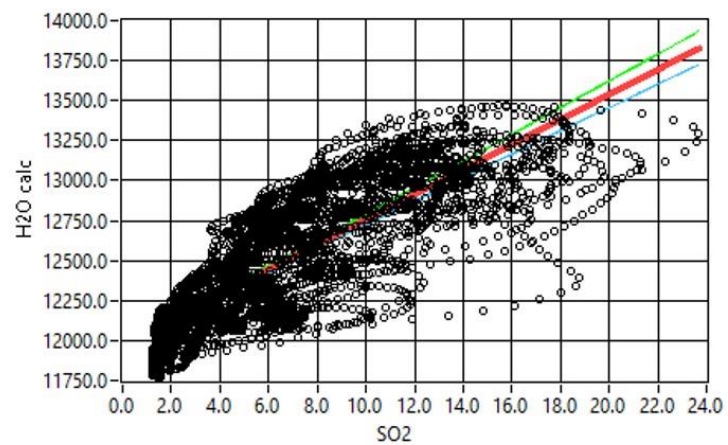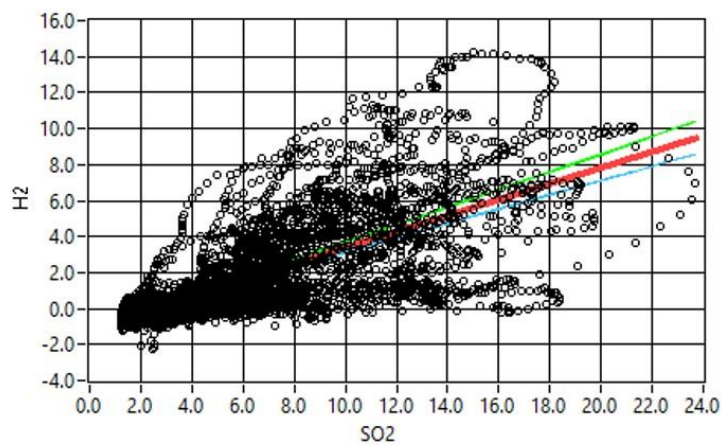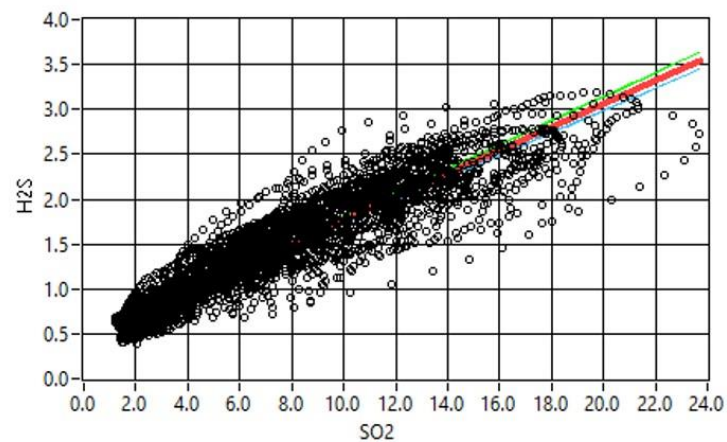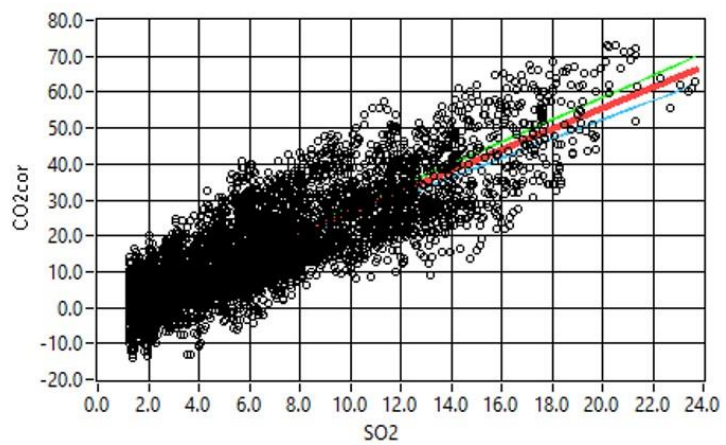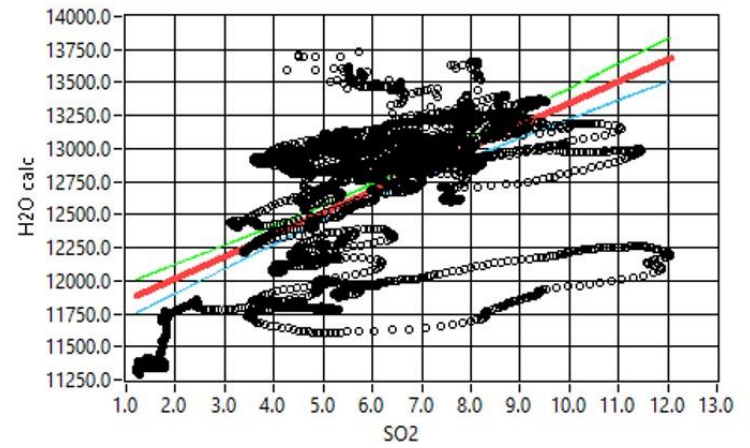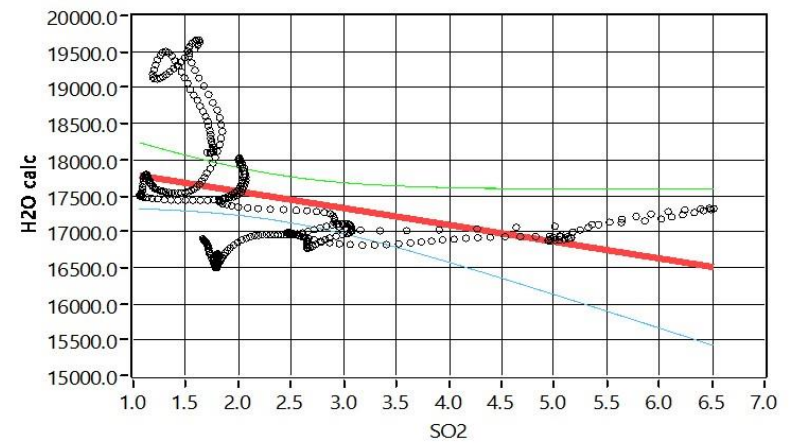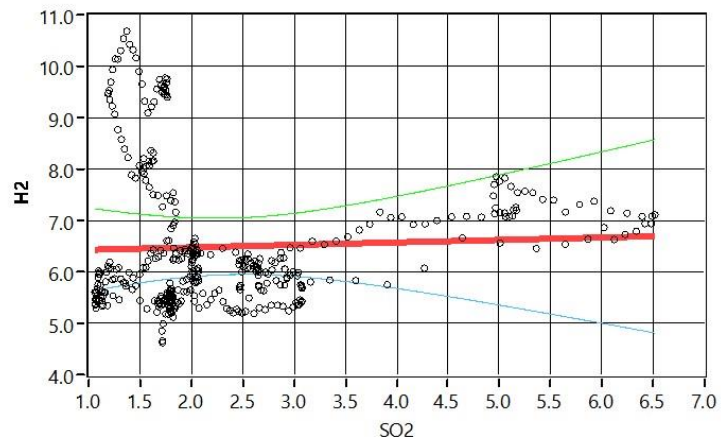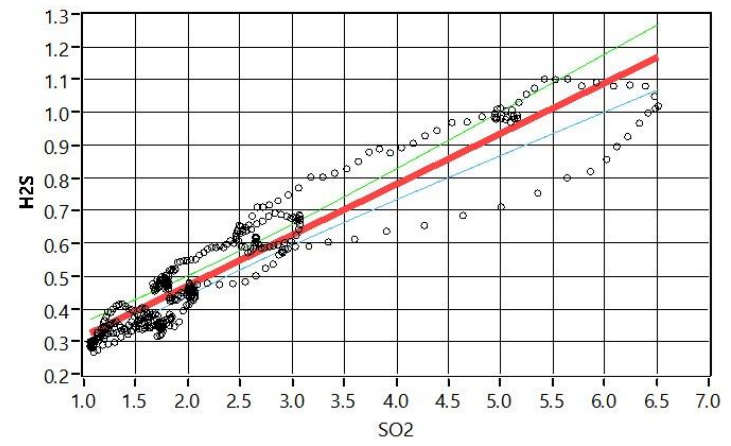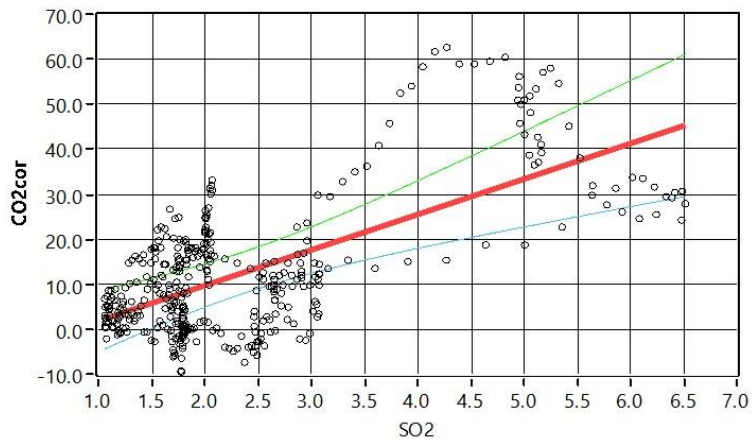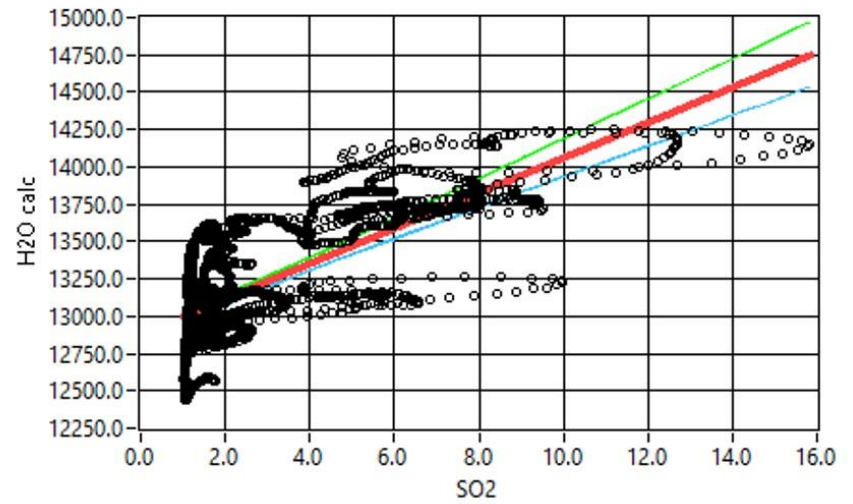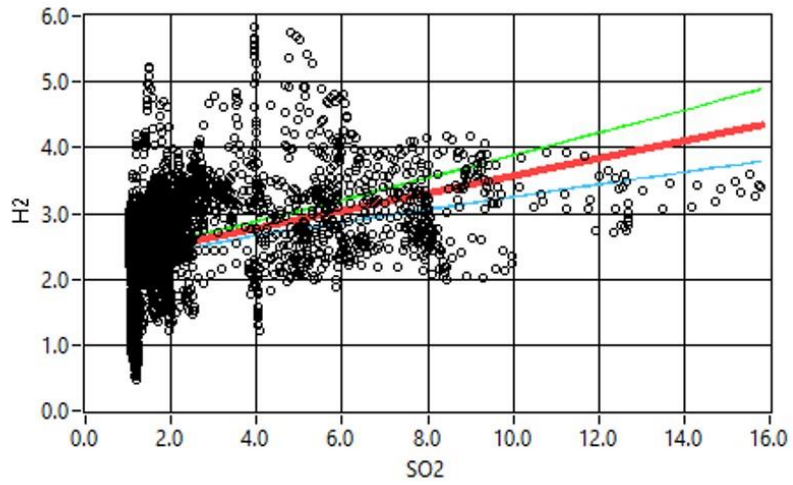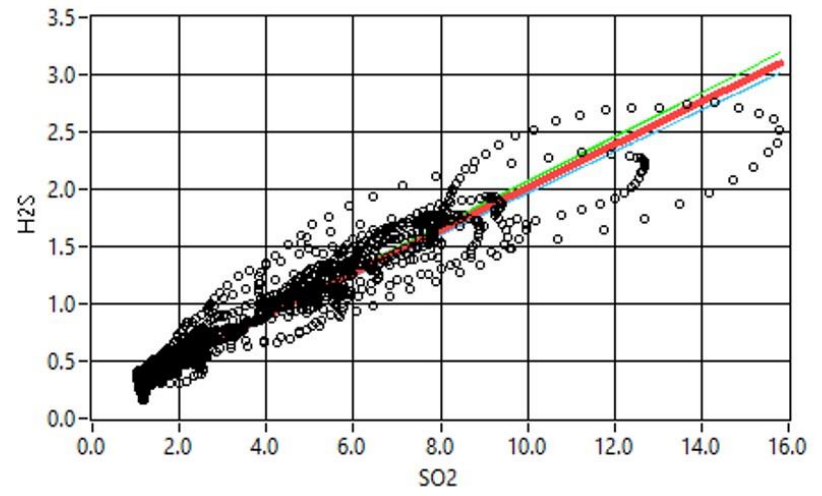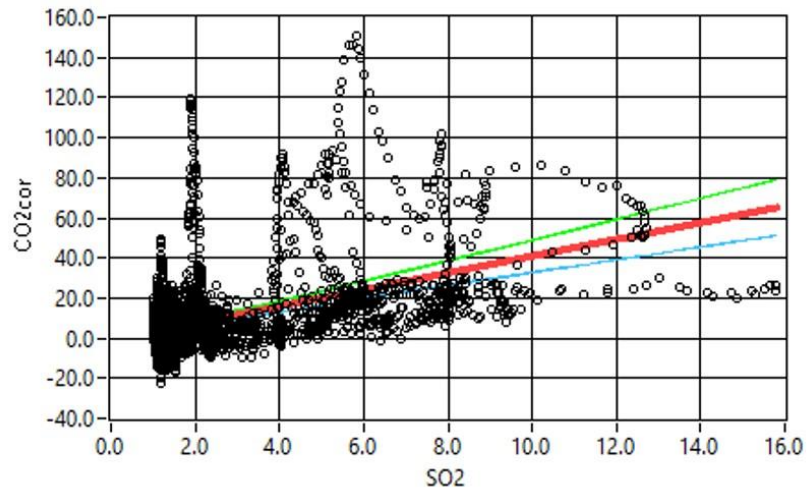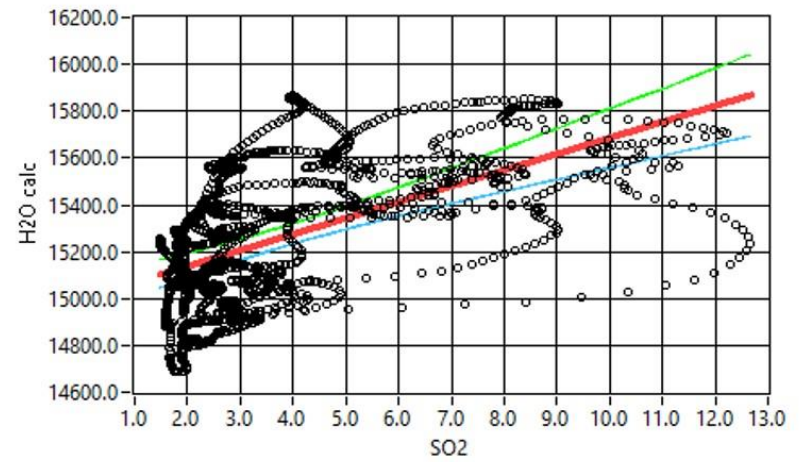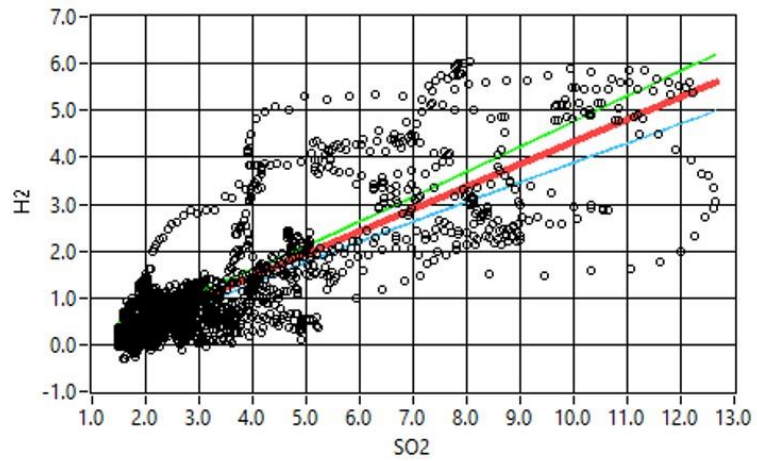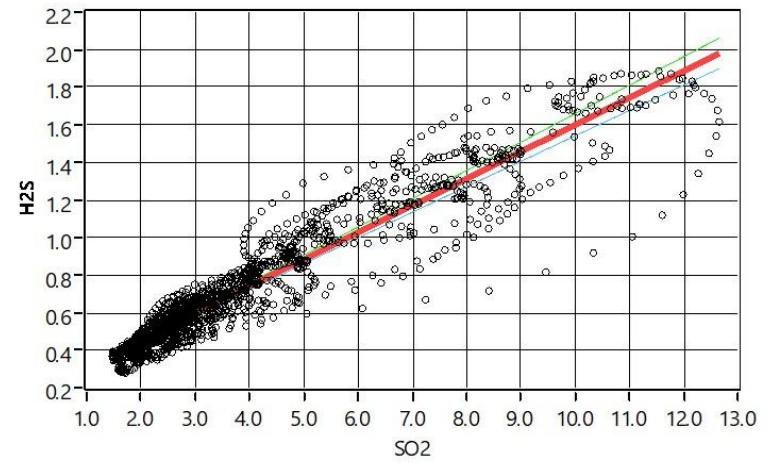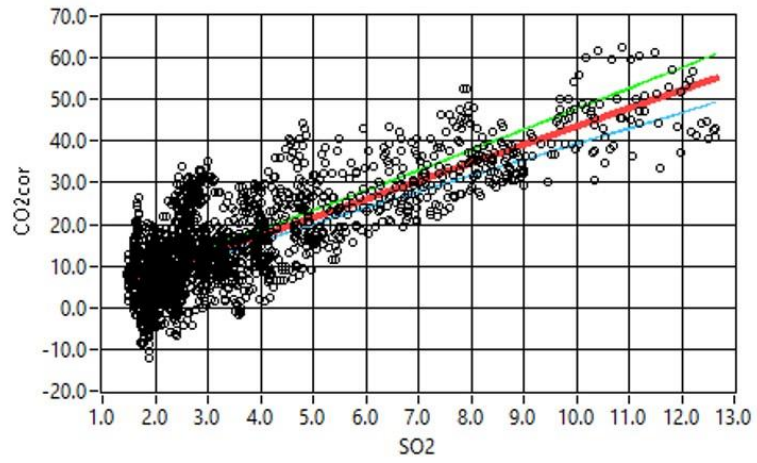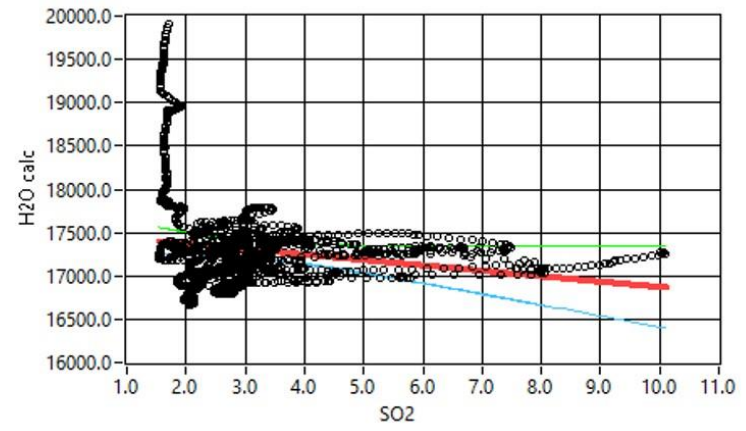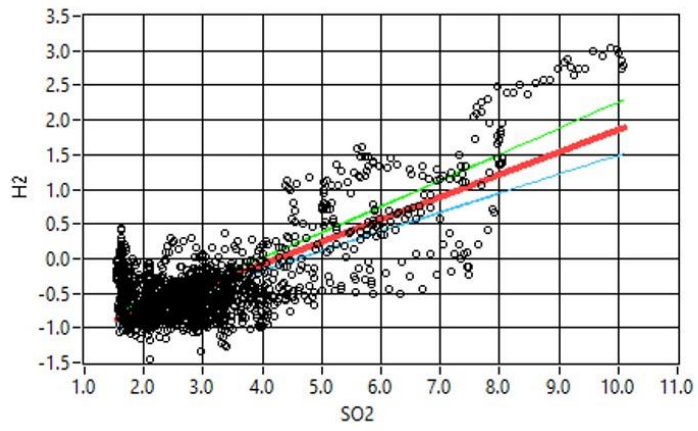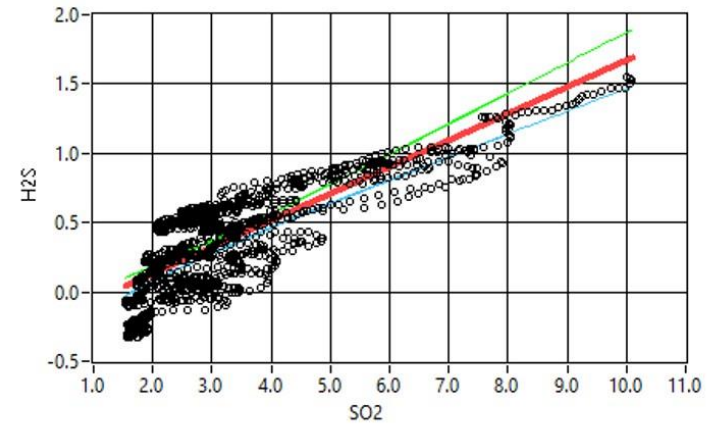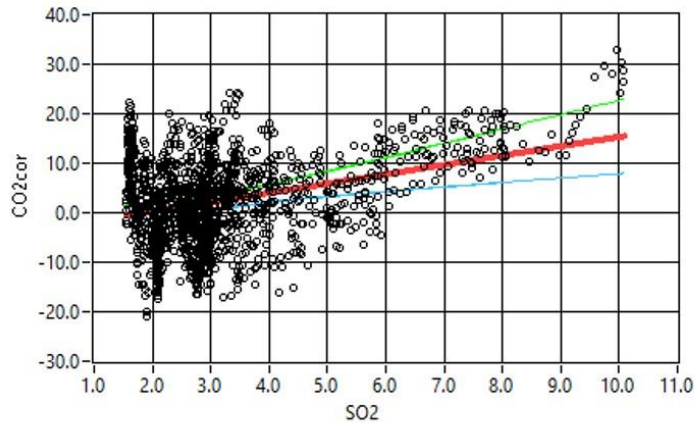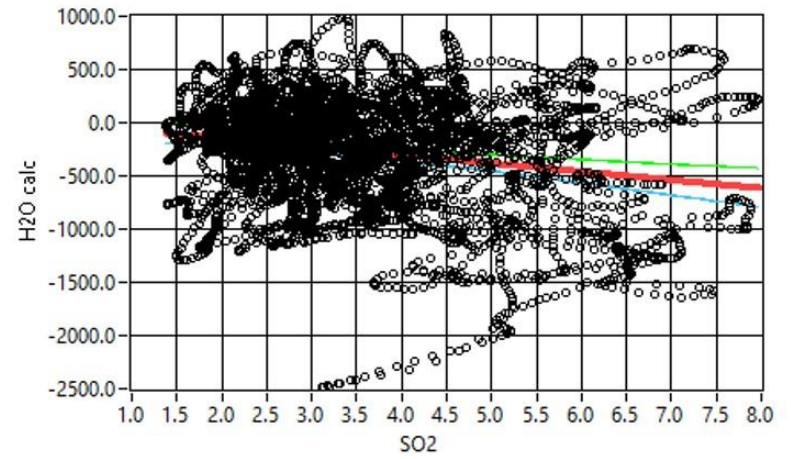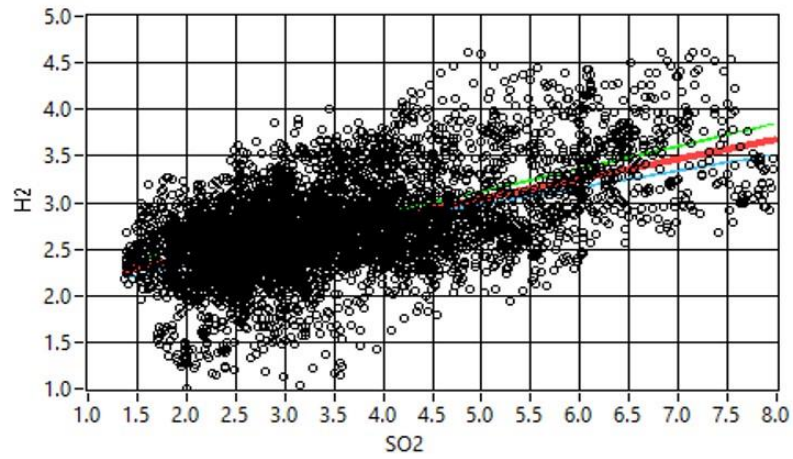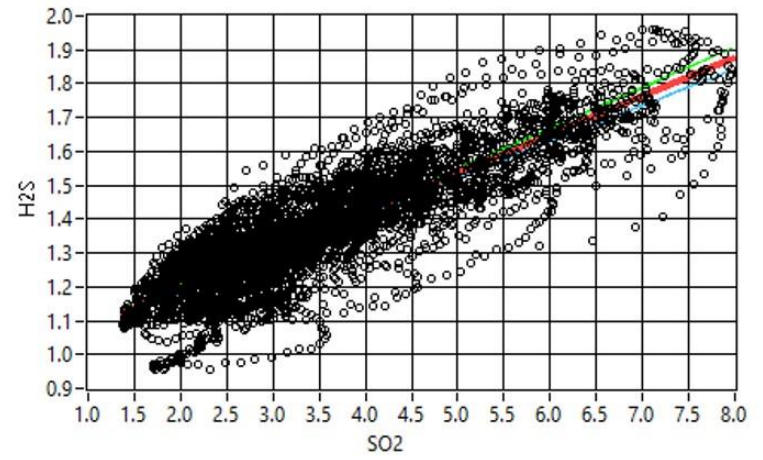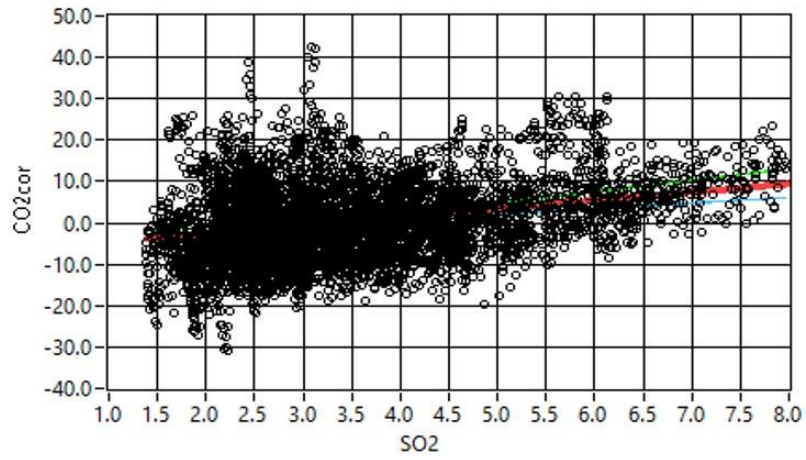
Table S6. CO_2, H_2S, H_2 and H_2O to SO_2 molar ratios obtained at San Miguel, El Salvador with the SN instrument

Date	sampling place	SO₂ max	CO₂/SO₂	error	R²	H₂S/SO₂	error	R²	H₂O/SO₂	error	R²	Data points
13/07/2018	SM plateau	3.52	9.19	4.74	0.661	0.10	0.03	0.880				157
06/02/2019	SM rim	5.20	7.01	2.14	0.625	0.12	0.02	0.841	221.06	56.47	0.704	449
06/02/2019	SM rim	5.25				0.13	0.03	0.902	59.90	27.85	0.645	197
07/02/2019	SM rim	4.60				0.07	0.02	0.709				372
07/02/2019	SM rim	5.74	5.15	1.51	0.695	0.14	0.01	0.972				362
07/02/2019	SM rim	4.70				0.12	0.04	0.852	70.54	29.51	0.758	150
27/03/2019	SM rim	3.18				0.19	0.06	0.886				121
27/03/2019	SM rim	3.29	11.11	5.00	0.624				111.82	46.07	0.664	225
27/03/2019	SM rim	6.07	5.57	1.47	0.787	0.11	0.02	0.866	83.44	19.70	0.822	284

Figure S15 – 18. Set of scatter plots of CO_2, H_2S, H_2 and H_2O vs SO_2 concentrations and the calculated best-fit line (red) obtained at San Miguel (2018 - 2020) using the SN device
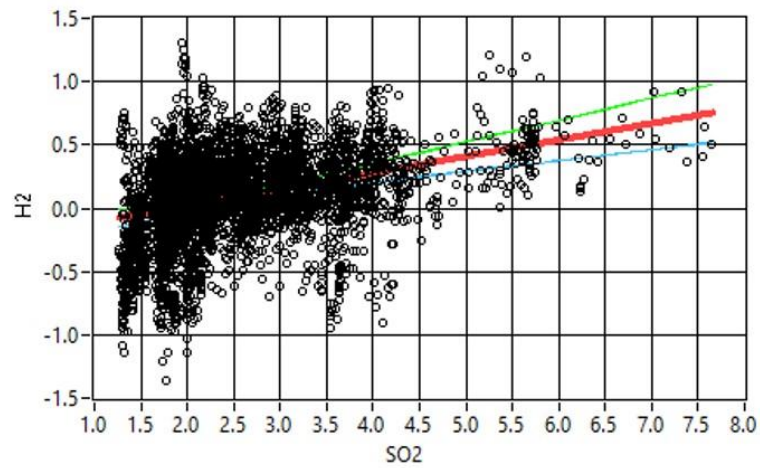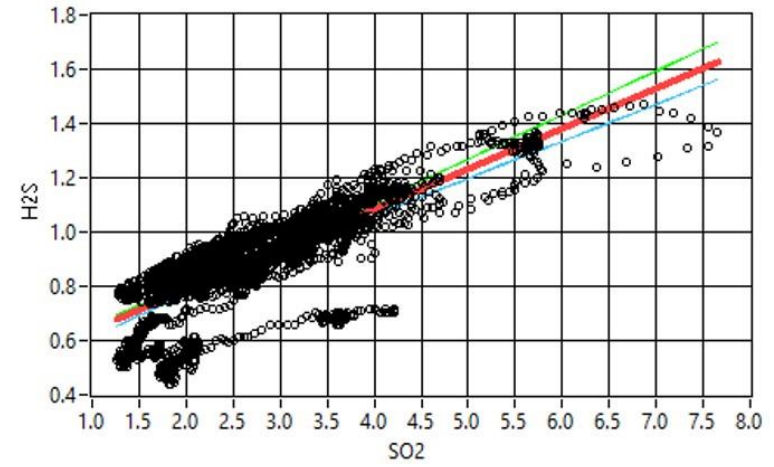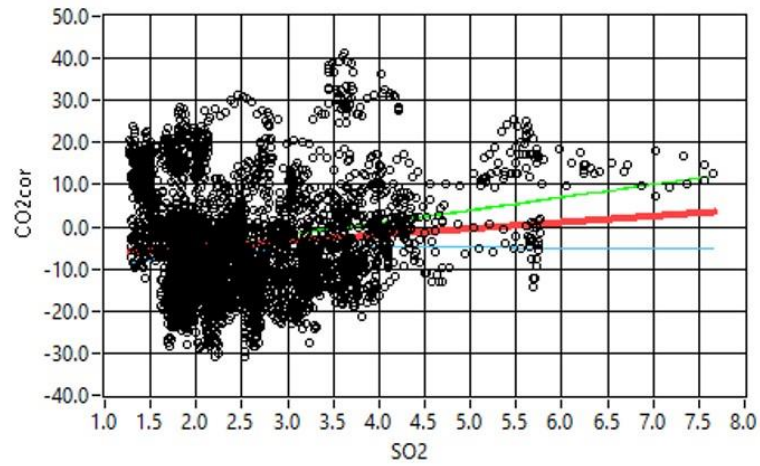
13.07.2018
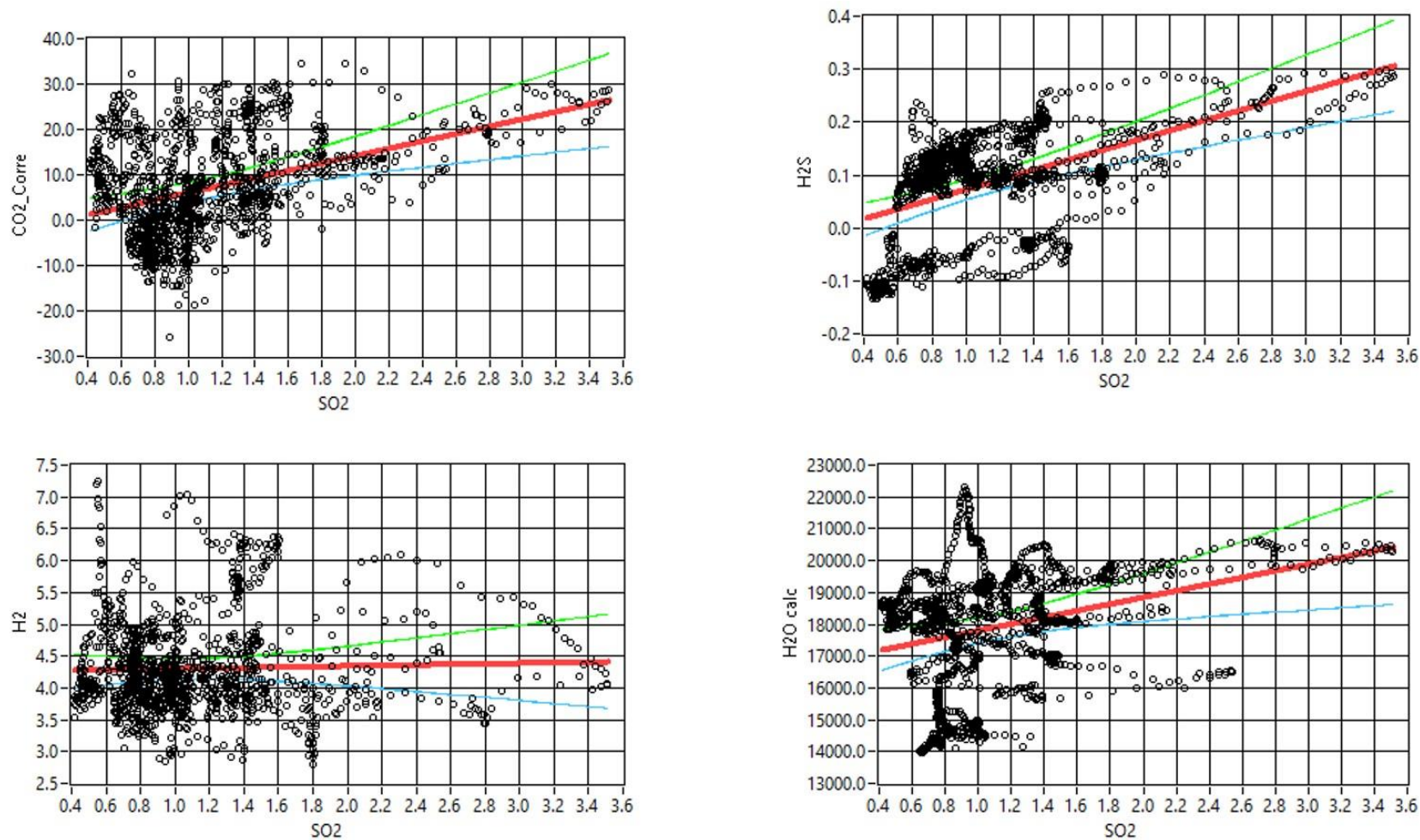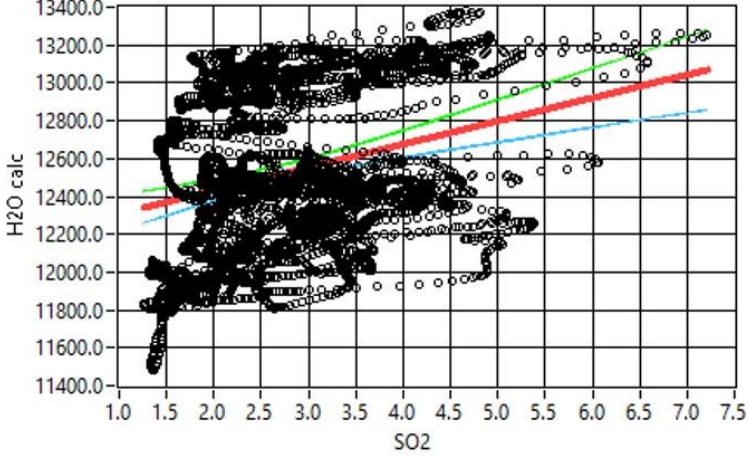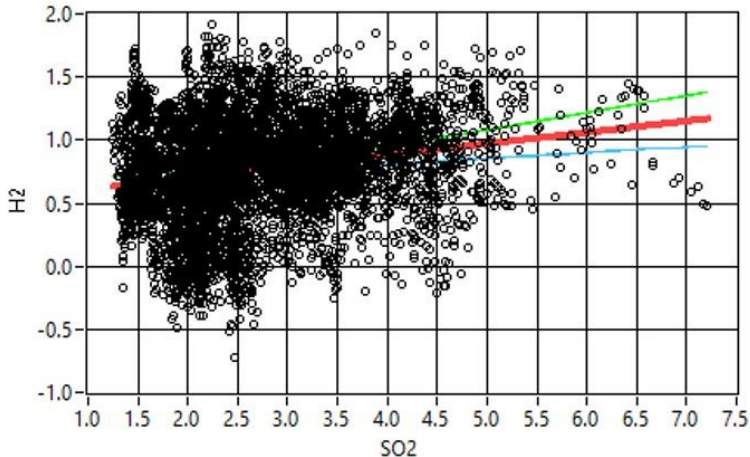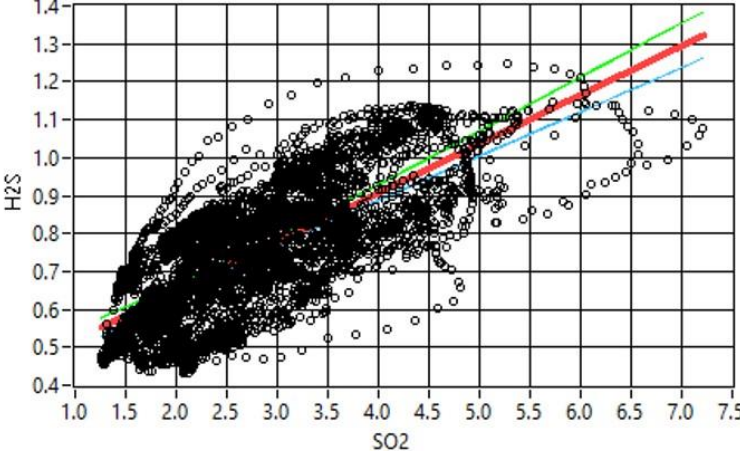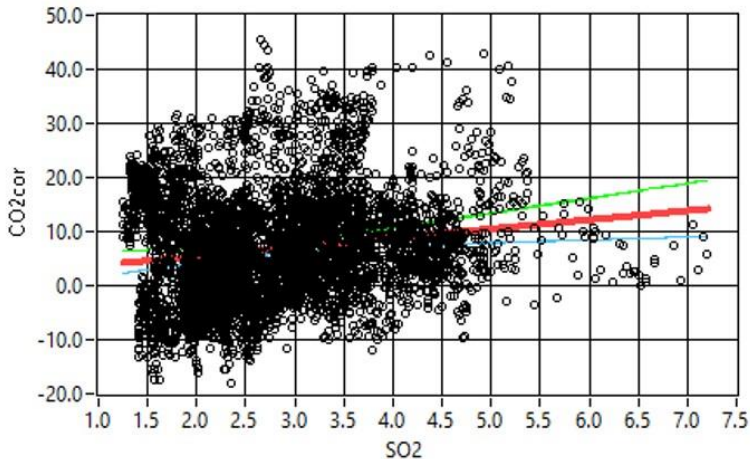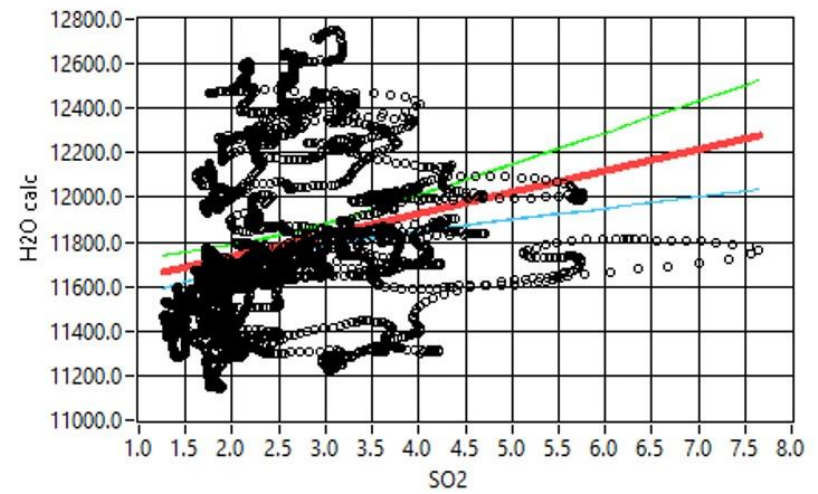
8. Acknowledgements

I would like to express my gratitude to all the people who supported and guided me during the time as a PhD candidate. First, I would like to thank my supervisor Prof. Dr. ██████████████ for giving me the opportunity to work on this research project. I am very grateful for his support, patience and guidance in each stage of my research, mostly throughout challenging periods. I really appreciate his support on the field and on the laboratory.

Special thanks to ███████████ for allowed me and encourage to write the proposal that led me to get my scholarship as well as to consider to perform studies at El Salvadorean volcanoes. I am sincerely thankful for her support on the field and her accurate observations in each writing I made.

Many thanks to ██████████ for stepping up to accompany me on my first field trip, teaching me how to prepare everything and for guiding me on the processing of the data.

I also like to thank people from the El Salvadorean Observatory, ████████████████ mi querido Maestro; ████████████████████████████████ for their collaboration on the field trips and the availability and access to data. Special thanks to ████████ for keeping the collaboration, honoring my Maestro's commitment with this research. Thanks to the people from the Nicaraguan Observatory, specially ██████████████ for helping me with the logistics to our survey on Masaya volcano and their collaboration on the field.

Thanks to ██████████ for providing me with the scripts and advice on how to evaluate the DOAS data for Santa Ana and San Miguel volcanoes. Special thanks to ██████████ for his assistance regarding the scripts and processing of the data but also his moral support and guidance thorough my whole PhD.

Thanks to all the current members of the ██████████ workgroup, since you provide my last years with a nice working environment and also leisure time at the big office. Special thanks to ██████████ for making the GC-MS troubleshooting times more enjoyable, you really made me feel I had a partner to rely on.

Finally, I would like to thank the most important people to me, my family. Gracias mami for not letting me fall and being my rock. Gracias ████████████████████ for supporting my dream of keep learning. The three of you are my parents and I cannot thank you enough for believing in me. Thanks to my siblings ███████████████████████████████████████ for giving me all the love and encouragement I needed to get through these years. Thank you to the little ones of this family, for bringing joy to my life. Thanks to my friends for always cheering me up and reminding me that I am capable to do everything that I put my mind on it.

9. Poster presentations

Rüdiger, J.; Schmitt, S.; Pitton, D.; Tirpitz, J.L.; Gutmann, A.; <u>Gutiérrez, X.</u>; Pöhler, D.; Lampel, J.; Horbanski, M.; Sander, R.; Zetzsch, C.; Hoffmann, T.; Held, A.; Platt, U.; Bobrowski, N.: HALVIRE: HALogen activation in Volcanic plumes In Reaction chamber Experiments, *European Geosciences Union General Assembly*, Vienna, Austria, April **2018**.

<u>Gutiérrez, X.</u>; Bobrowski, N.; Rüdiger, J.; Hoffmann, T.; Gutiérrez, E.; Dinger, F.; Montalvo, F.; Villalobos, M.: Remote and in-situ gas measurements at Santa Ana volcano, El Salvador, *Physics of Volcanoes*, Mendig, Germany, March **2019**.

<u>Gutiérrez, X.</u>; Bobrowski, N.; Rüdiger, J.; Hoffmann, T.; Gutiérrez, E.; Dinger, F.; Montalvo, F.; Villalobos, M.: SO2 and CO2 gas measurements at Santa Ana and San Miguel volcanoes, El Salvador, *European Geosciences Union General Assembly*, Vienna, Austria, April **2019**.

<u>Gutiérrez, X.</u>; Bobrowski, N.; Hoffmann, T.; Gutiérrez, E.; Dinger, F.; Montalvo, F.; Escobar, D.: Variation of SO2 and CO2 in the volcanic gas plumes of Santa Ana and San Miguel volcanoes: an overview by real-time measurements, *European Geoscience Union General Assembly*, online, April **2021**.

10. Curriculum vitae

Xochilt Gutiérrez

Personal Information

Date of birth: 10.10.1983 (San Salvador)

Nationality: El Salvador

E-mail: xcarito.guti@gmail.com

Language skills: Spanish (native speaker)

                        English (fluent)

                        German (basic knowledge)

Working experience

2015 – 2017
Manager of Centros Interactivos para el Aprendizaje de Ciencias (CIAC), Ministry of Education, El Salvador

2012 – 2014
Research Assistant, Bayerisches Geoinstitut, Bayreuth University, Bayreuth, Germany

2011 – 2012
Chemist, Ministry of Education, El Salvador

2009 – 2010
Professional to support volcanic gas monitoring, Ministry of Environment and Natural Resources, El Salvador

Education

Since 2017
PhD studies at Johannes Gutenberg University Mainz, Germany/Institute of Inorganic and Analytical Chemistry/Workgroup of Prof. Dr. Thorsten Hoffmann

2012 – 2014
Master in Science in Experimental Geoscience at the University of Bayreuth/Bayerisches Geoinsitute

2001 – 2008
Bachelor in Chemistry/Universidad de El Salvador

2000
Abitur/Colegio La Asunción, El Salvador